JONAS STOCK

GEOMORPHOLOGY AND EVOLUTION OF THE MIOCENE ROCK COAST OF THE ALGARVE: A MULTI TOOL APPROACH

UNIVERSIDADE DO ALGARVE
FACULDADE DE CIÊNCIAS E TECNOLOGIA

2020

Jonas Stock

GEOMORPHOLOGY AND EVOLUTION OF THE MIOCENE ROCK COAST OF THE ALGARVE: A MULTI TOOL APPROACH

Master in Marine and Coastal Systems
Work performed under the supervision of:

Delminda Moura (UAlg, CIMA)
Sónia Cristina (UAlg, CIMA)

UNIVERSIDADE DO ALGARVE
FACULDADE DE CIÊNCIAS E TECNOLOGIA

2020

Declaração de autoria de trabalho / Declaration of Authorship of work

GEOMORPHOLOGY AND EVOLUTION OF THE MIOCENE ROCK COAST: A MULTI TOOL APPROACH

Declaro ser o autor deste trabalho, que é original e inédito. Autores e trabalhos consultados estão devidamente citados no texto e constam da listagem de referências incluída.

I declare to be the author of this work, which is original and unpublished. Authors and works consulted are duly cited in the text and are included in the list of references.

X

Jonas Stock

Faro, 30th of September 2020

Copyright

Dedication and Acknowledgement

I am most grateful for the supervision by both, Delminda Moura and Sónia Cristina, who guided and supported me throughout the process of this thesis including planning and execution of several field trips.

I would like to acknowledge i) the Laboratory of Geology of CIMA-UAlg for utilization and particularly Paulo Santana for the help with the $CaCO_3$ analysis; ii) the Direção-Geral do Território (DGT) under the scope of CIMA and Mara Nunes for providing the orthomosaic for comparison of cliff evolution; iii) the financial support through BAföG and my mother Ulrike Stock; iv) my dear friend Camila de Sá Cotrim, who was by my side and supporting me in all possible matters from day one; Vincent Kümmerer for constant input, motivation and a healthy work-life balance; Jasmine Haskell for keeping the fun alive; Pedro Ferrara Rocha for helping with the Portuguese abstracts; and last but not least my roommates for giving me peace and support during the Covid-19 quarantine.

Abstract

Rocky coasts are widely distributed around the world (ca. 80% of the world coasts) and are subject to natural (physical, chemical, and biological) and anthropogenic pressures. The coastal evolution and erosional processes of the southern Algarve coast in Portugal have been previously studied; however, a precise analysis of the link between lithological characteristics and cliff vulnerability is lacking. Therefore, in this work we focus on facies variation and calcium carbonate ($CaCO_3$) content, discontinuities, (faults, joints, and layering), and morphological features (karst, notches, and marine caves) present in the southern cliffs of the Algarve from *Olhos de Água* to *Albandeira*. We combine a variety of data, including those derived from traditional field-based rock assessments, lab-based $CaCO_3$ content analysis, remote sensing (satellite and UAV image analysis) and photogrammetry. We find that the exposed carbonate rocks (mainly of Miocene age) at the southern Algarve are highly vulnerable to erosion. Additionally, we identify multiple key forcers: high vertical facies variation, intense karstification, multiple notches and marine caves. In addition, our lab analysis revealed differences in $CaCO_3$ content for each lithofacies, resulting in alternating rock strength and leading to the formation of multiple structural notches into the cliff face. Surface features (Land Use Land Cover - LULC) were categorized using remote sensing data and photogrammetry. A classification of cliff vulnerability was developed based on a combination of these lithological and geomorphological factors. The sector *Arrifes - Galé* was classified as most vulnerable; Sector *Galé - Armação de Pêra Bay* was classified as least vulnerable in the study area.

Keywords: Cliff vulnerability; Driver mechanisms; Lithology; Lagos-Portimão-Carbonate Formation (LPCF); Remote sensing; Algarve (Portugal)

Resumo

Os litorais rochosos representam cerca de 80% dos litorais em todo o mundo. Ao contrário dos litorais arenosos, a litologia desempenha um papel fundamental no seu comportamento. Este, é o resultado de factores naturais e antropogênicos. A evolução costeira e os processos erosivos da costa sul do Algarve (Portugal) foram previamente estudados; no entanto, uma análise focada na relação entre as características litológicas e a vulnerabilidade das arribas recebeu pouca atenção. Assim, este estudo focou-se na variação de fácies e no conteúdo de carbonato de cálcio ($CaCO_3$), nas descontinuidades (falhas, diaclases e planos de camada), e aspectos morfológicos (carso, sapas e grutas marinhas) presentes no litoral rochoso do Algarve, de Olhos de Água a Albandeira (principalmente do Miocénico). Foram integradas várias fontes de dados para realizar o estudo, desde dados recolhidos durante as saídas de campo para a avaliação da composição das rochas, análise de teor de $CaCO_3$ em laboratório, análise de imagens adquiridas por detecção remota (satélite e Veículo Aéreo Não Tripulado-VANT), e fotogrametria. O presente trabalho, identificou como principais forçadores da vulnerabilidade à erosão das arribas carbonatadas na área de estudo: variação vertical de fácies, carstificação intensa, sapas e cavernas marinhas. Além disso, a análise de laboratório revelou diferenças no teor de $CaCO_3$ para cada litofácies, resultando na alternância da resistência da rocha entre diferentes camadas, formando-se múltiplas sapas estruturais na face da arriba. As características da superfície foram categorizadas usando dados de detecção remota e fotogrametria. A classificação de vulnerabilidade das arribas foi desenvolvida com base na combinação dos fatores litológicos e geomorfológicos analisados. O Setor *Arrifes - Galé* foi classificado como o mais vulnerável enquanto o Setor *Galé - Baía de Armação de Pêra*) foi classificado como o menos vulnerável na área de estudo.

Palavras-chave: Vulnerabilidade das arribas; Mecanismos de erosão; Litologia; Formação Carbonatada de Lagos-Portimão (LPCF); Detecção remota; Algarve (Portugal)

Resumo Alargado

Costas rochosas podem ser observadas em quase todas as zonas litorais do mundo. Em comparação com as costas arenosas, a evolução das rochosas é bastante lenta e a perda de material é irreversível. A intensidade e a rapidez dos processos erosivos nas costas rochosas dependem de múltiplos fatores, entre eles: (i) propriedades litológicas das rochas expostas, (ii) parâmetros oceanográficos (impacto das ondas, amplitude da maré, variações do nível médio do mar), (iii) químicos (carsificação, muito dependente do clima e das descontinuidades da rocha), biológicos (bioerosão) e antropogénicos (infraestruturas, turismo, utilização do solo). Além disso, as arribas rochosas podem incluir diferentes unidades litológicas (litofácies) com diferentes resistências química e mecânica. Devido às diferenças de resistência, as litofácies mais vulneráveis podem sofrer erosão mais rapidamente do que outras, resultando num recuo diferenciado da arriba e na formação de arcos e leixões. O processo de erosão e recuo das arribas rochosas é favorecido pela presença de descontinuidades como falhas e diaclases, pois proporcionam uma maior superfície para a ação da meteorização e da erosão. A ocorrência de movimentos de massa é uma das formas mais comuns da erosão das arribas litorais e depende principalmente de propriedades como a litologia, estratigrafia, descontinuidades, bem como da precipitação e cobertura vegetal. Além disso, o desenvolvimento de sapas marinhas na base das arribas, fruto do impacto das ondas, é um dos maiores forçadores do colapso das mesmas. Ademais, a meteorização química como a dissolução, e a hidrólie podem resultar na desintegração de afloramentos rochosos, tornando-se outro fator importante na evolução das arribas. A dissolução é particularmente importante em rochas carbonatadas. Em consequência, desenvolvem-se estruturas cársicas como algares e condutas cársicas. A haloclastia (cristalização de sal nas descontinuidades das rochas), e a bioerosão (erosão promovida por organismos) são também mecanismos que contribuiem para a erosão e evolução das costas rochosas. Por outro lado, o rápido crescimento urbano, elevada densidade populacional e intenso turismo nas zonas costeiras, as arribas estão sujeitas a grandes pressões antrópicas. Consequentemente, é urgente proceder ao ordenamento sustentável das zonas costeiras, baseado no conhecimento científico e na utilização de métodos apropriados capazes de analisar rápida e eficazmente a vulnerabilidade de vastos sectores litorais

A detecção remota está entre as ferramentas mais populares no âmbito dos estudos de erosão costeira. As técnicas de detecção remota têm evoluindo e melhorado rapidamente a sua precisão nas últimas décadas. Referem-se a todas as observações, sem contato com qualquer objeto, por meio de satélite ou imagem aérea. O principal objetivo desta tecnologia é obter informações de parâmetros físicos para um determinado local e período de tempo, bem como o desenvolvimento de classificações (p. ex., uso do solo e da água).

A área de estudo deste trabalho compreende o trecho costeiro entre Olhos de Água e Albandeira no centro-sul do Algarve (Portugal). Aqui, as falésias expõem principalmente rochas carbonatadas da Formação Carbonatada de Lagos-Portimão (LPCF), do Miocénico, com exceção do trecho entre Albufeira e Arrifes. O principal objetivo deste estudo foi investigar a ligação entre as propriedades litológicas e alguns aspectos morfológicos e a vulnerabilidade das arribas à erosão, neste sector litoral, através da aplicação de múltiplas ferramentas como trabalho de campo, análises laboratoriais, detecção remota e fotogrametria.

Neste trabalho, em contraste com estudos anteriores, a análise da vulnerabilidade das arribas foi focada principalmente nas características litológicas das rochas expostas, embora se tenha também parametrizado a exposição à direção predominante das ondas e aspectos morfológicos como as estruturas cársticas. Deste modo, para investigar possíveis relações entre os parâmetros mencionados e a vulnerabilidade das arribas à erosão e para obter os dados necessários, foi implementada uma abordagem multi-ferramentas, as quais incluíram trabalho de campo para explorar a variação vertical de fácies e características geomorfológicas, bem como análise de conteúdo de $CaCO_3$ de amostras de rocha, realizadas em laboratório. Além disso, foram utilizadas plataformas de detecção remota em termos de imagens adquiridas por satélite e Veículo Aéreo Não Tripulado (VANT), além de análises fotogramétricas. Além do mais, foram testadas a adequação e a precisão destas ferramentas, para o estudo da vulnerabilidade das arribas à erosão, tendo como estudo de caso, as arribas no sul do Algarve entre Olhos de Água e Albandeira. Por último, na parametrização dos fatores que geram vulnerabilidade, foi desenvolvida uma avaliação relativa dos mecanismos motores da erosão e dos fatores de proteção, atribuindo fatores de impacto para cada parâmetro. Os parâmetros considerados, foram: variação vertical de fácies, conteúdo em $CaCO_3$, inclinação das camadas, densidade de ocorrência de falhas, quantidade e extensão

das estruturas cársicas distribuição e extensão das sapas e grutas marinhas, exposição da linha de costa à direção predominante das ondas e a largura da plataforma litoral e da praia. Os dois últimos parâmetros representam estruturas de proteção contra o impacto directo das ondas na base da arriba.

A área de estudo foi dividida em seis setores de acordo com as respectivas características litológicas tal como avaliadas no campo. Os resultados mostraram que o setor *Arrifes - Galé* apresenta a maior vulnerabilidade com uma pontuação de 3, sendo 4 o nível mais alto. Os sectores de *Olhos de Água - Santa Eulália; Santa Eulália - Albufeira; Albufeira - Arrifes e Armação de Pêra - Albandeira*, apresentaram moderada vulnerabilidade à erosão. A vulnerabilidade mais baixa foi detectada no setor *Galé - Armação de Pêra* com uma pontuação de 1,6. Além disso, os maiores valores médios de conteúdo de $CaCO_3$ e, portanto, correspondendo à menor vulnerabilidade, foram observados na localidade de *Albandeira* (77,9 %), seguido por *Santa Eulália* (73 %), *Olhos de Água* (59,7 %) e *Maria Luísa* (56,6 %). Entretanto, o menor teor médio de $CaCO_3$ foi verificado nas falésias de *Alemães* (39,68 %). A análise das feições morfológicas das superfícies do penhasco na área de estudo através das imagens Sentinel-2, revelou diversos problemas devido à cobertura vegetal e à baixa resolução (10 m). No entanto, as principais características macro morfológicas como praias, arribas, vegetação e infraestruturas, puderam ser distinguidas e classificadas usando a ferramenta de classificação do programa *SNAP*. Em contraste, a análise fotogramétrica das imagens capturadas do VANT no AgiSoft Metashape apresentou uma resolução muito alta para além da possibilidade de observar as arribas de ângulos diferentes e geralmente inacessíveis. Assim, o modelo 3D criado com AgiSoft Metashape ajudou a identificar a morfologia geral, bem como características de escala maior, como evidências de eventos de queda de rochas, algares e leques de dejecção na base das arribas, além de medições de altura do topo das arribas.

Os resultados deste estudo revelaram vulnerabilidade à erosão moderada a elevada em quase todos os setores estudados (com exceção da baía de *Armação de Pêra*), realçando as pressões a que estas arribas estão expostas. Adicionalmente, a zona costeira da costa sul do Algarve está sujeita a elevadas pressões turísticas, fazendo com que a avaliação da vulnerabilidade e prevenção de acidentes seja de extrema importância. Portanto, estudos

como este, auxiliam os gestores do território a entender os processos de vulnerabilidade das arribas costeiras e a garantir um turismo mais seguro.

Palavras-chave: Vulnerabilidade de arribas; Mecanismos de erosão; Litologia; Detecção remota; Algarve (Portugal)

Table of Contents

Table of Figures

Table of Tables

1 INTRODUCTION

The research on evolution and processes of rocky coastal cliffs is of major importance, as these environments experience great natural and anthropogenic pressures and are highly sensitive to climatic changes or extreme events. Processes that affect the evolution of rocky sea cliffs, and are therefore crucial factors to investigate include lithological properties, discontinuities in the rock (joints, faults, karst features), coastline orientation, erosion due to wave impact, chemical- and biological solution, as well as the behavior of sandy beaches and shore platforms (Kelletat, 1989; Bird 2008; Prémaillon et al., 2018).

Several studies (Komar, 1976; Kelletat, 1989; Sunamura, 1992; Carter and Woodroffe, 1994; Griggs and Trenhaile, 1994; Bird, 2000; Trenhaile, 2002; Woodroffe, 2002; Masselink and Hughes, 2003; Davis and Fitzgerald, 2004; Bird, 2008; Davis, 2013; Stephenson et al., 2013; Davidson-Arnot, 2010; Bird, 2016) have been conducted concerning the aforementioned matters which are precisely summarized by (Naylor et al., 2010). However, thorough research on driver mechanisms in respect to the physical substrate is needed (Griggs and Trenhaile, 1994; Benumof and Griggs, 1999; Trenhaile, 2002; Naylor et al., 2010; Boye and Fiadonu, 2020). This involves the examination of cliff features such as lithology, karstic holes, conduits and sinkholes, marine caves and notches as well as faults and joints, which need to be analyzed and parametrized.

In the southern Algarve rock coast, coastal evolution has been increasingly studied in the past decades (Marques, 1998, 2008; Catalão et al., 2002; Moura et al., 2006a; Teixeira, 2006; Moura et al., 2006b; Redweik et al., 2008; Nunes et al., 2009; Bezerra et al., 2011; Moura et al., 2011a; Moura et al., 2011b; Gabriel et al., 2012; Moura et al., 2012a; Horta et al., 2013; Oliveira et al., 2019). However, the main focus is on wave impact, coastline orientation, shore platform evolution and impact of storm surges. Yet, erosional processes on sea cliffs are driven by far more factors and hence, need to be studied particularly (Teixeira, 2006; Nunes et al., 2009; Bezerra et al., 2011; Moura et al., 2011a).

1.1 Hypothesis and Objectives

The fundamental research hypothesis of this work is that cliff vulnerability varies depending on the constituent lithological attributes of the exposed rocks of the coastal cliffs in the southern Algarve. A multi tool approach is implemented to obtain data to support the hypothesis.

The overall aim of this study is to develop an interpretative evolution of coastal geomorphology of the Miocene rock coast in the southern central Algarve, Portugal between *Olhos de Água* and *Albandeira* with the following objectives:

- Characterization of different lithological units and structures throughout the coastal stretch;
- Correlation of lithological properties (dimensions and features) with cliff vulnerability of the coast in the study area;
- Use of multiple tools such as fieldwork to explore lateral facies variation and geomorphological features, laboratory analysis of rock samples, coupled with remote sensing platforms in terms of satellite and UAV images and photogrammetric analysis.

When concluding the Thesis, it should be possible to develop a wholistic evaluation of cliff vulnerability in the study area, as well as state, whether field- and laboratory work or remote sensing proved to be useful and constructive tools for achieving the aim of the work.

2 BIBLIOGRAPHIC REVISION

2.1 Evolution of Rocky Coasts

Most of the worlds coast have been shaped during the Quaternary Geological Epoch, where they underwent transformations depending on the controlling factors of marine climate and mechanical strength of the substrate. The morphology and evolution of coasts is the result of the interaction between marine, terrestrial, organic processes and anthropogenic actions (Inman and Nordstrom, 1971; Davis, 2013). Key parameters of these processes include lithology, climate, vegetation, mean sea level and availability of fluvial sediment input (Bird, 2000; Bird, 2016). Depending on these factors, rocky coasts recede over time. The rate of erosion is determined by the balance between sub aerial and basal erosion, where water infiltration and runoff lead to sub-aerial weathering and marine impact results in the excavation of the cliff foot (base erosion). This process is acting over different times, rates and scales and is dependent on the exposing cliff material (Summerfield, 1991; Davis and Fitzgerald, 2004). Despite lithological variables, factors like discontinuities (faults, joints, karst features), mass movements (rock fall, toppling, collapsing cliffs), mechanic destruction (wave impact), climatic changes (sea level rise) or chemical solution and bioerosion lead to a receding rock coast (Kelletat, 1989; Summerfield, 1991). Erosional processes occur on a daily basis with average wave conditions, but during storms, wave energy increases rapidly and enhances the erosional forces on the cliff until far behind the tidal limit (Bird, 2016). Certainly, these factors are strongly depending on locality, making a common statement regarding cliff evolution impossible.

For the present work, understanding the relationship between lithological characteristics and erosional drivers and processes, is of utmost importance and is therefore discussed in the following Sections.

2.1.1 Lithology and Rock Resistance

Rocky sea cliffs can consist of different lithologies with mechanically and chemically stronger (therefore more resistant to weathering) and weaker rock units (Kelletat, 1989) (Figure 1).

"Resistant" in this context means strength of the exposed rock or the resistance to physical, chemical and biological weathering (Bird, 2016).

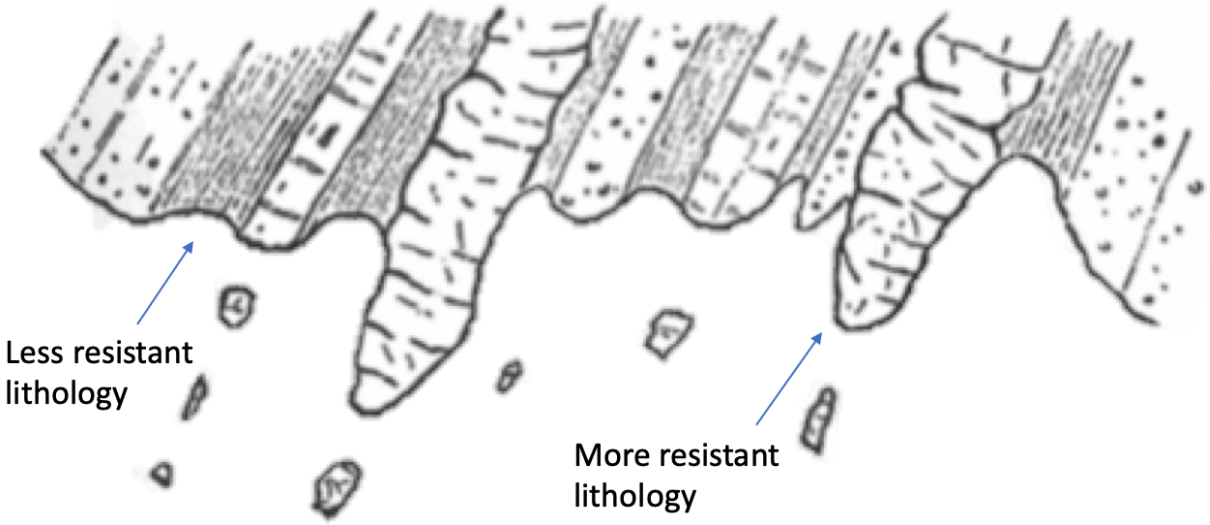

Figure 1: The evolution of a rocky coast is based on varying lithology, faults and joints. Rock units of more resistant lithology remain, whereas weaker parts get eroded more quickly (adapted from Komar 1976).

The resistance of a rocky cliffs is determined through its mechanical strength, which depends on the constituent lithology, calcium carbonate ($CaCO_3$) content and the presence of discontinuities (Moura et al., 2011b; Sunamura, 2015). Cliffs of thick layered, crystalline limestone, igneous or metamorphic rock without crevices or faults are under similar conditions much more stable and hence, more resistant to erosion compared to highly fractured and unconsolidated sediments (Davidson-Arnott et al., 2010; Griggs and Trenhaile, 1994). Dana (1857) classified rock strength according to mineral composition, ranging from the softest talc, to rock salt, calc spar, fluorspar, apatite, feldspar, quartz, topaz, sapphire to the hardest mineral diamond. However, this classification of comparative hardness was developed for comparison of different rocks and may be used to examine a rock specimen. Later, for example Clayton and Shamoon (1998) and Singh and Goel (1999) (original work John, (1971)) categorized different rock hardness from "1" to "4" with decreasing strength, which is more suitable for research on coastal cliffs:

1. Very hard quarzitic Sandstones and massive Granite, Gneiss, Marble
2. Moderately hard Slates, Shales, Grits and Basalts
3. Weak Limestones, Chalk and Sandstones

4. Very weak Claystones (defined as rock containing at least 90 % silt and clay), Siltstones

Regarding the differences in lithology and rock resistances, Prémaillon et al. (2018) compared their studies with those of Woodroffe (2002), where rates of erosion were linked to lithology (Figure 2). The results from Woodroffe (2002) exhibit a clear trend of increasing rates of erosion with decreasing rock resistance, which agrees with the outcomes of Prémaillon et al. (2018). However, hard rocks such as granite can erode as quickly as 1 m/yr $^{-1}$. Here, not only lithology but also influencing factors as fractures, wave energy and synoptic conditions need to be taken into account as well Prémaillon et al. (2018). As for the high diversity of rocky coasts, an absolute concordance of different studies is very unlikely. Thus, the outcomes are based on subjective classifications of rock classes and hence, leave space for interpretation and include some uncertainties.

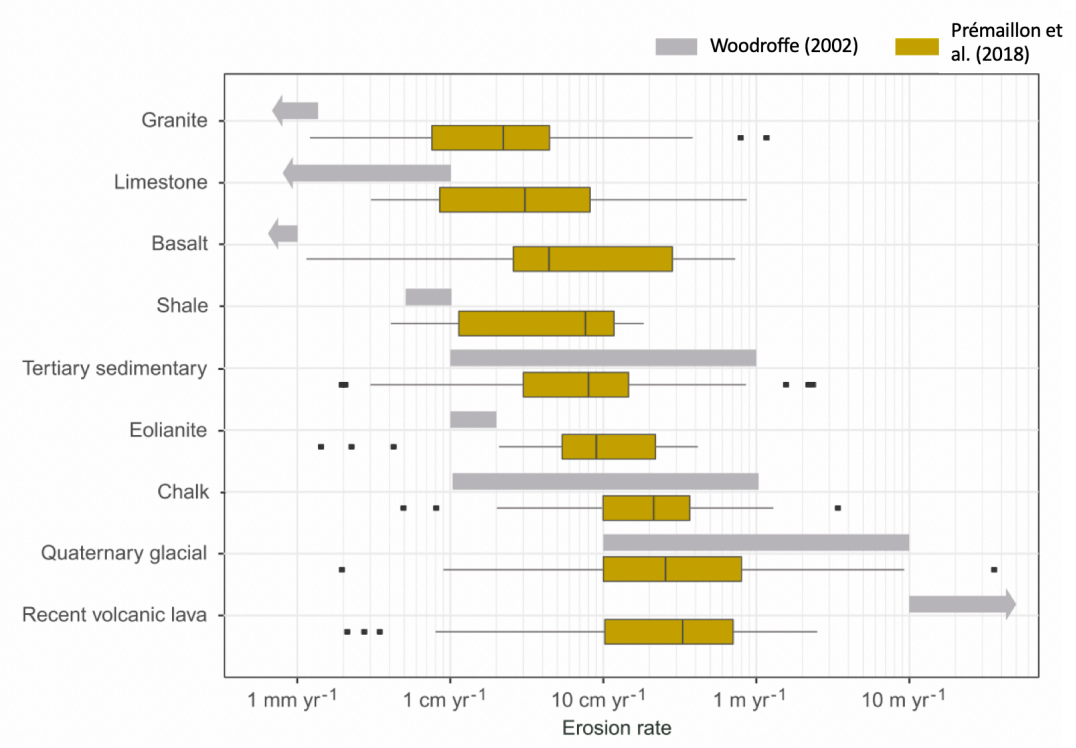

Figure 2: Erosion rates for different lithologies from two different studies (source: Woodroffe (2002).

Faults, fractures and crevices in the cliff enhance instability, as waves excavate and widen these discontinuities and develop structural notches, holes and caves. Due to constant wave impact on the cliff face, weaker lithofacies in the cliff get eroded more quickly than the

stronger layers in proximity. With time, the less resistant layers recess and create a structural notch, which contributes to instability in the cliff due to the overlying weight. This exerts an immense pressure on the notch and may lead to cliff collapse (Dias and Neal, 1992). A similar process takes place at the base of the cliffs. Here, during a phase of steady water level (mean-sea-level), the erosive forces of the waves can excavate a notch at the base of the cliff and thus, contribute to instability (Emery and Kuhn, 1982; Bird, 2016).

Often in combination with differential weathering and constant wave impact, susceptibilities in the rock result in the development of stacks and arches, as illustrated by Komar (1976) in Figure 1 and Bird (2000) in Figure 3 (Carter and Woodroffe, 1994; Davidson-Arnott et al., 2010).

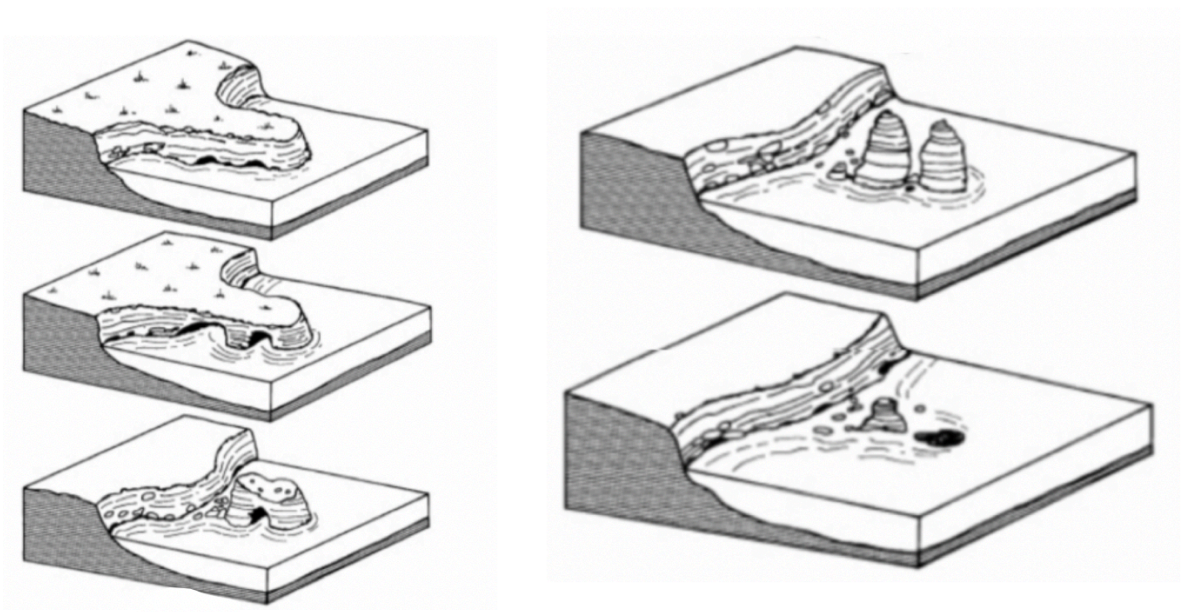

Figure 3: Process of headland erosion, where wave impact creates arches, which collapse with time and stacks of more resistant lithology remain (source: Bird 2000).

Due to the greater surface for erosion to act on, joints cracks and faults turn into indentations and embayments, which eventually get separated from the main cliff and result in stack formation. The morphology of stacks is relatively similar throughout the world, with a steep face towards the wave direction and a more convex shape at the more protected beach- facing side (Bird, 2000). In cliffs consisting of horizontally layered sedimentary rocks such as sand- and limestones, structural weakness results in the formation of arches. With constant wave impact in the lower and middle part of a headland or stack, excavations

advance into underpasses and a natural bridge develops (Davis and Fitzgerald, 2004; Bird, 2008; Stephenson et al., 2013). With time, these may erode as well and their debris deposits on the sea floor or gets transported along shore (Komar, 1976). Thus, the development of stacks and arches is mainly resulting from alternating layers of weak and more resistant rocks (Johnsons, 1919) and is supported by a high abundance of faults and joints in combination with marine weathering (Komar, 1976; Davis and Fitzgerald, 2004; Bird, 2008).

2.1.2 Shore Platform genesis and cliff protection

The development of shore platforms has been widely discussed in literature and different propositions regarding their genesis have been made. Concerning this, Bartrum (1926), Dana (1849), Edwards (1951) and Sunamura (1978) suggest wave action as the primary erosive process, whereas Bartrum (1916, 1938), Wentworth (1938, 1939) (Stephenson and Kirk, 2000) and Hills (1949) also hint at subaerial weathering as a possible alternative cause. Authors like Trenhaile (2002), Moura et al. (2006a) and Trenhaile and Kanyaya (2007) take rock porosity, faults and discontinuities in the platform into consideration, which result from karstification and enhance erosional processes. Consequently, many factors have to be considered when studying shore platform evolution as causes and processes may vary locally.

The most common wave induced process on shore platform evolution is abrasion. During the process of abrasion, sediments, ranging from fine sands to gravel, get washed over the shore platform by waves and grind the rock surface (Kelletat, 1989; Gomez-Pujol et al., 2014). Gradually, this produces a seaward dipping ramp, originating at the foot of the cliff. The rate of this abrasion and thus, the evolution of the shore platform, however, depends on the lithology, rock strength, wave energy, tidal range and presence of sediments (Summerfield, 1991; Trenhaile, 2002; Moura et al., 2011b; Bird, 2016). The latter can derive from the shore platform itself or gets transported from surrounding cliffs (Davis and Fitzgerald, 2004; Bird, 2016).

The evolution of shore platforms is further controlled by pressures from bio-erosive activities, however rates of downwearing vary depending on the lithological properties of the platform. Accordingly, in similar locations with similar climate and wave climate, calcarenite platforms

show higher rates of downwearing (0.25 – 2.97 mm/year), whereas for example siltstone appears to have lower values (0.07 – 0.33 mm/year (Moura et al., 2012a).

Depending on the tidal range, shore platforms vary in their visual appearance (Figure 4), where some are exposed entirely and only submerged briefly during high tide (Figure 4b), others are fully covered during the entire tidal cycle or are only shortly free from water during low tide (Figure 4c). Seaward-sloping ramps are in junction with the cliff foot and the high tide level and extend seawards to a level beneath low tide (Figure 4a). In locations with steep cliffs descending into the water (plunging cliffs), no shore platform is present (Figure 4d) (Bird, 2008).

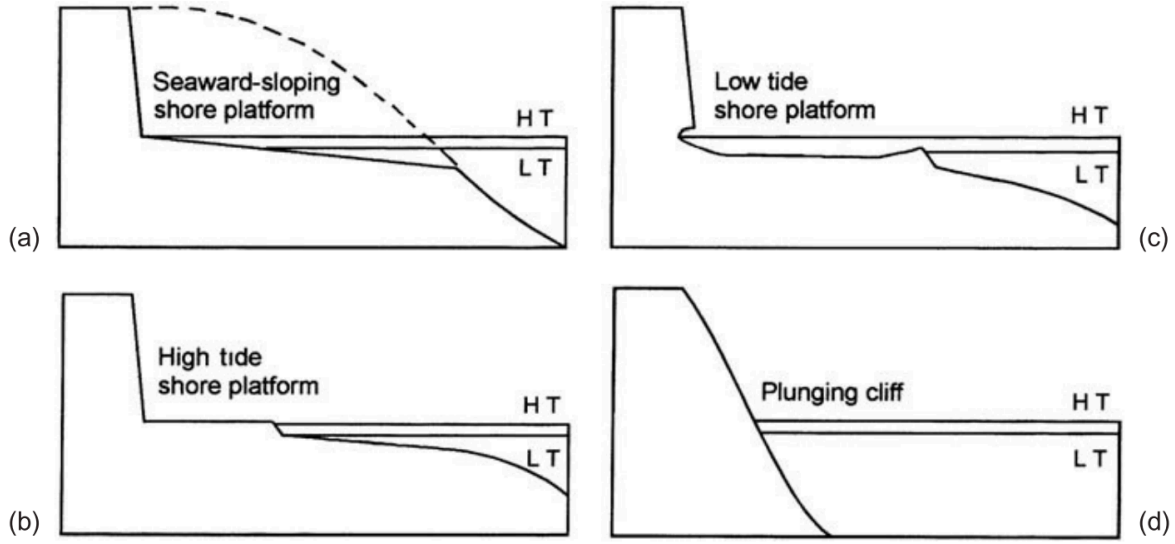

Figure 4: Shore platform scenarios on coasts. (a) Seaward sloping shore platform, (b) low tide shore platform, (c) high tide shore platform, (d) plunging cliff with no present shore platform (source: Bird 2008).

Another important factor for the genesis of shore platforms are tides. As tides are the controlling factor of where the waves impact the platform, it is crucial to consider the tidal range of coasts. In environments with a mesotidal tidal range, sub-horizontal wave cut platforms established, whereas macrotidal conditions formed seaward dipping ramps. Depending on the constituent lithology, topography, slope and roughness, the shore platforms of the intertidal zone vary in dimension and preservation, where widest shore platforms established in sheltered locations or at coasts with a high tidal range and direct wave exposition (Trenhaile, 2000; Trenhaile, 2002; Moura et al., 2011b).

Moreover, shore platforms play an important role for cliff protection against direct wave attack. When crossing the shore platform, waves dissipate energy and are forced to break further offshore and therefore, do not reach the cliff. However, depending on the offshore wave climate, coastline orientation, platform slope and local bathymetry, shore platforms can enhance wave heights and consequently increase erosional forces. Due to these opposing processes, shore platforms are an important factor when studying coastal evolution (Nunes et al., 2009; Moura et al., 2012b; Gabriel et al., 2013; Trenhaile, 2015).

2.1.3 Physical Processes

2.1.3.1 Waves

Amongst many parameters, waves are the most eroding factor on rocky coasts which is mainly dependent on wave climate, coastline orientation and cliff characteristics. However, erosion only occurs, when the assailing force of the waves is stronger than the resisting force of the constituent rock (Sunamura, 2015). In that case, waves act either hydraulic or mechanical on the cliff.

Hydraulic processes induce compression, shearing or tension. Erosion due to air compression (water hammer effect) occurs when waves break at a cliff and air gets trapped in between the rock and water, creating high pressure on the rock (Griggs and Trenhaile, 1994; Davis and Fitzgerald, 2004; Davidson-Arnott et al., 2010; Naylor et al., 2010; Bezerra et al., 2011). Shearing is the process of water moving up and downward on the cliff face when the waves hit the cliff. The procedure of tension occurs when the water recedes from the cliff (Kelletat, 1989; Davidson-Arnott et al., 2010; Sunamura, 2015).

Erosion due to mechanical action occurs when clastic sediments are smashed at the cliff by waves and dragged or grinded on the surface. The resulting abrasion process is very prominent on shore platforms and depends on the availability of material and wave energy (Kelletat, 1989; Summerfield, 1991; Sunamura, 2015).

Repeated wave impact and air being pushed into faults, crevices and fractures, results in an enlargement of these discontinuities and the dislodgement of particles from the cliff (quarrying). During storm surges and high wave energy, the erosional forces acting on the cliff are intensified and may lead to mass movements (Stephenson and Kirk, 2000; Davidson-

Arnott et al., 2010; Trenhaile, 2015). After the collapse or fall of rocks, the eroded material either stays at the foot of the cliff or gets reduced in size and transported by waves and littoral currents. While small particles get transported offshore, bigger eroded blocks function as a protection of the cliff (Costa et al., 2006; Trenhaile, 2015).

2.1.3.2 Mass movements

The most common mass movements are rock falls, topples and slides and mainly depend on cliff properties such as lithology, stratigraphy and jointing, climatic factors like precipitation and temperature, as well as on vegetation, hydrology and slope angle (Kelletat, 1989; Davidson-Arnott et al., 2010). Rock fall describes the vertical fall of cliff material, whereas rotating, stumbling material are classified as topples. Movements on a bedding plane or slip surface are shearing displacements and can be categorized into planar slides and rotational slides, depending on the shape of the sliding surface (Bird, 2008; Sunamura, 2015).

Landslides and rock fall are further results of weathering and layers of unconsolidated sediments, where high precipitation is an enforcing factor. Especially in humid areas, subsurface runoff contributes to cliff erosion, which is more or less effective depending on the present lithology (Bird, 2008).

Depending on the cliff profile, discontinuities and notches, mass movements may be indorsed (Bird, 2008). As previously mentioned, the development of marine notches at the cliff base or structural notches throughout the cliff face, creates high instability. The formation of notches is widely discussed, however, according to Trenhaile (2015), literature such as Sunamura (1992), Mottershead (2013) or Stephenson et al. (2013) mainly focuses on possibly inadequate field observations and suggests a classification into “tidal notches” (formation in intertidal zone) and “surf notches” (formation in high tide level). Moreover, notches may develop as a result of bioerosion, chemical dissolution, wave action, wetting and drying, abrasion and salt-weathering. This however, is reliant on the present lithology, tidal range and wave climate (Trenhaile, 2015).

2.1.4 Chemical Processes

Besides physical processes, chemical weathering such as solution, salt weathering (salt crystallization), mineral decomposition or base exchange may lead to the disintegration of

rock outcrops and is hence, another important process regarding cliff and shore platform evolution (Bird, 2008). Concerning salt weathering, two processes can be observed; Salt weathering and water layer weathering. Both act erosive on the rock surface due to pressures from solution, thermal expansion and hydration (Kelletat, 1989; Stephenson and Kirk, 2000; Masselink and Gehrels, 2014). Moreover, heavy, episodic precipitation increases runoff, lowers the infiltration rate and hence, promotes erosion. Given that rainwater contains dissolved carbon dioxide, it is slightly acid and therefore acts erosive on the rock. This is one of the main drivers for chemical weathering particularly on weak carbonate rocks, as fine particles are being washed out, leaving cracks and crevices behind. In granitic rocks, during the process of hydrolysis, feldspar transforms into clay minerals, which results in the collapse of the crystalline structure and a rapid disintegration of the rock into sand grains (Bird, 2008; An et al., 2020; Hayes et al., 2020). Accordingly, climatic conditions are a key factor concerning chemical weathering processes.

Especially in regions with carbonate rocks, which are strongly vulnerable to wave and rainwater impact, chemical weathering acts on the cliff and creates karst features like holes, conduits and crevices. This process creates a subterranean system of water circulation with highly instable features in the cliff (Oliveira et al., 2019). Depending on the lithotype and its mechanical strength, lithofacies in the cliff show more or less karst features, affecting the evolution of the cliff face in different fashion. Thus, the presence of karst features (caves and conduits) in the rock surface reduces the cliff's stability and promotes the risk of rock fall (Teixeira, 2009). Additionally, during events of heavy rainfall, rainwater infiltrates into the relatively permeable carbonate rock, dissolves the matrix and expands karst features. In the combination with sea water, the subterranean circulation of water creates a high risk of rock collapse and promotes cliff retreat (Bezerra et al., 2011; Oliveira et al., 2019).

A very common karst feature, which increases the vulnerability of rocky sea cliffs, are sinkholes (Figure 5). These highly hazardous depressions form through dissolution of the carbonate minerals within the rock and develop cavities (Forth et al., 1999). Sinkholes can evolve in different ways with various sub-categories. Dissolution sinkholes develop through a slow lowering of the surface as a result of subterranean small-scale collapses. Contrarily, collapse sinkholes experience an immediate and wholistic failure of the surface cover. Both

types create a small to large hole, which may afterwards be filled by surrounding sediments (Waltham and Fookes, 2003; Oliveira et al., 2019).

Figure 5: View from the beach into three different small sinkholes in the southern Algarve, Portugal (Olhos de Água beach), exhibiting high instability and vulnerability to cliff collapse (STOCK 2020).

2.1.5 Biological Processes

A process contributing and potentiating coastal erosion and shore platform genesis, which is often being neglected, is bioerosion (Bird, 2008; Kelletat, 1989). During the process of bioerosion, organisms directly act on lithic substrate, resulting in removal of the very same (Neumann, 1966). The intensity and distribution of bioerosion on a cliff or shore platform depends on factors like moisture availability, tidal regime and range as well as on the constituent substrate and thus, strongly varies (Stephenson et al., 2013; Trenhaile, 2015). Bioerosion can be separated into “direct” and “facilitative”. Grazing and boring species directly erode the rock material, whereas other bio-erosive species alter geological properties and geomorphic processes (Naylor et al., 2012). According to Moura et al. (2012a),

the main features of bio-erosive actions are initialized by macroborers and due to the grazing activity of limpets. Grazing organisms like invertebrate phyla are able to bore directly into the rock substrate up to tens of meters depth (Trenhaile, 2015). The grazing intensity of the organisms relies on spatial variation in grazer distribution, density of organisms, food availability and seasonality. Further, the development and alteration of mesoscale morphologies (e.g. rock-pools) is caused by bio-erosive activity, where discontinuities in the rock ease the process (Naylor et al., 2012). Boring organisms like echinoids, gastropods, sponges, barnacles and worms can support downwearing, especially on shore platforms (Summerfield, 1991) and thus, contribute to erosion. By enlarging crevasses and cracks, borers enhance weaknesses in the rock structure (Griggs and Trenhaile, 1994). Plants living on or near cliffs, may as well penetrate and expand cracks and joints in the rock surface, which supports the decomposition of rock outcrops (Bird, 2016).

The combination of the effects of bio-erosive activity, which act in different temporal and spatial scales, leads to a reduction of the resisting force of the rock while increasing the risk of meso- to macro-scale erosion (Naylor et al., 2012).

2.2 Remote Sensing Platforms

Remote sensing techniques have evolved and improved on a high frequency over the last decades and refer to all non-contact observations for any object by satellite or airborne image and spatial data acquisition. Main objective of this technology is to obtain information of physical parameters for a certain space and time frame as well as the creation of classifications (e.g. Land Use Land Cover – LULC). These derive from the translation of observations into visual categories on maps (Thenkabail, 2015; Toth and Jóźków, 2016; Gupta, 2017).

2.2.1 Satellites

Satellite based remote sensing can cover large swaths over long periods of time (years to decades) in a cost-effective way. Due to a variety of sensors onboard the satellite missions, this method can be applied to multiple studies on land, ocean and atmosphere (Drusch et al.,

2012; Lillesand et al., 2015). The European Space Agency (ESA) is the main executor for satellite remote sensing as they developed multiple missions (Sentinel-1 – 6) designed specifically for the needs of the Copernicus programme. The Sentinel missions consist of two parallel operating satellites to create fast revisit times and high spatial coverage. The applications are broad, containing radar and multi-spectral imaging for land, ocean and atmosphere monitoring (ESA, 2020 accessed on 20.01.2020).

Sentinel-2A was launched in 2015, followed by Sentinel-2B in 2017. This polar-orbiting mission is based on multispectral high-resolution imaging with spatial coverage of around 290 km for all land surfaces and coastal waters between -56° and +84° latitude (Drusch et al., 2012; Van der Meer et al., 2014). Applications include monitoring concerning coastal areas and supplement of data for risk management, land use, terrestrial mapping and natural hazards to name a few. According to Drusch et al. (2012), the system intends to complete the Landsat and SPOT (Satellite Pour l'Observation de la Terre) missions for data improvements. This is being done by using 13 bands of the visible, near infra-red and short wave infra-red electromagnetic spectrum for a broad spectral coverage and a high spatial resolution ranging from 10, 20 and 60 m (Drusch et al., 2012).

In order to identify the potential of Sentinel-2 Multi-Spectral Imager (MSI) data for geological use, Van der Meer et al. (2014) conducted research in southeast Spain. To see the resemblance of the simulated Sentinel-2 data to geological maps and mineral maps of the study area, the authors compare the high spectral resolution images and data to those generated from Advanced Spaceborne Thermal Emission and Reflection Radiometer (ASTER). ASTER is a high spatial resolution multi-spectral imaging radiometer with 14 bands, 60 km swath and spatial resolution between 15 – 90 m (Yamaguchi et al., 1999). Results show good correlations between the two systems and support the potential of Sentinel-2 data for geological applications (Van der Meer et al., 2014).

Research from Ge et al. (2018), who used both multi-spectral data from Sentinel-2 and ASTER data to categorize and map differences in lithology in the Shibanjiang ophiolite complex in inner Mongolia, China, shows, that the applied methods can differentiate rock units and improve classification accuracy. Subsequently, the obtained results regarding lithological mapping from the comparison of Sentinel-2A with ASTER, demonstrate the benefit of

Sentinel data and prove, that the use of satellite images is an economical and efficient tool for lithological mapping.

Generally, the use of satellite imagery has proven to be a very useful tool to obtain continuous datasets for global land surface monitoring and to study biophysical and biochemical parameters (Bishop, 2013; Van der Werff and Van der Meer, 2016).

2.2.2 Airborne

Airborne remote sensing describes the acquisition of data from sensors or cameras mounted to aircrafts, which constantly developed in the last decades and provide highly accurate mapping (Toth and Jóźków, 2016). When using airborne Light Detection And Ranging (LiDAR) with high resolutions of around 1-4 m, topographic data can be acquired for large swaths despite possible vegetation or forest coverage (Grebby et al., 2010).

Research on coastal cliff retreat in Japan, using aerial photographs was conducted by Horikawa and Sunamura (1967). For this, aerial photographs were taken with a six-year interval in 1960 and 1966 and profile lines were drawn. Consequently, the eroded distance and changes in coastal cliffs could be examined quite accurately. However, due to a lack of advanced technology, multiple important factors influencing sea cliff evolution, such as the erosive force of waves, could not be considered. Airborne remote sensing was also used to study cliff evolution in southern Portugal (Marques, 1998; Teixeira, 2006; Nunes et al., 2009), where aerial image comparison and interpretation over several years was the key methodology. Accordingly, airborne remote sensing can cover large distances with different sensors, scanners and cameras, but lack continuous time-periods and are not cost-efficient.

2.2.3 Unmanned Aerial Vehicles

The variety of Unmanned aerial vehicles (UAVs) is quite large, ranging from “do it yourself” systems, to inexpensive consumer products or professional systems and are commonly referred to as drones. Systems with fixed wings tend to have an increased flight duration compared to rotating-wing drones, which, however, can take off and land basically everywhere (Toth and Jóźków, 2016). Nevertheless, both solutions can cover areas, which

are otherwise difficult to access with high resolution and preinstalled flight planes, depending on the drone and camera system (Thenkabail, 2015). Compared to the aforementioned satellite and airborne remote sensing techniques, UAV surveys are inexpensive, rapid and spatially flexible but lack a wide spatial coverage due to insufficient battery life (Niethammer et al., 2012; Toth and Jóźków, 2016; Gupta, 2017; Oliveira et al., 2019).

UAVs can be used for a variety of research areas but are most affective for small space studies with a limited time and financial budget. Amongst others, UAVs are used to study landslides, soil- and cliff erosion, as well as for morphological and sedimentary processes on coasts. For this, mostly orthophoto mosaics and digital elevation models (DEM) are developed, which provide data concerning displacements of material and changes in volume (Catalão et al., 2002; Niethammer et al., 2012; Kaiser et al., 2018).

3 STUDY AREA

The study area of this work is located in the southern Algarve coast, Portugal and includes the Lagos-Portimão-Carbonate Formation (LPCF) (except the coastal stretch from Albufeira – Arrifes). The surveys and methodology were applied to a coastal stretch from *Olhos de Água* beach until *Albandeira* beach, covering around 22 km of coastline. This includes the locations *Olhos de Água, Maria Luísa, Santa Eulália, Alemães, Arrifes, Coelha-Galé, Armação de Pêra Bay, Nossa Senhora da Rocha and Albandeira* (Figure 6), which were studied with particular attention. The following Section introduces the present marine climate, morphology, shore platforms, karstification, the role of rivulets as well as anthropogenic influences.

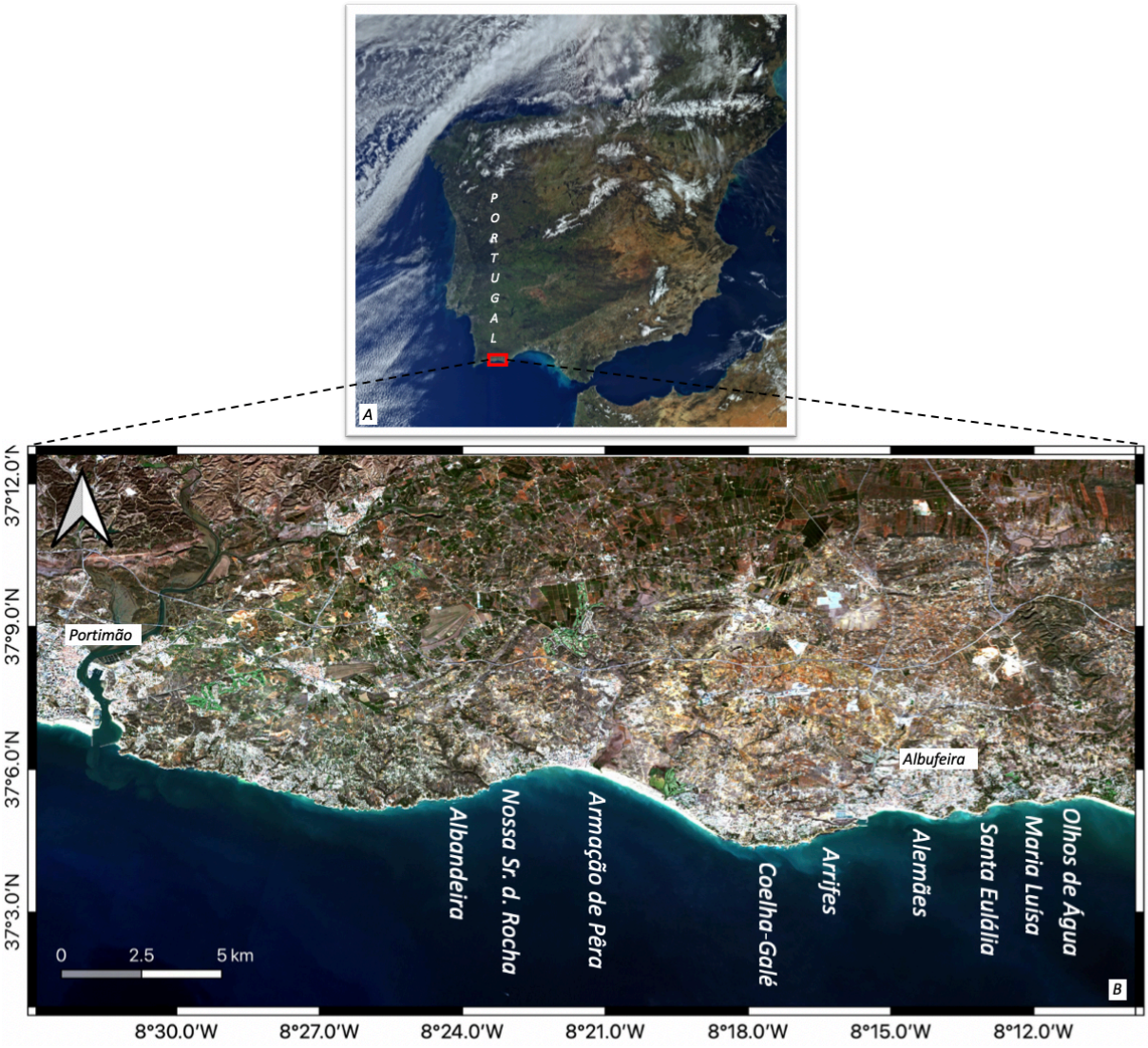

Figure 6: Geographic location of the study area from Olhos de Água beach until Albandeira beach (A: Copernicus Sentinel-3A data [01-03-2016], processed by ESA) (B: contains Sentinel-2A data [16.11.2019], processed by ESA).

3.1 Marine climate

The southern Algarve coast has a mainly Mediterranean climate, meaning mild winters and hot and dry summers. The average annual precipitation varies between 500 – 600 mm at the littoral zone, with +/- 80 % of it in the months between October to March. Mean yearly temperatures are around 19°C (Miranda et al., 2002). The southern Algarve coast has a mesotidal environment with a semidiurnal tidal regime, with an average range of 1.2 m at neap tide and 2.8 m at spring tide (Instituto Hydrogràfico 1990). The predominant wave directions offshore the southern Algarve coast are W-SW and E-SE, where W-SW directions occur 71 % of the time and E-SE conditions about 23 % (Costa et al., 2001). Average wave heights range from 0.3 m to 1.8 m, however, during storms, heights of more than 3.7 m can be reached (Pires and Pessanha, 1997). These events only occur during the time period of the maritime winter (October – March) and have an average duration of two days (Costa el al., 2001).

Since the occurrence of heavy winterly storms is quite common in the study area, the coastline is very sensitive regarding increasing wave- and wind-energy and therefore, its cliffs are highly susceptible to erosion. This has a strong influence on the evolution and geomorphology of the Algarve coast and can result in rapid cliff retreat rates (Nunes et al., 2009; Bezerra et al., 2011).

3.2 Morphology of the southern Algarve's rocky cliffs

The lithological and tectonically controlled Portuguese south coast mostly consists of crenulated rock coastline with sandy pocket beaches and bay-beaches, embayed by headlands and shore platforms (Figure 7) (Horta et al., 2013).

The cliffs in the southern Algarve coast vary from minimum heights of +/- 2 m up to +/- 40 m, with a predominant height between 15 m and 25 m (Marques, 1998). These relatively uniform stratified rocks are slightly dipping SE (up to 10°) and are moderately faulted (Romariz et al., 1979).

The coast in the study area, mainly exposes Miocene carbonate rocks, which are highly vulnerable to chemical attack such as karst exhumation. This presents a major factor

concerning coastal cliff evolution (Moura et al., 2006a). The paleokarst ranges from deep valleys to sinkholes, cutting through the Miocene carbonate rocks, which later were filled by fluvial and marine deposits from the Pliocene and Pleistocene geological Epochs.

Figure 7: Coastal section eastward of Albandeira beach, showing plenty of pocket beaches embayed by headlands (STOCK, 2020).

During the Early to Upper Miocene, the nowadays outcropping, +/- 60 m thick LPCF formed as a result of the deposition of sandstone and carbonate rudstones into a carbonate-siliciclastic platform (Forst et al., 2000; Pais et al., 2012). Additionally, Forst et al. (2000) suggest that the formation occurred along a narrow shelf platform and was frequently affected by eustatic cycles. Eventually, this led to a relatively concurrent facies variation.

In general, the main lithotype of the southern Algarve cliffs originates from the Miocene Epoch and includes limestones, siltstones, calcarenites and biocalcarenites (Moura et al., 2006a; Bezerra et al., 2011) (Figure 8). The only lithological different part in the study area is the coastal stretch from *Albufeira* until *Arrifes* beach, where outcropping Jurassic limestones and Cretaceous marls form the coastline (Figure 8).

The rocks from the Miocene Epoch in the study area can be categorised into two main lithological types: weakly cemented calcarenites and crystalline limestones, generally with a

high abundance of macrofossils (molluscs shells, sea urchins and carbonate algae). Research from Teixeira (2009) concerning mechanical rock strength of the outcropping Miocene rocks in the Algarve coast, identified the majority of the samples as low to very low resistant, which is positively linked to low $CaCO_3$ content (Moura et al., 2011b). Carbonate content analysis from Teixeira (2009) discovered $CaCO_3$ content values with average values of 87 % for calcarenites with a high lumashell abundance and around 73 % in fine calcarenites.

Lateral facies variations in the area is relatively persistent in the cliff face, whereas vertical facies variations alter on a high frequency. These changes in vertical and lateral facies along the coastline of the southern Algarve is subject to the height of the cliffs, coastline orientation, intersection of the topographic surface and displacements by faults and are of major importance concerning cliff stability Moura et al. (2011a).

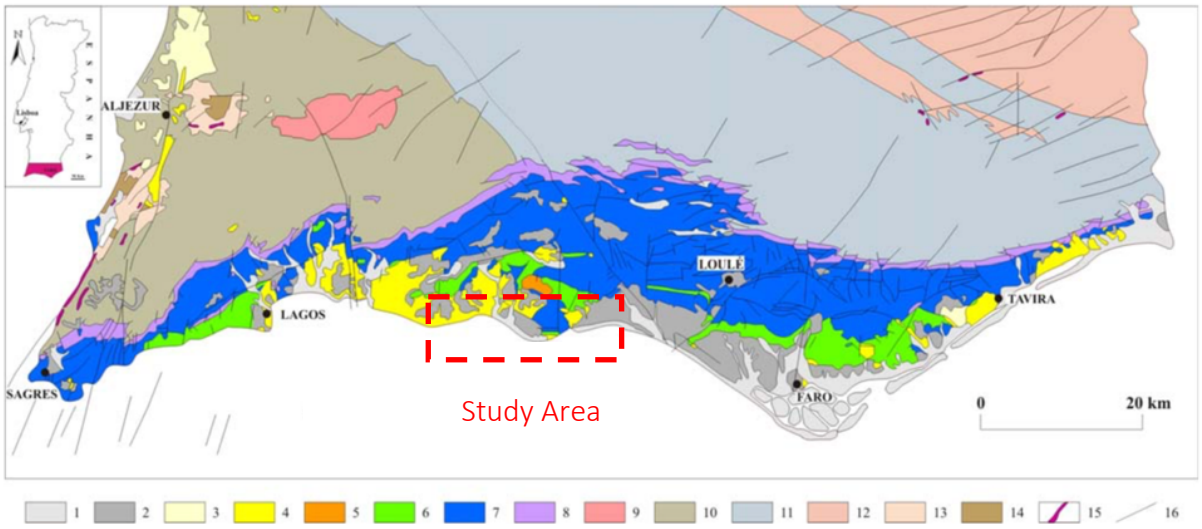

Fig. 1.1- Mapa geológico da Bacia Algarvia.

1- Holocénico; 2- Pleistocénico; 3- Pliocénico; 4- Miocénico; 5- Paleogénico; 6- Cretácico; 7- Jurássico; 8- Triásico/Hetangiano; 9- Complexo alcalino de Monchique; 10- Vestefaliano; 11- Namuriano; 12- Viseano; 13- Tournaisiano; 14- Fameniano; 15- filões; 16- falhas (adaptado da carta geológica de Portugal 1/500000, 1992)

Figure 8: Geological map of the Algarve, showing the distribution of cliff lithology and the study area (red dashed rectangle) (adapted from Terrinha et al. (2006)).

3.3 Shore Platforms

As previously mentioned, shore platforms are an important factor concerning cliff evolution and are widely present in the study area. The most extensive intertidal platforms in the study area occur east of *Galé*, at *Arrifes* and between *Santa Eulália* and *Maria Luísa*, where they reach a maximum width of around 80 m to 150 m, respectively (Moura et al., 2006a). Gabriel

et al. (2013) studied wave behaviour on shore platforms at *Olhos de Água* beach and determined, that depending on the wave conditions, the shore platform acts either dissipative or enhances wave heights, influencing the beach and cliff morphology. Moreover, energy dissipation of waves at the shore platform varies throughout the study area, where *Galé* presents a higher dissipating efficiency compared to *Olhos de Água*. This is also linked to the orientation of the coastline and the resulting exposition to incoming waves (Moura et al., 2012b). The exposed shore platforms in the study area vary depending on bio- and chemical processes (Section 2.1.4 and 2.1.5), where for example hydric erosion creates solution ponds (Figure 9).

Figure 9: Aerial photograph showing the exposing shore platform between Olhos de Água and Maria Luisa (left) and a close up view of the shore platform at Olhos de Água, indicating hydric erosion (right) (STOCK, 2019).

3.4 Karstification

The carbonate rocks of the southern Algarve coast are affected by strong karstification. This karstification in the study area occurred at least during two different karstogenic phases. The first before the Pliocene and the more recent, in the Quaternary. In the former event, which occurred during the Tortonian – Messinian (Upper Miocene) geologic time period, intense karstification took place due to sub-aerial weathering of the highly vulnerable carbonate rocks of the LPCF (Roberts and Plater, 1999; Moura et al., 2006a).

In the study area, particularly *Castelo* beach and the section from *Armação de Pêra* to *Albandeira* beach, sinkholes are abundant (Moura et al., 2011a). However, these fossil,

inactive dolines are free from sedimentary filling and reach down to the beach level (Forth et al., 1999) (Figure 10). When being exposed to direct wave impact, sinkholes may collapse and leave only parts behind (Figure 11). The majority of the sinkholes in the southern Algarve coast show a moderate fracture permeability, indicating water travelling through the existing fractures with a moderate speed. Due to the water's greater resistance time and hydraulic gradient, large amounts of carbonate material get removed as a result of dissolution (Forth et al., 1999).

Figure 10: Two openings of a large sinkhole in the cliffs near Albandeira beach (STOCK 2019).

Figure 11: An open carved sinkhole with cemented walls at the western end of Maria Luísa beach (STOCK 2019).

3.5 Rivulets

The hydrographical system in the southern Algarve is characterized by temporary, low drainage and highly irregular superficial outflows. Since the rivers and rivulets are barely capable of erosion and sediment placement at the shore, the Algarve coast lacks material from fluvial input and is therefore sensitive to beach erosion and longshore drifts (Ramos-Pereira et al., 2006; Martins et al., 2012).

Rivulets reaching the beach can be found at *Maria Luísa* beach and *Santa Eulália* beach, where rather small rivers temporary reach the backshore and deposit sediments (Figure 12). Another location, where rivulets play an important role, is *Armação de Pêra* bay. This is one of the few areas of accretion in the study area and is highly dependent on fluvial input from the *Alcantarilha* and *Espiche* rivers, which are opened artificially once a year (Moura et al., 2006b). This induces morphological changes on the beach slope and creates a dissipative

profile. After closure of the inlet, which may be after 2 to 14 days, the beach recovers by connecting the swash bar to the beach-face and the berm (Pinto and Teixeira, 2002).

Figure 12: Rivulet reaching the backshore of Maria Luisa beach, transporting only little amount of sediment to the shore (STOCK 2020).

3.6 Anthropogenic pressures

According to the Estatística de Instituto National (2019), 22.8 million tourists visited Portugal in 2018, which creates and enhances pressure on infrastructure at and near the coasts, and especially the southern Algarve region. For this reason, anthropogenic impacts need to be included when calculating hazard and vulnerability statistics and maps (Martins et al., 2012).

In addition to the already very high physical vulnerability in the southern Algarve region, coastal erosion is also highly affected by anthropogenic impacts such as intense tourism, industrialisation, urban growth and different kinds of land use. This region has experienced a tremendous touristic boost especially between 1966 and 1977 (Cavacao, 1997) and again since the 1980s, creating a high pressure for local infrastructure at and near the coast (Teixeira, 2006; Nunes et al., 2009; Proença et al., 2011). The following urban expansion occurred in the main tourist locations, namely *Portimão*, *Carvoeiro*, *Armação de Pêra* and *Albufeira*, where human impact increased until less than 4 km from the shoreline (Martins et al., 2012). The growth of anthropogenic pressures in the way of construction of infrastructure

(highways, buildings) and an increasing population density in the coastal zone of the Algarve intensifies the risk for both people and natural environment (Dias and Neal, 1992; Teixeira, 2006). Teixeira (2006, 2009) also hints at incidents (e.g. at *Maria Luísa*) including injuries and deaths of people due to falling cliff material as well as mass fluxes, which destroy houses, restaurants, and beach facilities.

In order to enhance protection, recovery, governance and management of the coastal zones in Portugal, an Integrated Coastal Management (ICM) has been developed since 1990. Accordingly, laws were established, linking water management, coastal management and terrestrial issues to create comprehensive strategies. However, due to multiple entities with different fields of interests, common agreements on certain procedures is often difficult (Oliveira et al., 2020).

4 METHODOLOGY

To achieve the aims of this research, various methods were applied. These include fieldwork, laboratory analysis, application of remote sensing tools, photogrammetric image analysis and the parameterization of driver mechanisms. These and specific workflows are outlined below.

4.1 Fieldwork

The fieldwork conducted for this study was split into several parts and took place along the Algarve south coast from *Olhos de Água* to *Albandeira* beach. The main purpose of the field survey was to observe the present cliff face, its geomorphological and lithological characteristics, structures and karst features. This included the identification and description of both lateral and vertical facies variation and their contact zones. In addition, rock samples were taken from each identified layer along the coast, whenever changes in lithology were detected. The samples were stored in small, labelled plastic bags for further analysis.

Moreover, the presence or absence of shore platforms as well as rivulets reaching the shore and the extent of karst features were noted to obtain knowledge concerning cliff vulnerability.

With the aim to access the quickest possible understanding of the lateral facies variation between coastal sectors, pictures were taken along the coast with both, a digital camera (Panasonic Lumix GH4) and an UAV (DJI Spark). These images target a better perception of the vertical and horizontal progress of the cliffs' layered structure. Moreover, vertical (top-down) images were taken with the UAV for photogrammetric analysis and for comparison and evaluation with results obtained from satellite image analysis.

In total, nine specific coastal sites were studied, including *Olhos de Água*, *Maria Luísa*, *Santa Eulália*, *Alemães*, *Arrifes*, *Coelha*, *Armação de Pêra* bay, *Nossa Senhora da Rocha* and *Albandeira*. However, as for constraints by national security at this time (Covid-19), some of the sites could not be accessed and were therefore described based on literature and previous research.

4.2 Laboratory Work

The performed work in the laboratory included the quantification of $CaCO_3$ content of each sample as this parameter is directly linked to mechanical rock strength (see Section 2.1.1). According to literature such as Hulsemann (1966) and Lamas et al. (2005), the most efficient method for this purpose is the determination of released CO_2 after the reaction of the sample with hydrochloric acid (HCl). This was done with a Bernard Calcimeter (Figure 13).

To start, a "zero determination" had to be done to determine a reference value for pure $CaCO_3$. To do so, the following steps were executed:

a) Uncapping both the ampoule and the Erlenmeyer;
b) In the Erlenmeyer, adding ca. 0.2 g of pure $CaCO_3$ and a small tube with 3 ml of pure HCl;
c) Moving the ampoule down and up until the liquid in the ampoule matches the level in the burette. Recording the value (L1);
d) Capping both, the ampoule and the Erlenmeyer;
e) Stirring the Erlenmeyer, so that the acid spills on calcium;
f) Moving the ampoule down and up until the liquid in the ampoule matches the level in the burette. Recording the value (L2);
g) L1- L2= "zero" or L carbonate

The same steps were performed with the samples; however, the ampoule stayed caped.

During the process, HCl reacts with $CaCO_3$. Hence, by measuring the amount of CO_2 released during the reaction, the percentage of $CaCO_3$ in the sample can be determined. With equation (1) the percentage of $CaCO_3$ in each sample could be determined.

$$\%\ of\ \mathrm{CaCO_3}\ \text{in the sample} = 100 * \frac{\text{weight of } \mathrm{CaCO_3} * \text{L sample}}{\text{weight of sample} * \text{L carbonate}} \quad (1)$$

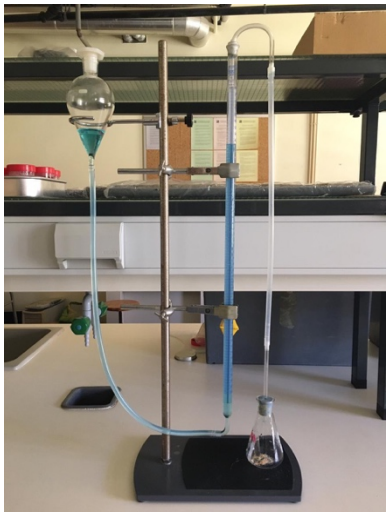

Figure 13: The used Bernard Calcimeter to conduct $CaCO_3$ content analysis (Stock, 2020).

4.3 Remote Sensing Tools

4.3.1 Satellite Data acquisition and processing

For processing of satellite images and to classify surface features (LULC) of the cliffs in the study area, the software *Sentinel Application Platform* (SNAP) version 7.0.0 was used. This software allows the processing of satellite image for multiple purposes. For this study, a classification of surface properties was executed to complement the other used methodologies and to analyse cliff conditions. In SNAP, two methods are available, the *Unsupervised Classification* and the *Supervised Classification.* Both tools develop a distinction of surface features (LULC) such as vegetation, lithology and infrastructure. The *unsupervised classification* is based on the spectral numbers of each pixel, which are being grouped accordingly, without any human intervention. For the *supervised classification* however, training data is necessary. This is obtained by locating representative samples and by creating groups of interest (Gupta, 2017).

These classification tools were chosen to test, if this method can be applied to coastal cliffs, to categorize surface features and to discover possible limitations.

The needed data from the Sentinel-2 satellite mission was downloaded from the *Copernicus Open Access Hub* website (ESA, 2020a).

To compare possible seasonal influence, Sentinel-2 MSI Level-2A satellite images from three distinct dates were selected (16.11.2019, 23.08.2019, 10.03.2020). For easier and accurate processing of images from Sentinel-2 missions, cloud coverage should be the closest to zero, which was the main factor for the image selection. The specifics of the downloaded and used data are listed in Table 1.

Table 1: Specifics of the satellite data (Sentinel-2 mission) obtained from the Copernicus Open Access Hub website that was used for the classification analysis.

Satellite	Sentinel-2B	Sentinel-2A	Sentinel-2A
Processing level	Level-2A	Level-2A	Level-2A
Instrument abbreviation	MSI	MSI	MSI
Date	2019-11-16	2019-08-23	2020-03-10
Cloud cover percentage	0.127385	0.118888	0.145209
Bands used	B2(490 nm), B3(560 nm), B4(665)	B2(490 nm), B3(560 nm), B4(665)	B2(490 nm), B3(560 nm), B4(665)

After uploading the downloaded zip-file into *SNAP*, the image was *resampled* in order to have 13 bands with the same spectral resolution (10 m) and 3 subsets were created (Subset 1: *Olhos de Água – Albufeira*; Subset 2: - *Arm. d. Pêra*; Subset 3: - *Albandeira*). Prior to the classification, each subset had to be reprojected to convert the image from UTM to Geographical Lat/Long (WGS84) (Table 2).

With these files, the *Unsupervised Classification* could be performed by applying the *K-means Cluster Analysis* tool. Processing parameters like the number of clusters, iterations, as well as the bands and ROI-masks can be adjusted beforehand as required.

Table 2: Latitude/Longitude coordinates of the chosen Subsets, where subset 1 correspond to …, Subset 2 …. And Subset 3 ….

Subdivision	Latitude (N)	Longitude (W)
Subset 1	37° 4' 4.80"- 37° 6' 35.9"	8° 10' 48"– 8° 15' 25.1"
Subset 2	37° 3' 43.2"– 37° 6' 35.9"	8° 14' 24"– 8° 21' 36"
Subset 3	37° 4' 12"– 37° 6' 35.9"	8° 21' 36"– 8° 28' 12"

This procedure provides a very rough classification of surface properties of the chosen area, which can give an idea about possible LULC or lithological differences in the studied area.

To further increase the precision of the classification, the *Supervised Classification (Maximum Likelihood Classifier (ML)* and *Random Forest Classifier (RF)* was performed. The *ML Classifier* calculates the probability for each pixel to belong to a certain class, based on the assumption, that the statistics for each class in each band is normally distributed (Richards and Jia, 2006). The *RF Classifier* uses a random sample selection based on a set of decision trees (Breiman, 2001; Niculescu et al., 2018).

In order to execute these tools, *New Vector Data Container* were necessary. By drawing multiple polygons in the chosen area, a manual classification of various LULC categories could be carried out. The *ML Classifier* tool uses the provided vector data for comparison with each pixel. This generates a detailed classification of the superficial features according to the created *Vector Data Container*. The same operation was done for the *RF Classifier*, where the same *Vector Data Container* could be used.

By exporting the results as a *KMZ*-file, the images could be uploaded into *Google Earth*, where with the help of the *transparency* tool, they could be compared to *Googles* internal data.

4.3.2 UAV Image acquisition and processing

The aim of this tool was to obtain an integrated mosaic image as well as a 3D model of the study area, captured by an UAV. For this, the cliffs between *Olhos de Água* and *Albandeira* beach were photographed in two ways, vertical (top-down) and parallel to the cliffs' face. The top-down images were used for a classification of the surface geomorphology in *SNAP*, as well as for comparison to aerial images from 2001. These were provided by the the Direção-Geral do Território (DGT) and digitalized and mosaicked by Nunes et al., (2009). In order to identify possible changes of cliff position, the two mosaics (UAV from the present study and the one from Nunes et al., (2009)) were georeferenced with the *QGIS* software and lines were drawn along the foot of the cliff.

The UAV images were taken in an altitude of 50 and 70 meters with an overlap of around 40 % for the best possible mosaicking. Due to the higher cliffs in certain parts of the study area,

the altitude had to be adjusted to up to 100 m above sea level. In order to identify vertical facies variations and to create vulnerability maps of the cliffs in the study area, horizontal images of the cliff face were taken with the UAV.

4.4 Photogrammetric Analysis using AgiSoft Metashape

For better visualization of the study area and to quantify sinkholes, the captured UAV images were further processed in *AgiSoft Metashape*. This software allows the 3-dimensional visualization of images and the creation of orthomosaics and DEMs.

For this, the UAV images from each sector were uploaded separately into the software for easier and faster processing. In the following, the steps of the tab *Workflow* were carried out. The first step was to align the images, before building a *Dense Cloud.* This tool creates points out of the information in the image, which can then be further transformed into a *Mesh.* In the next step, the *Texture* was built, which finished the 3D model.

To overview the study area, orthomosaics of the captured images were generated as well.

4.5 Parametrization and Vulnerability Evaluation

In order to develop a parametrization and vulnerability evaluation of the cliffs, the study area had to be divided into subsections, which was done according to the differences in cliff lithology. This provided six sectors (see Section 5.5, Table 6).

The parametrization of the overall cliff vulnerability in the study area was done with all the studied parameters (Table 3), their amount or extend and the according impact factor. The impact factors were assigned in order to provide a proportional impact-distribution of the parameters according to each parameter's importance concerning cliff vulnerability (weighted average).

Table 3: The used parameters for the parameterization of driving factors and vulnerability to erosion in the study area.

Lithologic features	Geomorphological features
Vertical **facies variation**	Density of **faults**
Average percentage of **$CaCO_3$**	Quantity/Extend of **karstification**
Average **layer inclination**	Distribution/extend of **notches**
	Quantity/Extend of **marine caves**
	Shoreline **exposition** to dominant **waves**
	Width of **abrasion platform**
	Width of **beaches**

In the parametrization, the "vertical facies variations" describes the number of different lithologies (layers or lithofacies) in the cliff face, the "layer inclination" expresses their geometrical behavior (dip direction), meaning upsloping (vulnerability 1), horizontal (vulnerability 2), vertical (vulnerability 3) and down-sloping (vulnerability 4).

The faults were counted with the help of geological and tectonic maps of the southern Algarve such Dias and Cabral (2002), Terrinha et al. (2006) and Cunha (2012) as well as from observation during fieldwork. The latter is also the base for the parametrization of karst features, which include ducts, caves and sinkholes. The evaluation of karst elements is based on visual comparison between the sectors. Marine caves and notches were counted in similar fashion, where field observation and UAV images were consulted.

Information regarding shore platform and beach width was taken from literature such as Moura et al. (2006a) and Moura et al. (2012b) as well as from measurements in the 3D model using *AgiSoft Metashape*.

Finally, the exposition to waves was taken from literature such as Nunes et al. (2009), Moura et al. (2011a) and Horta et al. (2013) as well as from *Google Earth*.

The number of available parameters however varied for each sector, as not every location could be sampled. Nevertheless, the parametrization provides a total vulnerability-value and a weighted average for each sector according to the classification in Table 4.

Table 4: Vulnerability classification from 1 (low risk) to 4 (very high risk) that was used to evaluate the overall vulnerability of each parameter and sector.

1	Low vulnerability
2	Moderate vulnerability
3	High vulnerability
4	Very high vulnerability

This parametrization was done without including the thickness of each lithofacies. As for possible differences in the results, particularly concerning the impact of $CaCO_3$ when including this parameter, a new table was created, in which the layer thickness was considered (Annex A).

For this, each layer was measured with the help of the images from fieldwork and the ruler tool in *AgiSoft Metashape* and converted into a percentage of the entire cliff height. With this, a weighted average of $CaCO_3$ content in the entire cliff could be calculated for each location (see Section 5.2, Table 5).

5 RESULTS

In the following Sections, the results from field work, laboratory analysis, Satellite and UAV data processing, as well as the parametrization and vulnerability evaluation are presented.

5.1 Field Work

As previously described in Section 4.1, the fieldwork was performed along the southern Algarve coast, where sections of cliffs were described and sampled, whenever changes in lithology and geometry of the layers could be detected. In addition, numerous photographs with both, a digital camera and an UAV were taken, aiming to access the quickest possible understanding of the lateral and vertical facies variation along the coast. In addition to the performed fieldwork, images from previous research and literature concerning geological profile depiction in the southern Algarve coast were used for field site descriptions and in order to identify lithological characteristics for certain locations (see Section 4.1).

Considering that variations in vertical facies and density and spacing of fractures are major factors concerning cliff instability, different lithotypes and intensity of karstification highly affect the erosional processes and need to be studied in more detail (Moura et al., 2011a). For this reason, this Section is dedicated to the description of said features of the exposed rocks in the study area, starting at *Olhos de Água* beach and continuing westwards. The study area, presented in Figure 14 extends between *Olhos de Água* and *Albandeira* and includes the distinctively studied locations *Olhos de Água*, *Maria Luísa*, *Santa Eulália*, *Alemães*, *Arrifes*, *Coelha-Galé*, *Armação de Pêra* bay, *Armação de Pêra* bay - *Albandeira* and *Albandeira*.

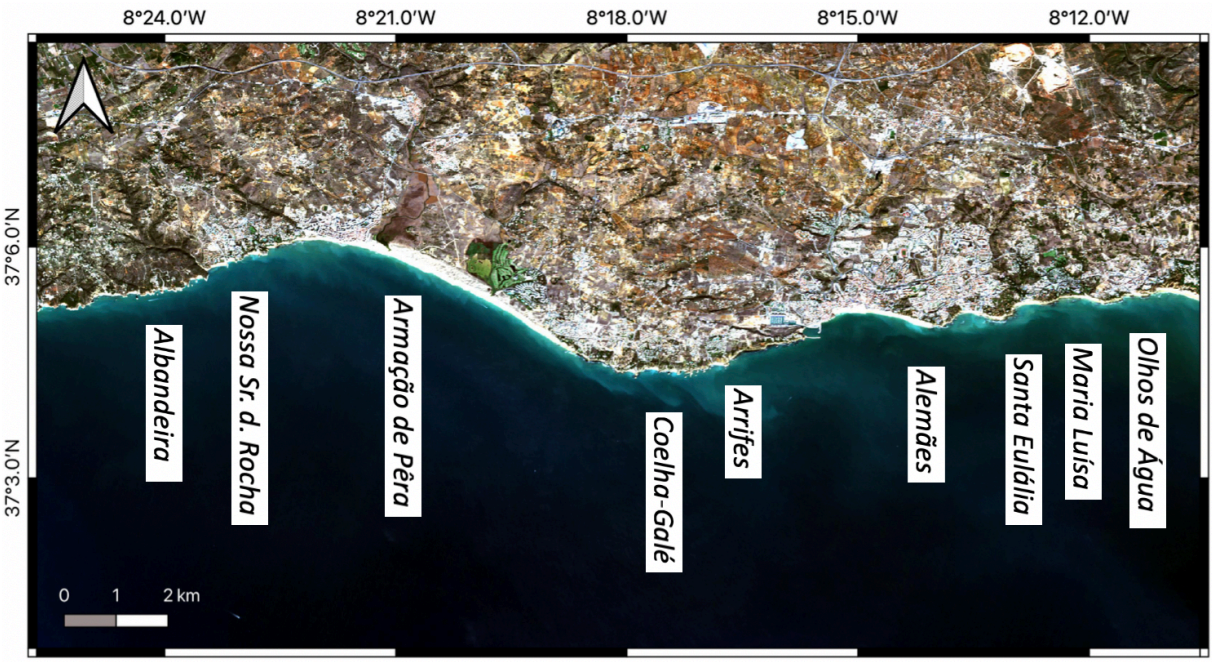

Figure 14: Resampled and reprojected Sentinel-2B MSI Level 2 RGB satellite image from 16.11.2019 of the study area, showing all locations under particular research (Stock 2020, contains Copernicus Sentinel-2 data (2019)/ESA).

5.1.1 Olhos de Água

The most eastern part of the study area are the cliffs near *Olhos de Água* as this location acts as the boundary between the western rocky and the eastern sandy cliffs (Figure 14). Here, the WSW-ENE oriented cliffs expose Miocene rocks with various lithologies. The paleorelief developed into the LPCF and is mostly filled by Plio-Pleistocene sands. These advance to yellow-reddish sediment fans, piling up in the hanging valleys and intercepting the LPCF (Figure 15).

As a result of the changing topography, the cliff height is not uniform, but ranges between +/- 5 and +/- 10 meters. The cliff profile in this section is concave in its lower part and convex in the upper part, indicating both, marine and subaerial erosion respectively (Figure 16). The latter is favored by the softer Plio- Pleistocene sediments on top and is highly important for natural beach nourishment. However, marine erosion acts on the cliff foot, carving caves and notches (Figure 16 and 17). The high cliff vulnerability is further represented by chaos of blocks, which accumulate at the cliff foot in multiple spots (Figure 16). The cliffs directly connect to a shore platform, which is only partially and at times covered by sand.

In the section of *Olhos de Água* two shore platforms can be observed, which act as a protective feature against the dominant WSW incoming waves (Figure 18). The present shore platform reaches out up to 150 m in exposed width and extends offshore up to 7 m below the current mean sea level. It is slightly SW dipping (3-5°) and strongly bioturbated, leading to the formation of a well-developed biokarst (Figure 19b) and solution ponds with accumulation of sands (Figure 19a). An older raised shore platform is preserved at the easternmost zone of this site, however suffering very rapid erosion (Moura et al., 2006a). This platform has a maximum width of 30 m and preserves large karstic holes which are mainly situated at the interception of joints. Wave-cut notches occur at the foot of the raised platform, in the junction with the current one (Figure 17).

Like in many other locations in the study area, the exposing cliffs show plenty of karst features, which are associated to active or former water circulation in between layers. These include crevices, conduits, holes and caves, surfacing in multiple lithofacies and at the base of the cliff, whenever layers are less permeable. Various cemented cliff faces with lines of incomplete conic sections at *Olhos de Água* indicate a high abundance of former sinkholes, which collapsed as a result of instability and erosional driver.

Additionally, multiple fresh-water springs can be detected in this section, especially emerging in the current shore platform, leading to the formation of solution ponds (chemokarst).

Figure 15: Sediment fan from Plio- Pleistocene deposits in the Paleovalley, advancing downwards from the cliff and intercepting the beach and the LPCF (STOCK, 2019).

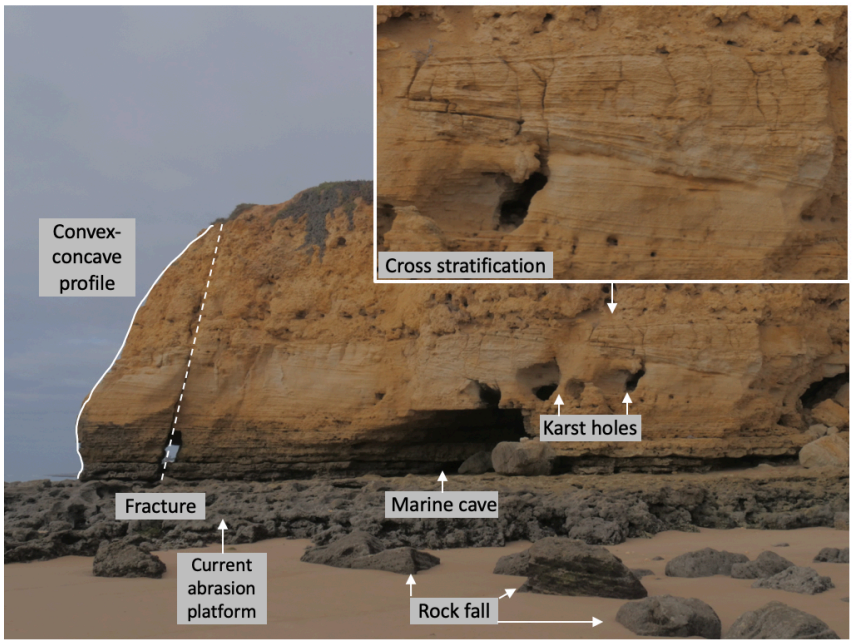

Figure 16: Convex-Concave cliff profile at Olhos de Água with indicators of rock fall, marine caves, fractures and cross stratification (STOCK, 2019).

Figure 17: Wave cut notch in the junction of the cliff with the current shore platform during low tide at Olhos de Água (STOCK, 2019).

Figure 18: The raised and current shore platform at Olhos de Água during low tide (STOCK, 2019).

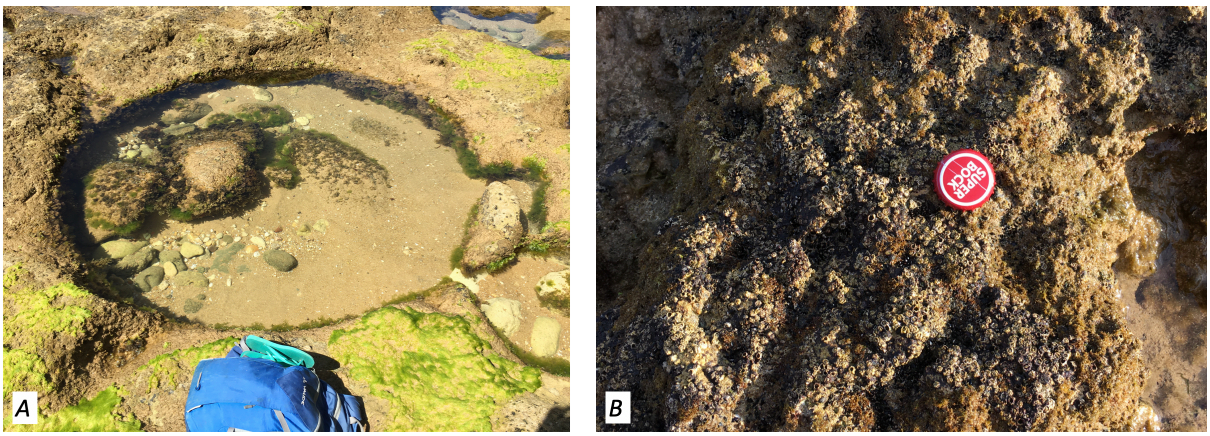

Figure 19: Images of the current shore platform at different locations at Olhos de Água. The left image (A) presents a solution pond, which derived from hydric erosion with sand accumulation. The right image (B) shows features deriving from bioerosion (STOCK, 2020).

The vertical facies variation of the cliffs of *Olhos de Água* is quite low with only 3 distinct lithofacies (Figure 20).

The bottom layer OA-A is a biocalcarenite and varies in its thickness along the section, but averages in +/- 2 m visible thickness. In its base, the shore platform is carved. This massive fossiliferous layer does not display any internal structure, organization or sedimentary structures but contains a high density of fossil shells, such as oysters, fragments of divert mollusks and barnacles (Figure 21). The contact between this layer OA-A and the overlaying Layer OA-B is of an erosive type, which may promote fragility, rock fall, and favor the water circulation.

Layer OA-B is a calcarenite of around 2,55 m thickness and displays beach typical cross lamination (Figure 20). In between the non-fossiliferous calcarenite layer and the harder carbonate horizon in this lithofacies, a siltstone bed can be detected. The contact zone to layer OA-C is erosive.

Due to changes in the topographic surface, the top layer OA-C strongly varies in its apparent thickness and consists of biocalcarenite lithology with a high abundance of sea urchin fossils (Figure 22).

As a result of erosional processes and interceptions by the topographic surface westwards of this section, layer OA-C is partially inexistent, whereas layer OA-B gains thickness. On the

contrary, this scenario flips on the eastward side, where layer OA-B loses its apparent thickness and layer OA-C is more developed.

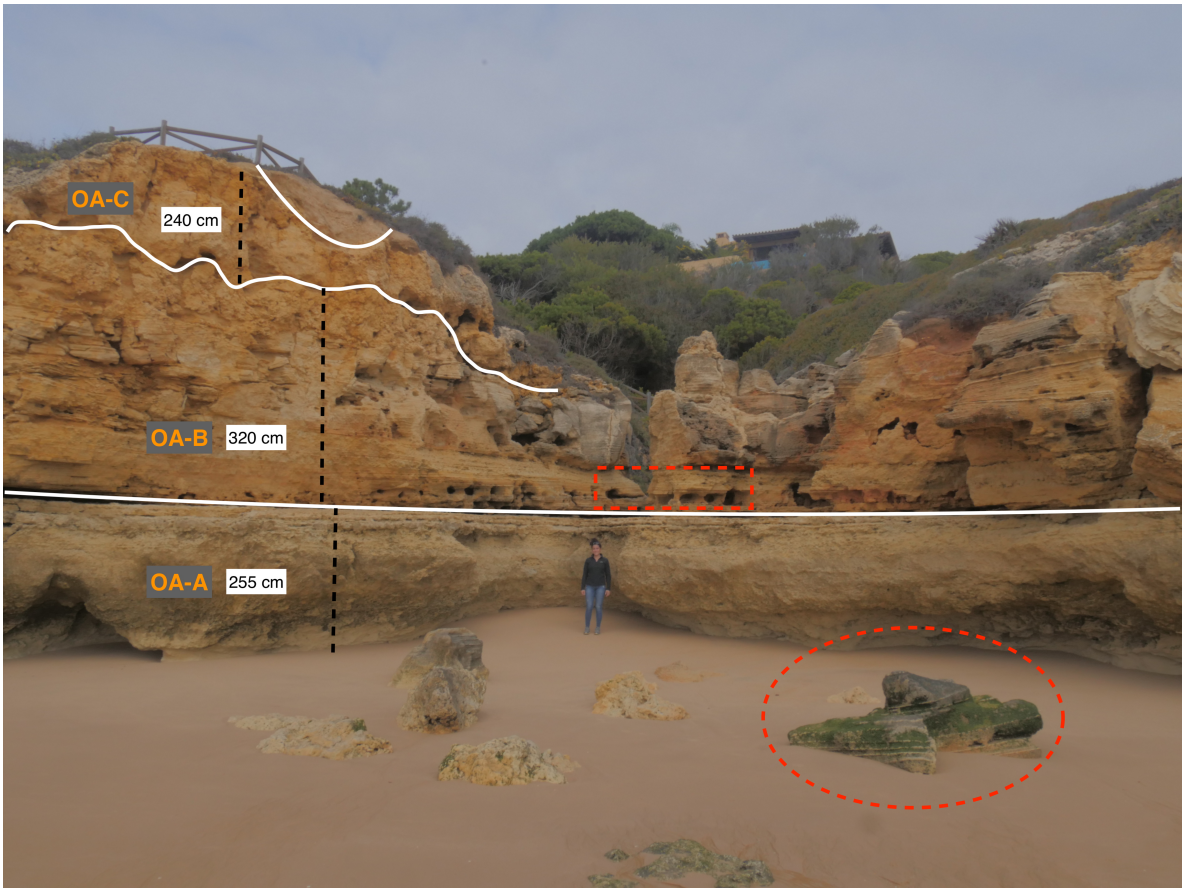

Figure 20: Cliff profile of Olhos de Água showing lithofacies, layer thickness, karst features (red squared) and elements of rockfall (red circled) (STOCK, 2019).

Figure 21: Fossil rich lithofacies OA-A with multiple sea urchins (STOCK, 2020).

Figure 22: Biocalcarenite top- layer OA-C with high abundance of sea urchins (STOCK, 2019).

The cliffs of *Olhos de Água* appear in varying morphological conditions throughout this section. Some cliffs are highly affected by karst processes and rock fall, which erodes parts of the cliff face and hence changes its appearance (Figure 23). On the contrary, Figure 24 shows a relatively smooth cliff face and karst features only appear in the top layer. Marine caves and notches can be observed almost in the entire section.

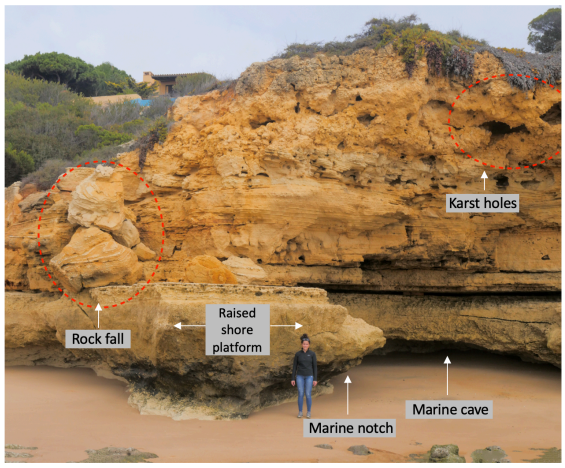

Figure 23: Cliff face of Olhos de Água with multiple features that affect its appearance (STOCK, 2019).

Figure 24: Cliff face of Olhos de Água with karst features in the upper layer and thin lithofacies and marince caves in the lower part (Moura, 2019).

5.1.2 Maria Luísa

Further to the west from *Olhos de Água*, *Maria Luísa* beach is located (Figure 14). This NW-SE orientated section is directly exposed to the main swell direction and tectonically controlled, resulting in faults and changing lithology with mainly cemented detrital and partially lumashell-rich carbonate rocks. On top of the cliff, accumulation of Pliocene and Pleistocene sands fill the paleo-relief of the Miocene formation and add to an already high vulnerability of this cliff (Teixeira, 2009; Moura et al., 2011a; Bezerra et al., 2011). Due to a varying topography, the cliff height alters but averages in about 15 meters with the highest cliffs up to 30 m. The predominant cliff profile is convex, promoting landslides and indicating prevailing aerial erosion. However, multiple marine caves developed at the foot of the cliff, signifying wave impact as an additional marine erosional process (Figure 25). In contrast to the quite obvious erosional processes of rock fall at the previous location, the cliff retreat of the sandier cliffs (Plio- Pleistocene material) of *Maria Luísa* beach occurs through mass fluxes

and is therefore relatively discreet. The cliff is directly connected to the current shore platform, which is largely covered by sand. These sediments derive from offshore, the surrounding cliffs and from Plio- Pleistocene mass fluxes.

There are two shore platforms present, where the raised platform is reached by waves during high tide (Moura et al., 2006a). In various parts of this section, the raised shore platform shows a wave cut notch in the junction of the current platform (Figure 26). The current shore platform reaches out to a similar extend as at the previous location (+/- 150 m) and its visibility is dependent on the marine climate and sand availability.

Karst features are widely distributed throughout this section, where mainly holes and conduits accumulate at the base and in the upper part of the cliff. Here, holes and crevices are affected by wave impact, leading to high cliff instability. Often, parts of the cliffs are entirely disturbed by dissolution as a result of intense karstification. Another indicator of strong karstification is clay transport through karstic ducts, surfacing and depositing in layer-contact zones (Figure 27).

Figure 25: Marine cave developed at the foot of the cliff at Maria Luísa beach, supported by the presence of a discontinuity (STOCK, 2019).

Figure 26: Wave cut notch in junction with the current platform (covered by sand) at Maria Luísa (STOCK, 2020).

Figure 27: Surfacing of clay in the layer contact zones through karstic ducts (STOCK, 2020).

The vertical facies variation shows 7 different lithotypes plus a clay intrusion, which cannot all be presented in one figure, as their geometric relation is quite complex, and their contacts obliterated along the cliff profile. The detected layers are labeled increasing with cliff height and distance to the west. Layers ML-A, -B, -C and -D are shown in Figure 28. Lithotypes ML-D and -E are presented in Figure 29, ML-E and -F are shown in Figure 30 and ML-G in Figure 31.

Layer ML-A of the cliffs in the section of *Maria Luísa* beach is a biocalcarenite and varies in +/- 3 m thickness. In this highly fossiliferous layer, there is no internal structure noticeable, but just like in OA-A, a high abundance of oysters, fragments of mollusks and barnacles can be found.

After this fossiliferous, non-layered block, a very thin (+/- 1 m), and partially discontinuous laminated sandstone layer ML-B can be identified. The numerous changes in thickness of this layer implies a mostly tangential behavior of layer ML-A and ML-C and is the result of intersections in the topographic surface and faults.

Layer ML-C is of biocalcarenite lithology, with a high abundance of sea urchins and a strongly varying thickness due to variations in the topographic surface.

The vertical position of the biocalcarenite layer ML-D varies along this section and represents a former high energetic environment with calcarenite fragments of past cliffs or shore platforms (Figure 32a) as well as remobilized and chaotic distributed fossils like barnacles (Figure 32b).

Lithotype ML-E consists of Plio- Pleistocene, reddish coarse sands with pebbles and cross stratification. In the most western part of this section, where the lithology is mainly detrital (sand) with only a few carbonate rocks in the bottom of the cliff, layer ML-F is defined by laminated siltstone.

Layer ML-G is of calcarenite lithology and is located below the top layer ML-H. This layer consists of a very stratified sandstone.

Figure 28: Lithofacies variation at Maria Luísa beach, showing layers ML-A, -B, -C, -D as well as karst features (STOCK, 2019).

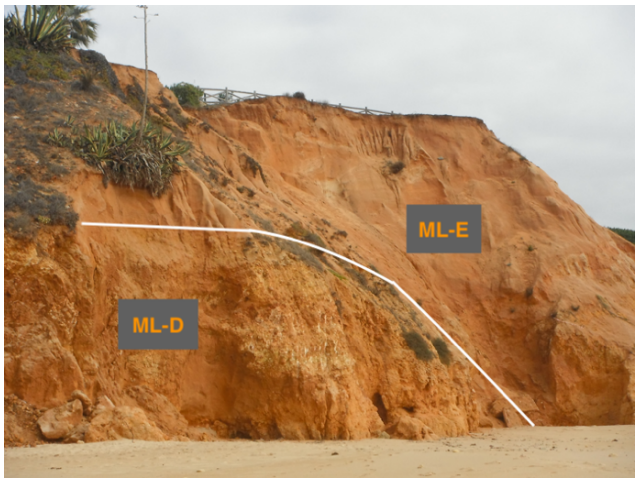

Figure 29: Lithofacies ML-D and -E (MOURA, 2019).

Figure 30: Lithofacies ML-E and -F (MOURA, 2019)

Figure 31: Lithofacies ML-G at the most western part of the beach (MOURA, 2019).

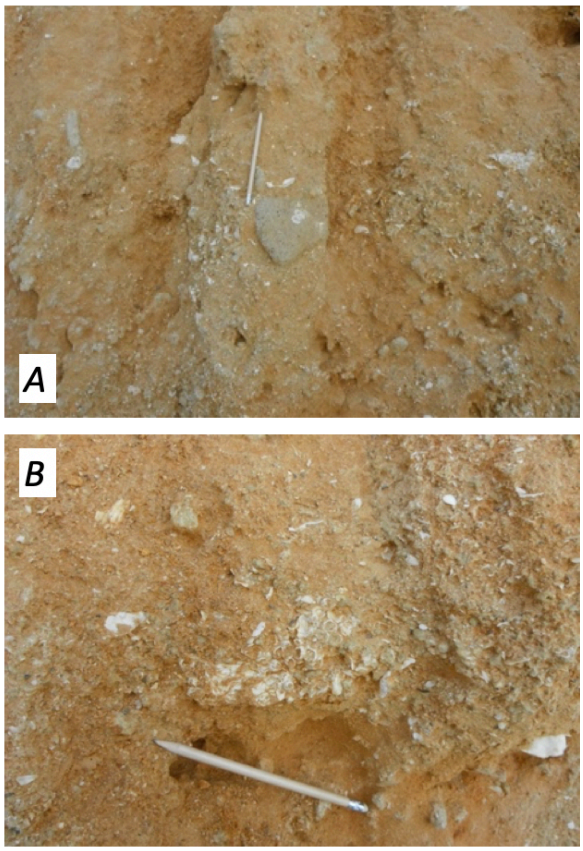

Figure 32: Lithotype ML-D with rock particles (A) and fragments of fossils e.g. barnacles (B) (MOURA, 2019).

5.1.3 Santa Eulália

To the west of *Maria Luísa* beach, the SE exposed beach of *Santa Eulália* is situated (Figure 14). This area is tectonically controlled, suggesting a fault-regulated geometry with high structural disturbance (Moura et al., 2006a). Similar to previous sites, Plio- Pleistocene sediments fill paleo-valleys from the top of the cliff (Figure 33). Furthermore, the visibility of features throughout the cliffs at and near *Santa Eulália* beach change due to varying topography. As a result of variations in the topographic surface, whole layers or parts of the cliff can be covered by sand, which is, however, subject to temporal limitation depending on sand availability. The height of the cliffs in this section averages in around 5 m.

The cliff profile is mainly convex, indicating high pressure from aerial erosion, which is also reflected in the formation of channels, cutting through Plio- Pleistocene sediments in the top part of the cliff (Figure 33). The profile of the cliffs at the eastern and western limits of the beach follow an almost vertical angle.

Evidence of rock fall or mass fluxes could not be observed during the time of the fieldwork. Mainly as a result of energetic events, sand is frequently being transported to the cliff foot, where it may cover rock fall or sediment slides.

Shore platforms can only be detected at the cliffs between *Maria Luisa* beach and *Santa Eulália* beach, where the cliff foot is directly connected to it. Apart from this, sand covers the platform and is in junction with the base of the cliff.

The intense karstification in the study area is particularly visible in the upper part of the cliffs at *Santa Eulália*, where crevices and conduits are abundant. Nevertheless, karstification also promotes instability in certain lithofacies like layer SE-B (Figure 34).

Unlike cliff profiles from previous observation in the study area such as those at *Olhos de Água*, the geometric relationship of the layers in *Santa Eulália* is more complex. The contact between the layers is erosive and thus follows an irregular geometry, resulting in a variation of thickness in each layer. This erosive contact zone can be observed between layer SE-A and SE-B, shown in Figure 35. Due to collapses of parts of the cliffs, the individualization of the layers is more complicated compared to previous locations. As it can be seen in Figure 34, layer SE-B cannot be entirely identified throughout this section, as it partially collapsed. Yet, 4 different lithological facies can be detected (Figure 33 and 36).

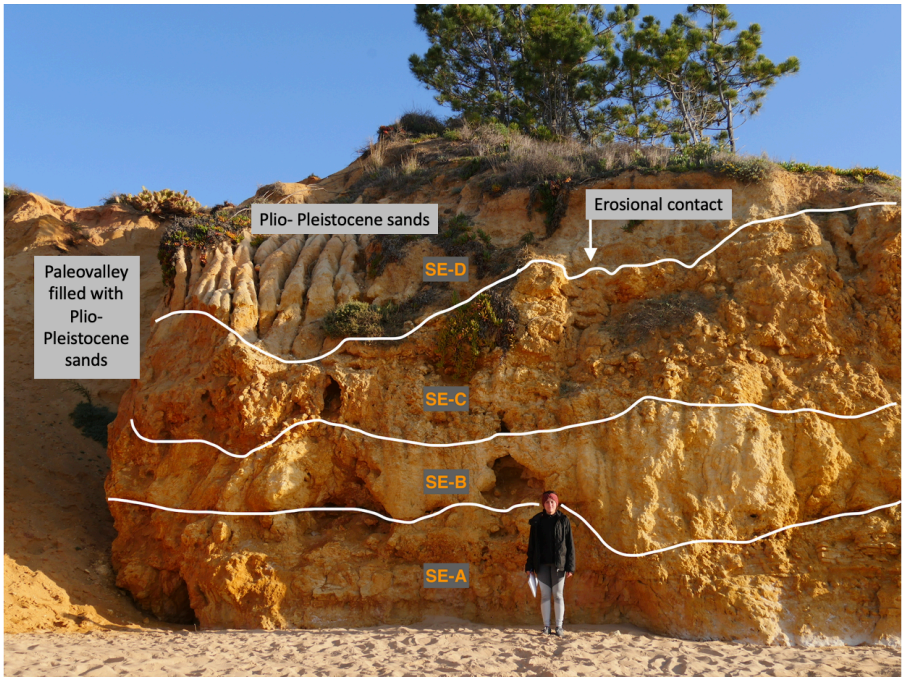

Figure 33: Cliff characteristics at Santa Eulália beach, where Plio- Pleistocene sediments are situated on the top and erosional contacts between layers (STOCK, 2019).

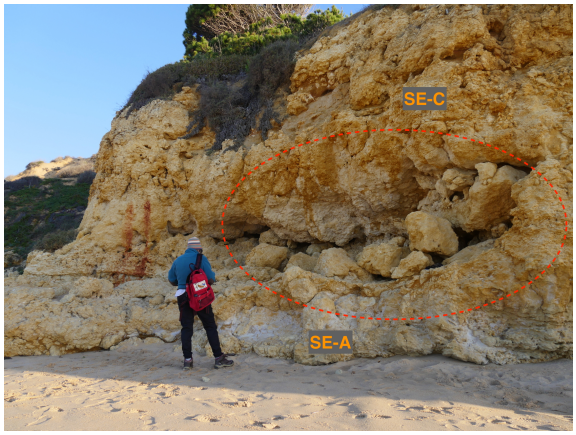

Figure 34: Collapsed parts of layer SE-B (red circled) at Santa Eulália beach (STOCK, 2019).

Figure 35: Example of irregular contact zone between layer SE-A and SE-B at Santa Eulália beach (STOCK, 2019).

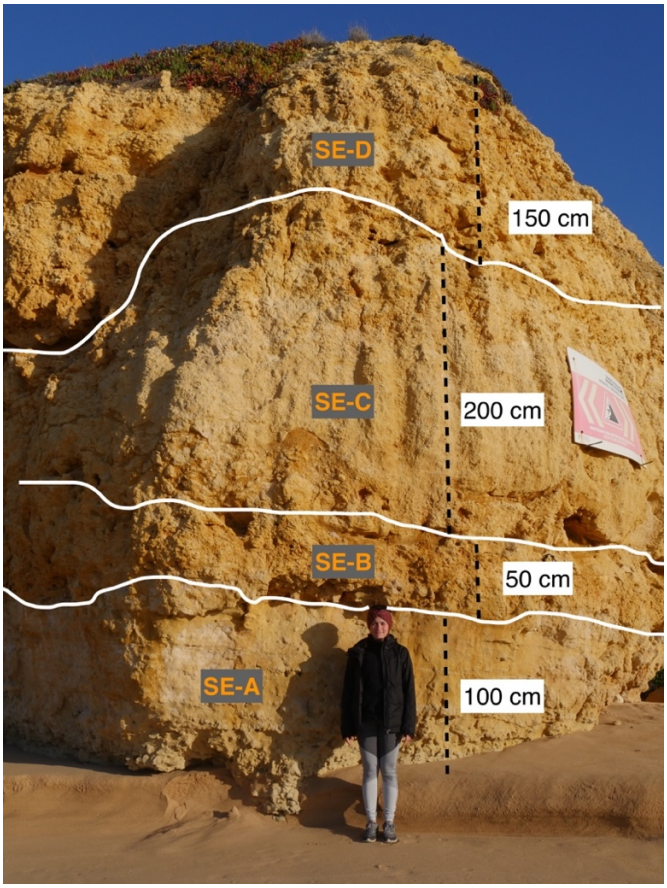

Figure 36: Lithofacies variation at a cliff at Santa Eulália beach, showing the stratified layer SE-A, the fossil- rich layer SE-B, layer SE-C from the LPCF and the strongly disturbed top- layer SE-D (STOCK, 2019).

The bottom layer SE-A (+/- 1 m) of the cliffs of *Santa Eulália* beach is the only one being stratified in this section. It contains a large amount of detrital sediments and is partially truncated by layer SE-B (+/- 0,5 m), which shows the erosional contact between the layers in

the section. Layer SE-B is more fossiliferous and includes shells and pathways of former living fauna (paleochannels). The most important remobilized fossils in this layer are sea urchins, indicating former high removal and transport energies.

Like the previous layers SE-A and SE-B, lithotype SE-C belongs to the LPCF from the Miocene epoch and averages in +/- 2 m thickness. Material and formations of lithofacies SE-D are of detrital sediments and are separated by a highly erosional contact zone to the lower layer SE-C. Due to different iron content in this +/- 1,5 m thick layer and the resulting oxidation process, as well as different levels of karstification, layer SE-D is highly disturbed by dissolution and is separated into two parts (disturbed calcarenite and overlaying Plio-Pleistocene sands) but can be classified as the same facies.

5.1.1 Alemães

In the next westward section of the study area, the NW-SE orientated beach of *Alemães* is located and is connected to *Santa Eulália* beach by a cliff (Figure 14). At the eastward end of the beach, where calcarenite sediments are the main type of limestone deposits, a groin was built to keep sediments at the beach and to reconnect the cliff to the stack in order to rebuild the headland (Figure 37).

At this location, Plio- Pleistocene sands can only be observed in the uppermost part of the cliff, where they overlay the top carbonated lithofacies. The topography of this section is highly variable, resulting in an alternation of small valleys and hills (Figure 38). The cliffs average in around 14 m in height.

The cliffs between *Alemães* beach and *Santa Eulália* beach are highly affected by marine erosion, where wave impact undercuts large parts of the cliff, forming a landwards carved notch. This concave profile in the base of the cliff presents a high vulnerability for the overlaying and unsupported material to collapse. As a result, accumulation of material from rock fall can be observed at the foot of the cliffs throughout the entire stretch (Figure 38).

In this part, the raised shore platform shows an unprecedented extend and a landward carved formation (Figure 38).

On the contrary to the previous locations, the cliffs near *Alemães* beach show only very little number of karst features. At the raised platform however, numerous sinkholes, which are mostly partially collapsed, can be observed.

Figure 37: Groin at the eastward end of Alemães beach to prevent sediments from following the longshore drift and thus promoting accretion at the beach (STOCK, 2020).

Figure 38: The landward carved cliffs and platform between Santa Eulália and Alemães beach showing the vertical facies variation, with piles of fallen rocks and plenty of marine caves (STOCK, 2020).

In this section of *Alemães* beach, 3 vertical facies of different lithotypes can be detected (Figure 38).

Layer A-A is very fossiliferous with a high abundance of fossilized sea urchins and can be identified as the continuation of layer SE-B. The present sea urchins in Layer A-A are larger and more conserved compared to other parts of the study area (Figure 39a). Additionally, pectens are widely spread in this more or less 7,5 m thick part of the cliff profile (Figure 39b).

Above layer A-A, a ca. 4 m thick siltstone layer A-B1 can be detected, which is presented in Figure 40a. The top layer A-B2, shown in Figure 40b, can be associated to one or multiple storm or even tsunami events, as this layer includes shells, sea urchins, barnacles, pectens, round quartz pebbles from small to large as well as lumashells. Its thickness is about 1.5 m.

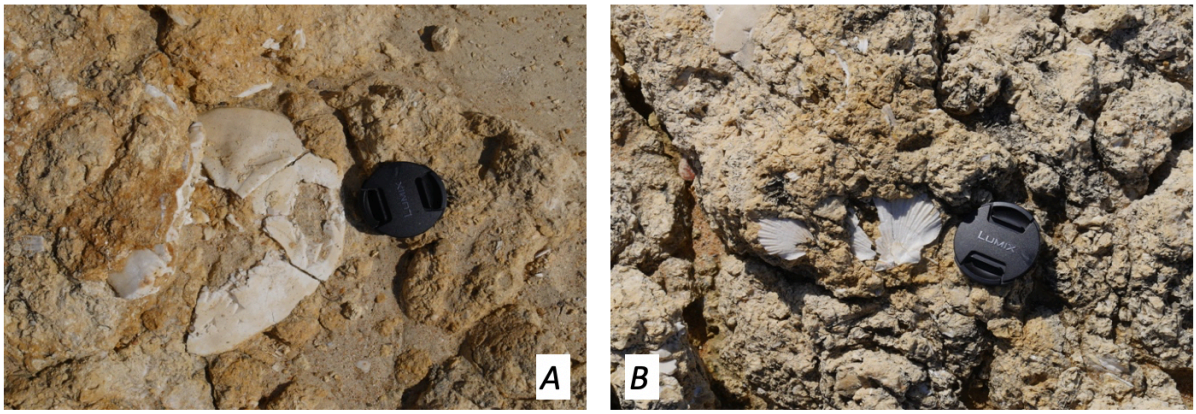

Figure 39: Well preserved sea urchins (A) and high abundance of pectens (B) in lithofacies A-A at Alemães beach (STOCK, 2020).

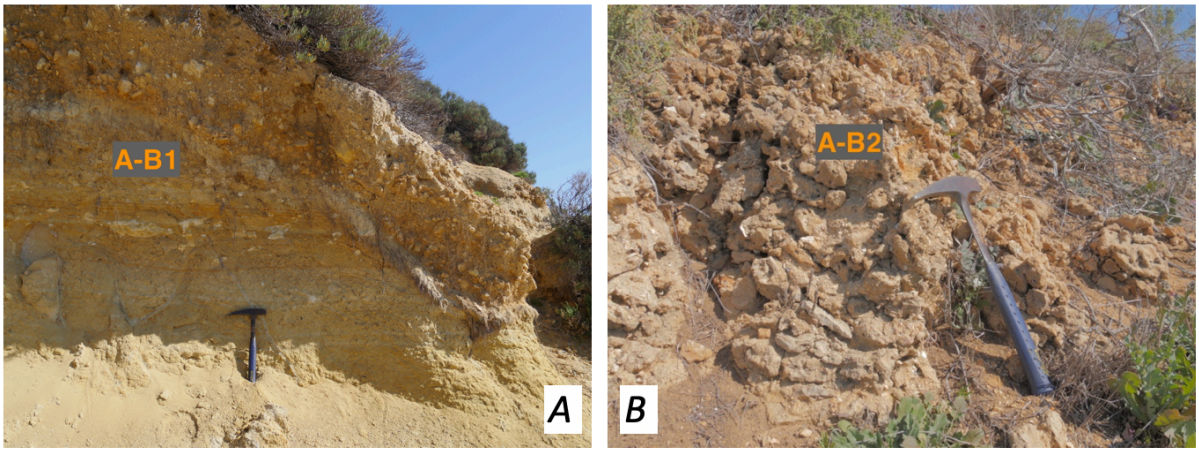

Figure 40: Siltstone layer A-B1 (A) and storm or even tsunami depositions A-B2 (B) at the cliffs of Alemães beach (STOCK, 2020).

5.1.2 Arrifes

From *Alemães beach*, the following westward section of *Arrifes* is the only lithological different region from all the studied locations in the study area (Figure 14). Here, Cretaceous and Jurassic cliffs are exposed at the SW-NE orientated coast and intercept the LPCF. Due to tectonic movements during halokinesis of the *Albufeira* diapir, the rocks are folded and vertically disposed (Figure 41). These vertical layers of Jurassic limestone, with an inclination of up to 30°, are mainly Cretaceous marls and clay-stones. Into these softer and fractured claystone formations, caves are shaped (Moura et al., 2011a). According to Moura et al., 2011a) the faults may be the reason for the relatively straight coastline in this section. Due to its SE exposition, *Arrifes* beach is protected from the main swell direction.

Figure 41: Vertically displaced cliffs of Cetaceous marls and claystones at Arrifes beach (MOURA, 2019).

5.1.3 Coelha - Galé

The coastal stretch to the west from *Arrifes* beach, that includes *Coelha*, *Castelo*, *Evaristo*, *Manuel Lourenço* and *Galé* beach, is highly crenulated with plenty of pocket beaches which are embayed by headlands and shore platforms (Figure 14) (Moura et al., 2011a; Horta et al., 2013; Oliveira et al., 2019). The exposition of this section is split, where *Galé* beach and

Evaristo beach are NW-SE orientated and therefore directly exposed to the main swell direction. *Castelo* beach and *Coelha* beach are exposed to the south, however, *Castelo* beach is more affected by the W-SW swells, whereas *Coelha* beach is sheltered by the dividing headland (Horta et al., 2013). Nevertheless, the entire section is affected by marine erosion, when swells from E-SE hit the S and SE exposed beaches without any protection. This is represented by multiple marine caves at the base of the cliff. The cliffs mainly exhibit an almost vertical profile with slight down-sloping tendencies, meaning aerial and marine erosion are more or less in equilibrium (Figure 42). The cliffs in the back of the beaches exhibit a rather convex profile, indicating high impact of aerial erosion. The presence of marine caves and the steep profiles increases cliff vulnerability, resulting in cliff collapse and rock fall (Figure 42). With +/- 14 m, the cliffs in the area of *Coelha* beach are among the highest in the study area.

Shore platforms can be observed at the cliffs' foot and at the ocean-facing tips of cliff-stacks.

Concerning karst features, plenty of holes and conduits are well developed in the base and the top part of the cliff. Additionally, lithofacies of siltstone show both, marine and structural notches in the bottom and the middle and upper part respectively (Figure 42). As already mentioned, this section is highly affected by the abundance of sinkholes. Only at *Castelo* beach, studies from Oliveira et al. (2019) count 26 sinkholes with an average depth of 5,47 m in an area of +/- 22 km^2, primarily situated in a maximum distance of 10 m from the coastline. Some of these features are filled by Plio- Pleistocene sediments, others are open and constantly washed out by waves. This intense karstification decreases cliff stability and promotes rock fall.

The cliff face of *Coelha* beach shows 9 different vertical lithofacies (Figure 42). The lowest lithofacies C-A is only partially visible and consists of fossiliferous limestone (Moura, 2011a). Above, 3 siltstone layers (C-B, C-D, C-F) are alternating with light-yellow limestones (C-C, C-E). The lithofacies C-G is rich in fossils like *Celleporaria palmata* (Bryozoas) and parts of the coral *Culizia parasitica* (Pais et al., 2012). Between this layer and the top lithofacies C-I, another siltstone layer C-H is situated.

At *Galé* beach, research from Forst et al. (2000) suggest 3 different horizontally bedded lithofacies. According to this, the lowest layer G-A consists of a +/- 3,4 m thick limestone

(Rudstone) with a high abundance of rhodolites at the base and higher sand contents as well as foraminifera and bivalves in the upper part.

Layer G-B is +/- 4 m thick fossiliferous sandstone with strong bioturbation, plenty of bivalve shells and gastropod imprints in its lower part. This unit contains a condensed layer of around +/- 0,4 m thickness full of flat domed sea urchins (*Clypeasteroida*).

On top, layer G-C, a gray sandy rudstone (+/- 0,4 m thickness) is situated and separated by an erosive contact to the previous lithofacies. This top layer contains oysters, pectens, and parts of sea urchins (Terrinha et al., 2006; Pais et al., 2012).

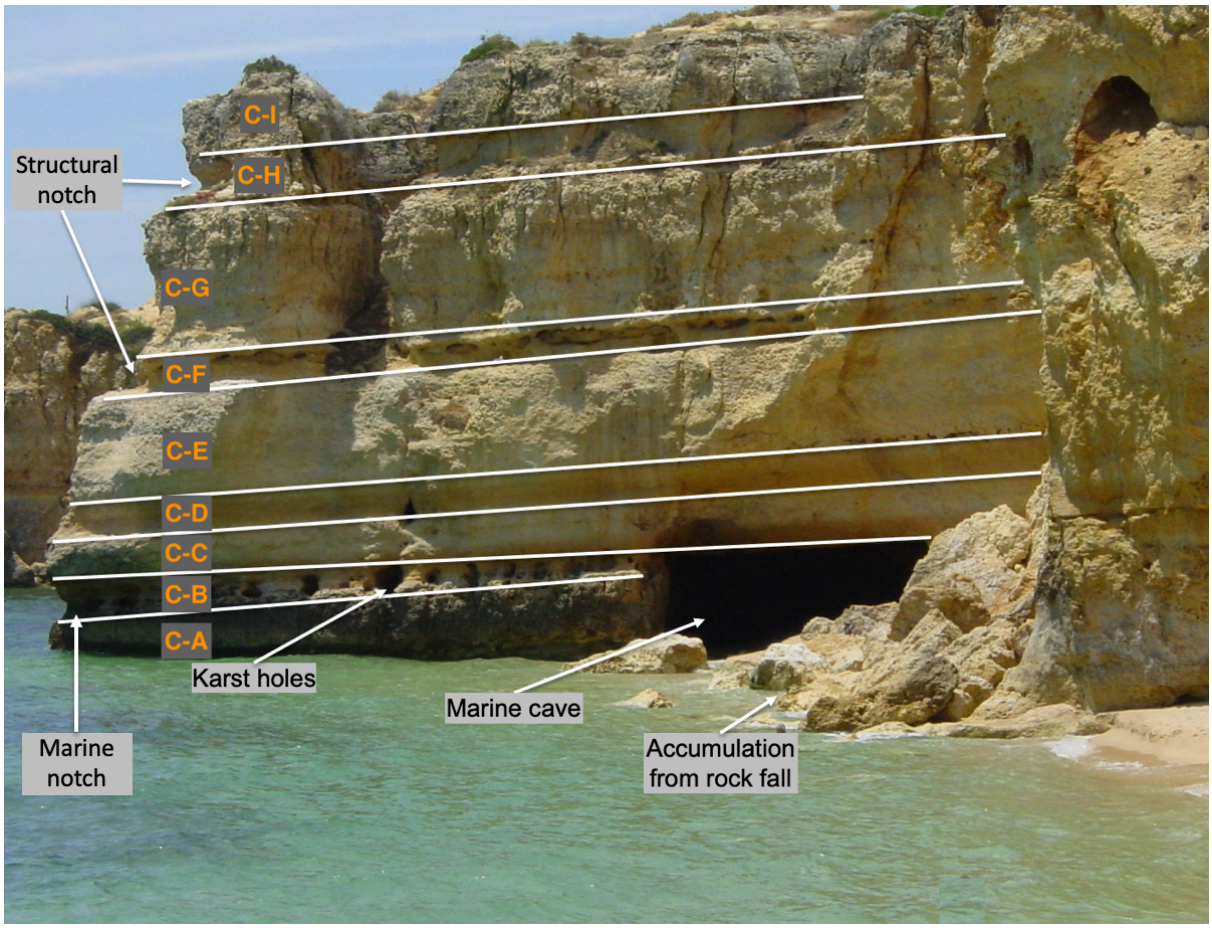

Figure 42: Lithofacies variation of a cliff at Coelha beach, showing 9 different vertical lithofacies, marine caves, wave cut and structural notches, accumulation of material from rock fall at the foot, as well as karst features (MOURA, 2019).

5.1.4 Armação de Pêra Bay

The zeta shaped *Armação de Pêra* bay is located westwards of *Galé* beach and is constraint by horizontally bedded Miocene calcarenite outcrops (Figure 14 and 43). This coastal sector

is NW-SE orientated and therefore highly impacted by the main swell direction (W-SW). According to studies from Moura et al. (2006b), a well-cemented beachrock formation is exposed in the shoreface and in the backshore, where aeolianite formations crop out. Aeolianites and beachrock developed as a result of sandy dune cementation by carbonates and are often covered by younger free dunes (Vousdoukas et al., 2007; Davis, 2013).

The *Armação de Pêra Bay* is highly dependent on fluvial sediment inputs through rivers. As described in Section 3.5 both, the *Alcantarilha* and *Espiche* rivers intercept the paleokarst in the backshore before draining to the beach, where they are responsible for the beach evolution. However, nowadays the rivers don't reach the shore through their natural bed. In fact the river mouth is artificially opened several times a year to support sediment inputs (Dias, 1988; Moura et al., 2006b).

Figure 43: View over Armação de Pêra bay towards west (STOCK, 2020).

5.1.5 Armação de Pêra bay - Albandeira

The section from *Armação de Pêra Bay* to *Albandeira* beach is heavily crenulated with pocket beaches, which are embayed by steep and high cliffs, forming headlands and bays (Figure 14 and 44). The mainly SW-NE orientated cliffs are moderately protected from the main swell direction.

The exposing rocks are limestones, calcarenites or siltstones of the LPCF and are less fossilized compared to other sectors. The cliffs are in average +/- 17 m high with some ranging up to 20 m and are subject to marine erosion, forming marine caves at the junction with the beach. This reduces the stability and promotes rockfall, building up rock piles at the foot of the cliff (Figure 45).

Owing to the presence of pocket beaches, shore platforms are covered by sand or are submerged.

The cliffs show multiple siltstone layers with structural notches and karst is again abundant, where holes and conduits can be observed throughout the entire cliff face.

When studying the cliffs of *Senhora da Rocha* beach, which are situated halfway between *Armação de Pêra and Albandeira*, 9 different horizontal lithofacies can be detected. Multiple siltstone layers form structural notches in the lower and upper part of the cliff (Figure 46).

Figure 44: View from Albandeira to Armação de Pêra, where pocket beaches and headlands build the coastline. (STOCK, 2020).

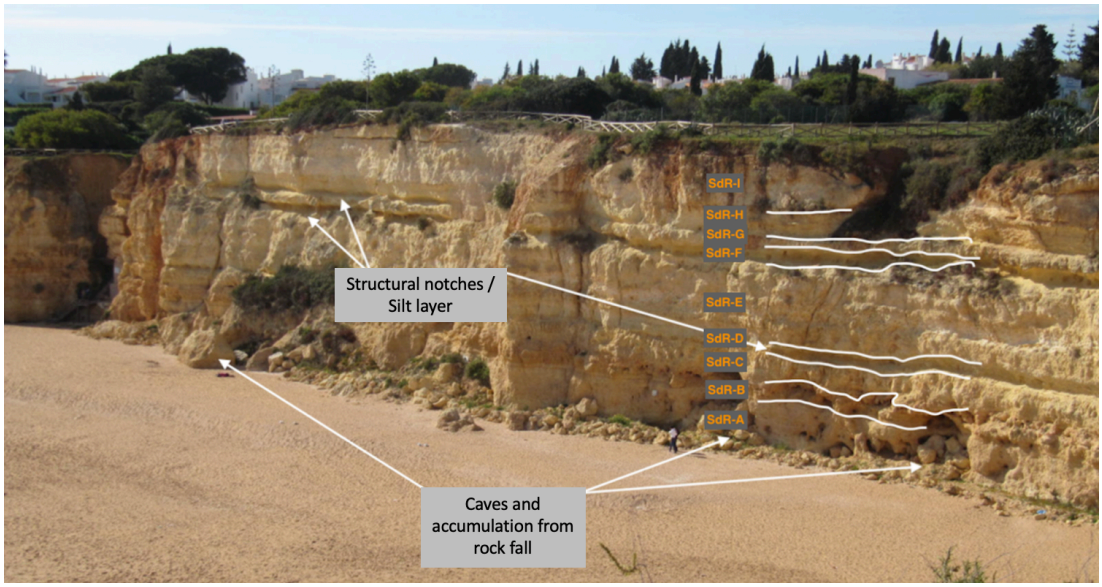

Figure 45: Cliff at Nossa Senhora da Rocha beach, showing 9 vertical facies variation, marine caves, structural notches, accumulation of rocks at the base, as well as karst features (MOURA, 2019).

Figure 46: Structural notches in the cliff of Nossa Senhora da Rocha beach (MOURA, 2019).

5.1.6 Albandeira

The SW-NE orientated cliffs of *Albandeira* Beach (Figure 14) are very similar to the previous site (Nossa *Senhora da Rocha*), showing headlands and pocket beaches. The topography also

continues in similar fashion as the previous location, with cliff heights between 14 and 21 m. The cliffs show a very straight profile with plenty of undercuts and marine caves, indicating prevailing marine erosion (Figure 47). Accumulation of rocks at the base of the cliff point to rock fall events and signify high vulnerability (Figure 48).

Equal to the previous location *Senhora da Rocha*, shore platforms are covered by sand or are submerged.

Karst features like holes and ducts can be detected in the cliff face and mainly accumulate in the upper middle and lower part of cliff (Figure 48). Large sinkholes, connecting the ocean to the littoral platform, are outstanding characteristics of this coastal stretch and increase cliff instability (Section 3.4) (Oliveira et al., 2019).

Moreover, the identification of siltstone layers along the cliff profile is a good way to detect the position of the observer and to confirm the layering structure. Additionally, the thickness and location of these lithofacies are extremely important due to their direct link to rockfall events (see Section 6.1.1).

Figure 47: The steep cliffs near Albandeira beach with headlands and pocket beaches (STOCK, 2020).

The vertical facies variations of the cliffs at *Albandeira* beach show 8 different lithotypes (Figure 48).

The bottom layer AL-A mainly consists of rhodolites (Figure 49). This lithified concentric red algae can be associated to former warm water reefs, where it accumulates after dying and now acts as a reference level for comparison of vertical facies variations to other field sites such as *Galé* beach.

The next overlaying layer AL-B is separated by an erosive contact to layer AL-A. This horizontal layer varies in its thickness but is with +/- 1,5 m relatively thin overall. It is highly shelly and fossiliferous (lumashell) mainly with pectens and large oysters (Figure 50).

Layer AL-C consists of brownish and less fossiliferous rock and averages in +/- 1,55 m thickness.

The next two lithotypes AL-D and AL-E are of a high similarity and measure around 2,35 m and 1,6 m respectively. Both are light yellow colored and are separated by a thin horizontal layer, full of karstic conduits. From this layer upwards, a layer of soil, AL-F, is situated and averages in about 1,5 m thickness.

Above that, bioturbation seems to have acted on the very thin (+/- 0,45 m) siltstone layer AL-G, causing a very saturated yellow color. The last layer AL-H is with +/- 1,55 m relatively thick and just like lithotype AL-F, consists of highly stratified, lithified soil.

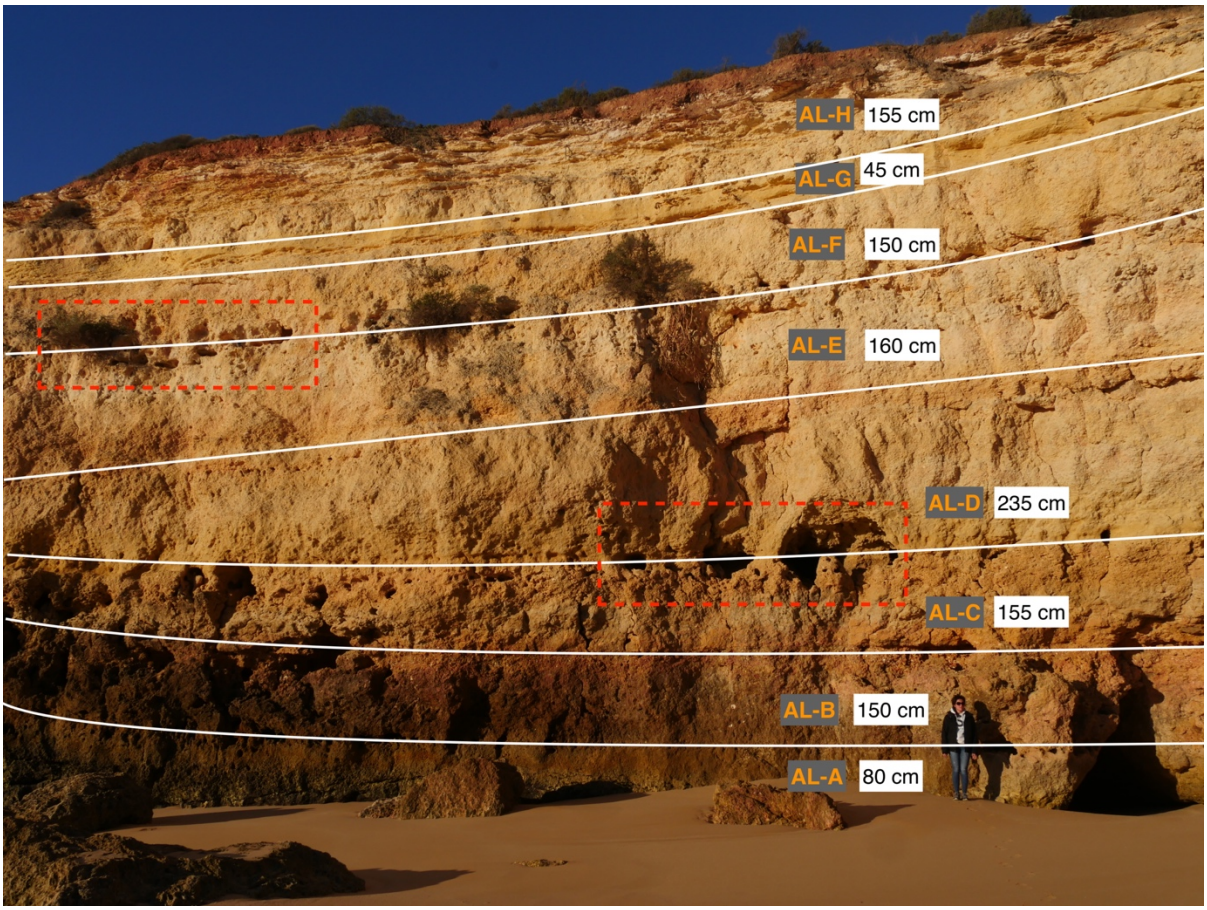

Figure 48: Lithofacies variation, evidence of rock fall events at the foot of the cliff and karst features (red squared) at the cliff at Albandeira beach (STOCK, 2020).

Figure 49: Layer AL-A with a high abundance of Rhodolites (STOCK, 2020).

Figure 50: The highly fossiliferous and shelly layer AL-B at Albandeira beach (STOCK, 2020).

5.2 Laboratory Work – $CaCO_3$ Content Analysis

The samples collected during the fieldwork were further analyzed in the laboratory. As described in Section 4.2, a Bernard Calcimeter was used in order to determine carbonate content for each sample. The outcome is presented in Figure 51 and shows a slight trend in increasing $CaCO_3$ content from east (OA) to west (AL). The transparent background colors indicate the grade of vulnerability to chemical attack, that was used in the parametrization (Section 4.5) where green represents low vulnerability, yellow moderate vulnerability, orange high vulnerability and red very high vulnerability. At the same time, it shows the grade of mechanical strength, where low values (red) represent mechanical weak and high values (green) mechanical strong layer.

The highest values in $CaCO_3$ content can be observed in the cliffs at *Albandeira* with an average of 77,9 %. Followed by *Santa Eulália* (73 %), *Olhos de Água* (59,7 %) and *Maria Luísa* (56,9 %). Lowest average $CaCO_3$ content can be found in the cliffs of *Alemães* (39,68 %).

In the locations OA and SE, higher $CaCO_3$ content can be observed in the top layers (OA-C, SE-B/-C/-D), compared to the lower lithofacies.

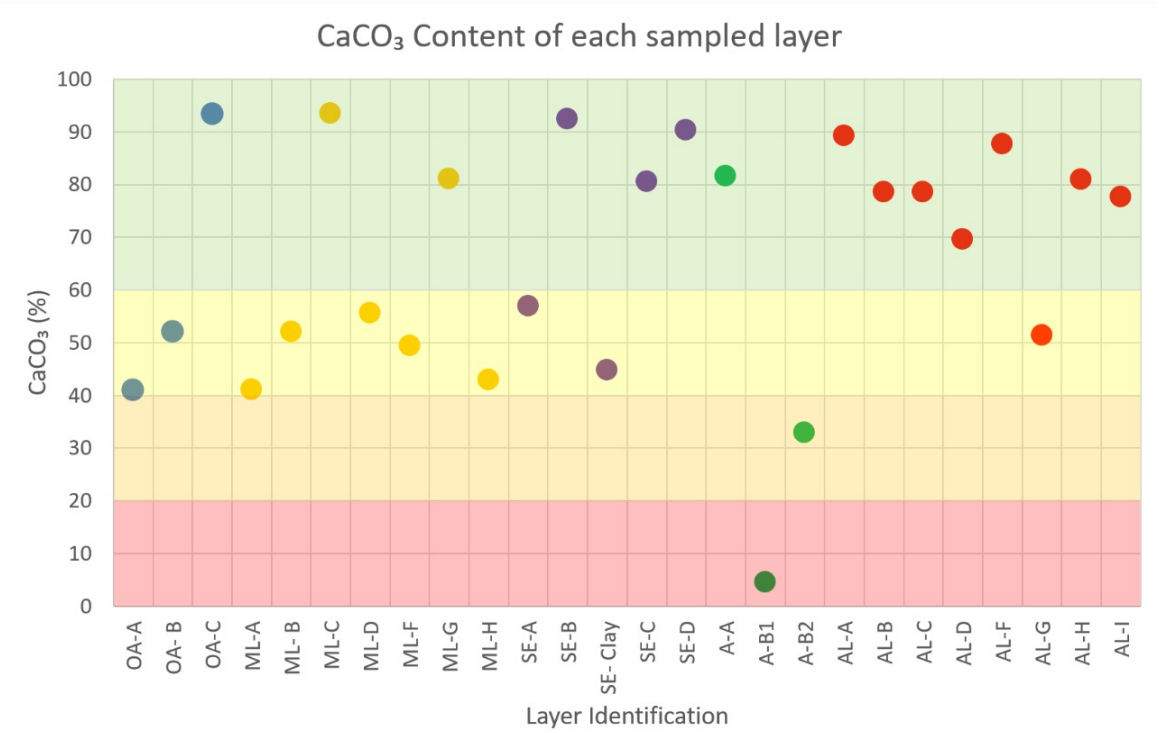

Figure 51: $CaCO_3$ content of each sampled lithofacies organized from East to West with distinctly colored dots according to the locations. Low values can be observed in the locations OA, ML and SE, whereas the cliffs of Albandeira show very high values. $CaCO_3$ values >60 % (green) indicate low vulnerability to chemical weathering, 60-40 % moderate vulnerability, 40-20 % high vulnerability and values lower 20 % very high vulnerability.

When only considering $CaCO_3$ content, vulnerability maps of cliff faces can be created by coloring the layer according to its respective vulnerability-value (Figure 52, 53 and 54). These images show the percentage of $CaCO_3$ in the respective layer and hence, the grade of vulnerability to chemical attack.

Green layers correspond to the upper layer of the LPCF, which contain large fossils of sea-urchins and pectinids. The upper siltstone layer A-B1 (in red) at location *Alemães* (Figure 53) overlying the LPCF with only 4,5 % of $CaCO_3$, belongs to the younger *Cacela Formation* of the Late Miocene- Messinian (Cachão et al., 1998; Cachão and Freitas, 1998). These siltstones are mechanically weaker than the underlying fossiliferous limestone with 81,6 % of $CaCO_3$. Thus, siltstones of the *Cacela Formation* erode and recede more easily and rapid than the LPCF, creating a structural notch in the contact zone of these two very different mechanical resistant layers. During more energetic conditions, the swash of the waves impacts the cliff by washing the surface of the platform and hence, widening it.

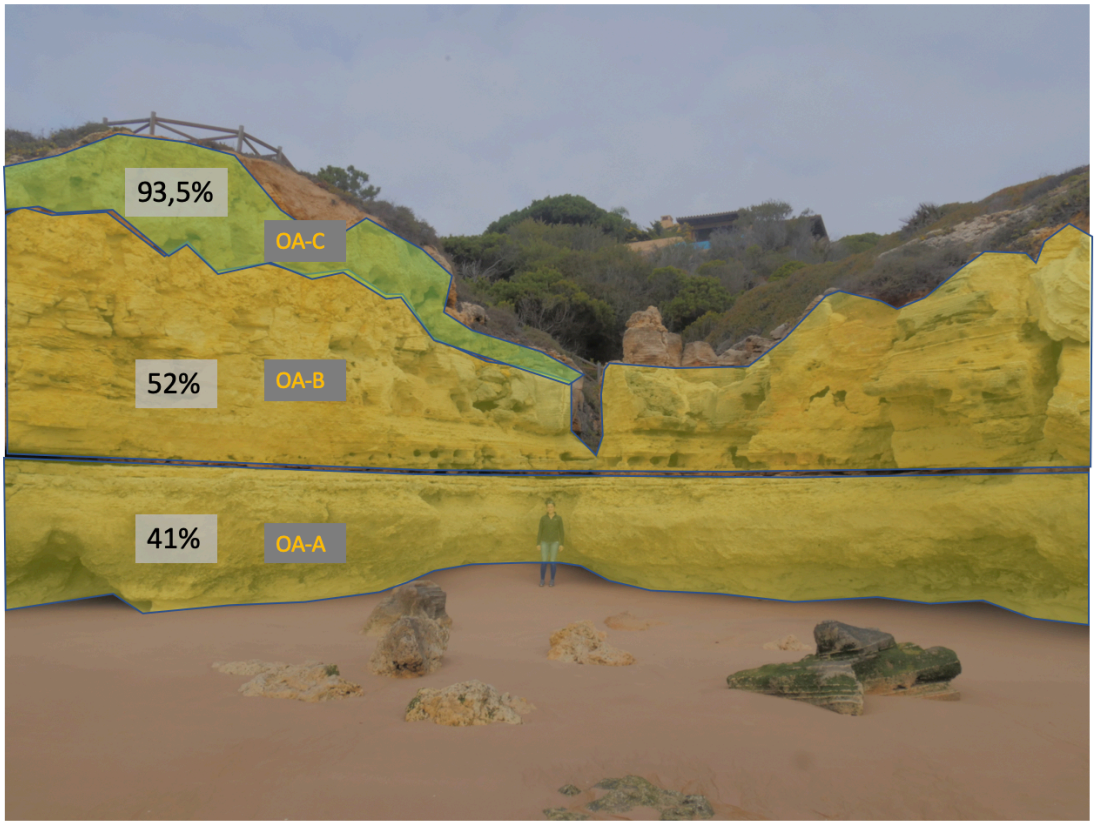

Figure 52: CaCO3 content and respective grade of vulnerability in each layer at location Olhos de Água (STOCK, 2020).

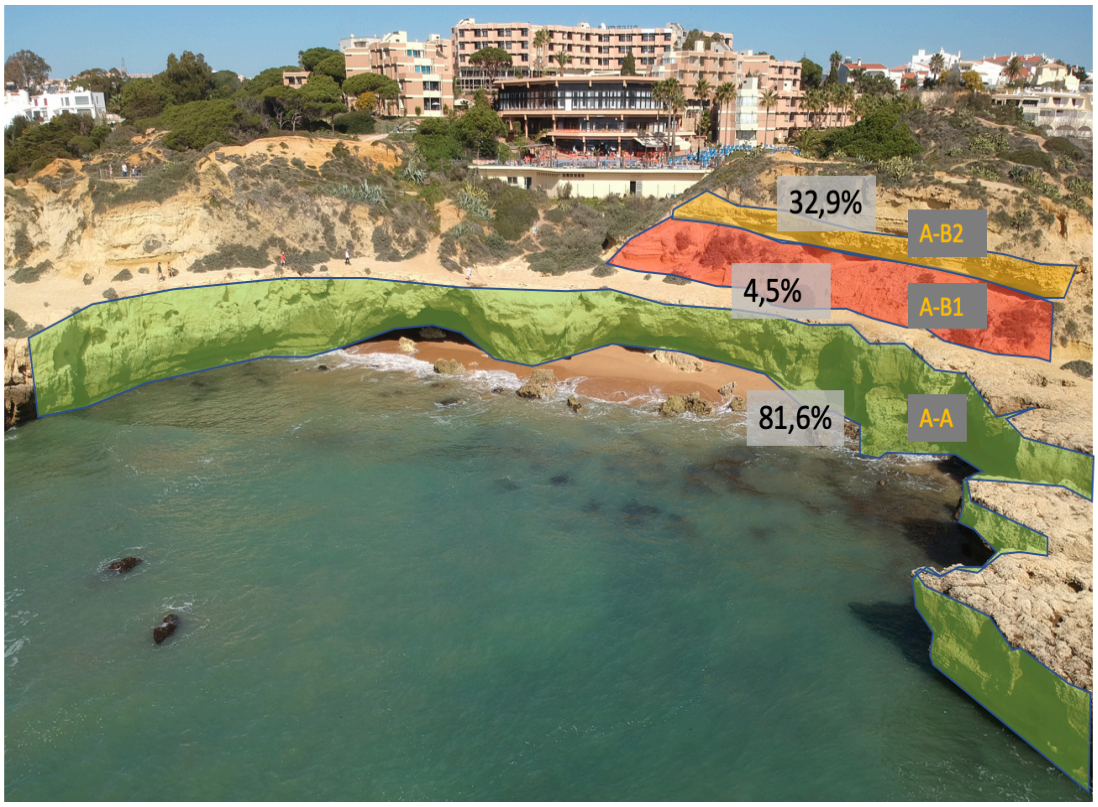

Figure 53: $CaCO_3$ content and respective grade of vulnerability in each layer at location Alemães (STOCK, 2020).

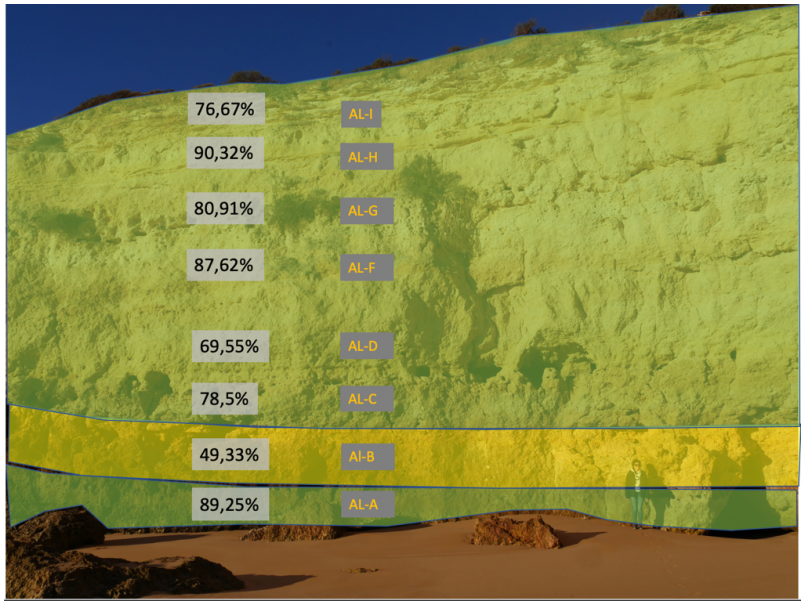

Figure 54: CaCO3 content and respective grade of vulnerability in each layer at locations Albandeira (STOCK, 2020).

As previously mentioned, and further discussed in Section 6.6, this evaluation was done without taking into account the cliff height and layer thickness. Concerning $CaCO_3$ content, this however, could influence and change the resulting vulnerability for each location. Thus, new calculations were made for sectors I, II and VI, for which all the necessary information was available ($CaCO_3$ content and layer thickness).

The outcome (Table 5) shows, that for these three sectors I, II and VI, the thickness of the layers does not alter the vulnerability classes, but, with the exception of *Alemães (A)*, the weighted averages are lower. Even though the difference for locations OA, ML, SE and AL is only very little (0,12 % - 1,6 %), it shows, that when taking into account the layer thickness, the vulnerability of the cliff to chemical weathering slightly increases.

Table 5: Calculation of averages of $CaCO_3$ content in each cliff. Arithmetic averages exclude layer thickness. Weighted averages represent layer thickness being considered.

Location	Facies variation	Arithmetic Average of $CaCO_3$ (%)	Weighted Average of $CaCO_3$ (%)	Difference (%)
OA	3	62,19	60,81	-1,38
ML	7	59,35	58,5	-0,78
SE	4	80,05	79,94	-0,12
A	3	39,69	52,28	+12,59
AL	8	76,67	75,08	-1,6

5.3 Remote Sensing

5.3.1 Satellite image analysis

The analysis of satellite data from the Sentinel-2 missions (August and November 2019, March 2020) involved multiple methods and tools as described in previous Sections (4.3) The chosen methods aim to test, if satellite images (open source Sentinel-2 data) can be used for the identification and analysis of morphological features at coastal cliffs in the study area.

The most noteworthy results from the *unsupervised* and *supervised classification* are presented in this Section.

5.3.1.1 Sentinel-2 Unsupervised Classification

The unaltered result of the *unsupervised classification* of a Sentinel-2 image from November 2019 in SNAP shows a very broad categorization of the surface features in the study area (Figure 55). The colors were automatically assigned. The performed color manipulation, where the 14 classes were combined and reduced to five groups corresponding to *Grassland*, *Sand*, *Infrastructure*, *Vegetation (Soil, (unvegetated) farmland)* and *Water*, provides a slightly better understanding of the different surface properties (Figure 56).

With the aim to decrease the size of the files and to identify smaller features, the study area was divided into subsets and the classification was carried out again while applying the same color palette (Figure 57 and Annex B).

The *unsupervised classification* shows, that this tool is able to distinguish main features such as beaches, cliffs, vegetation and other objects (e.g. infrastructure), however, it shows difficulties, differentiating between similar colors and reflections such as those from houses and sand (Figure 58).

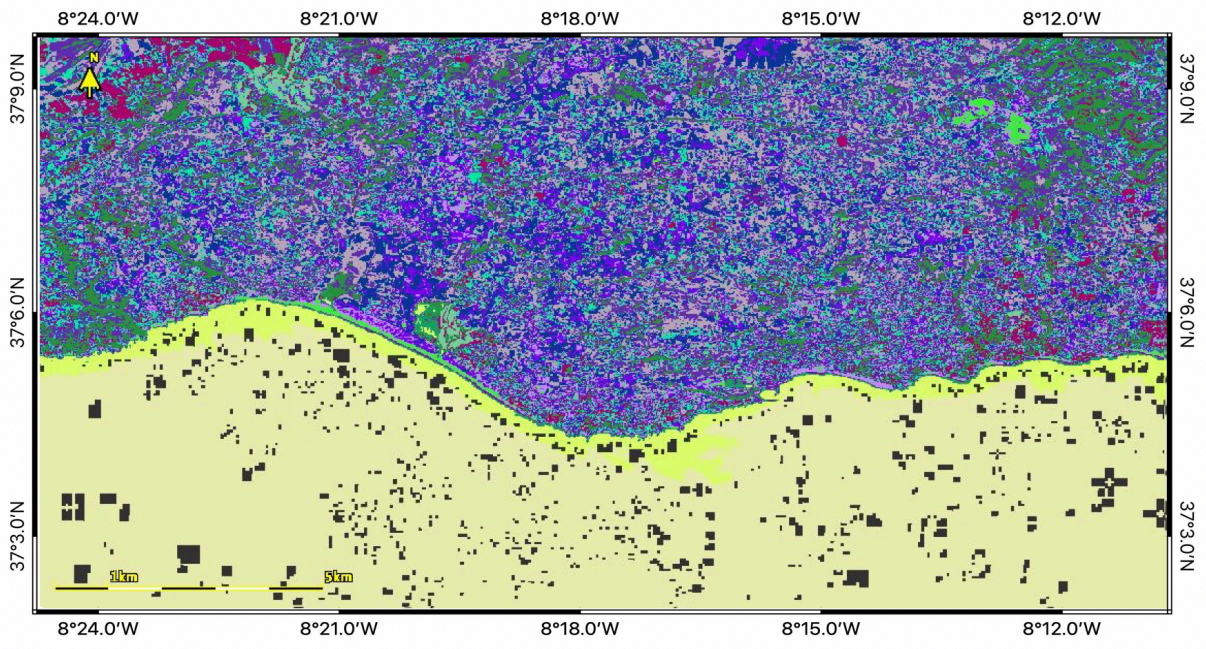

Figure 55: Unsupervised classification of a Sentinel-2 image from November 2019 of the entire study area without any alterations showing 14 different colored categories (STOCK, 2020. Contains modified Copernicus Sentinel data (2019), processed by ESA).

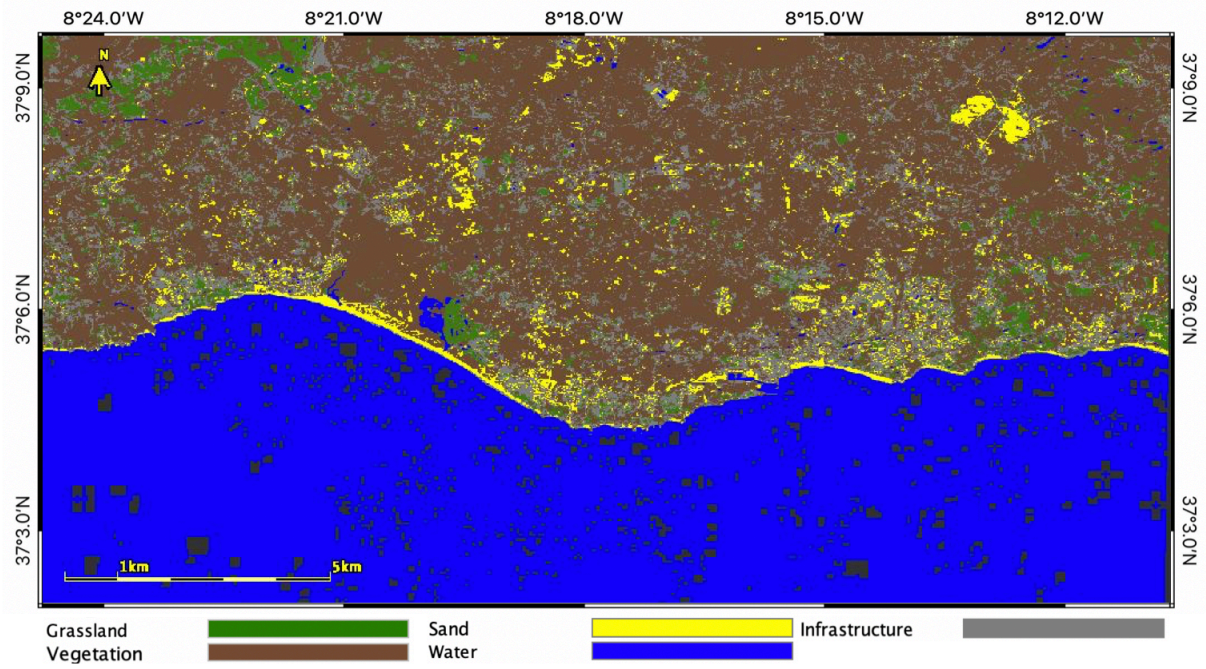

Figure 56: Unsupervised classification of a Sentinel-2 image from November 2019 of the entire study area after color manipulation and reducing/combining the classes to 5, which provides a more profound understanding of the present categories (STOCK, 2020. Contains modified Copernicus Sentinel data (2019), processed by ESA).

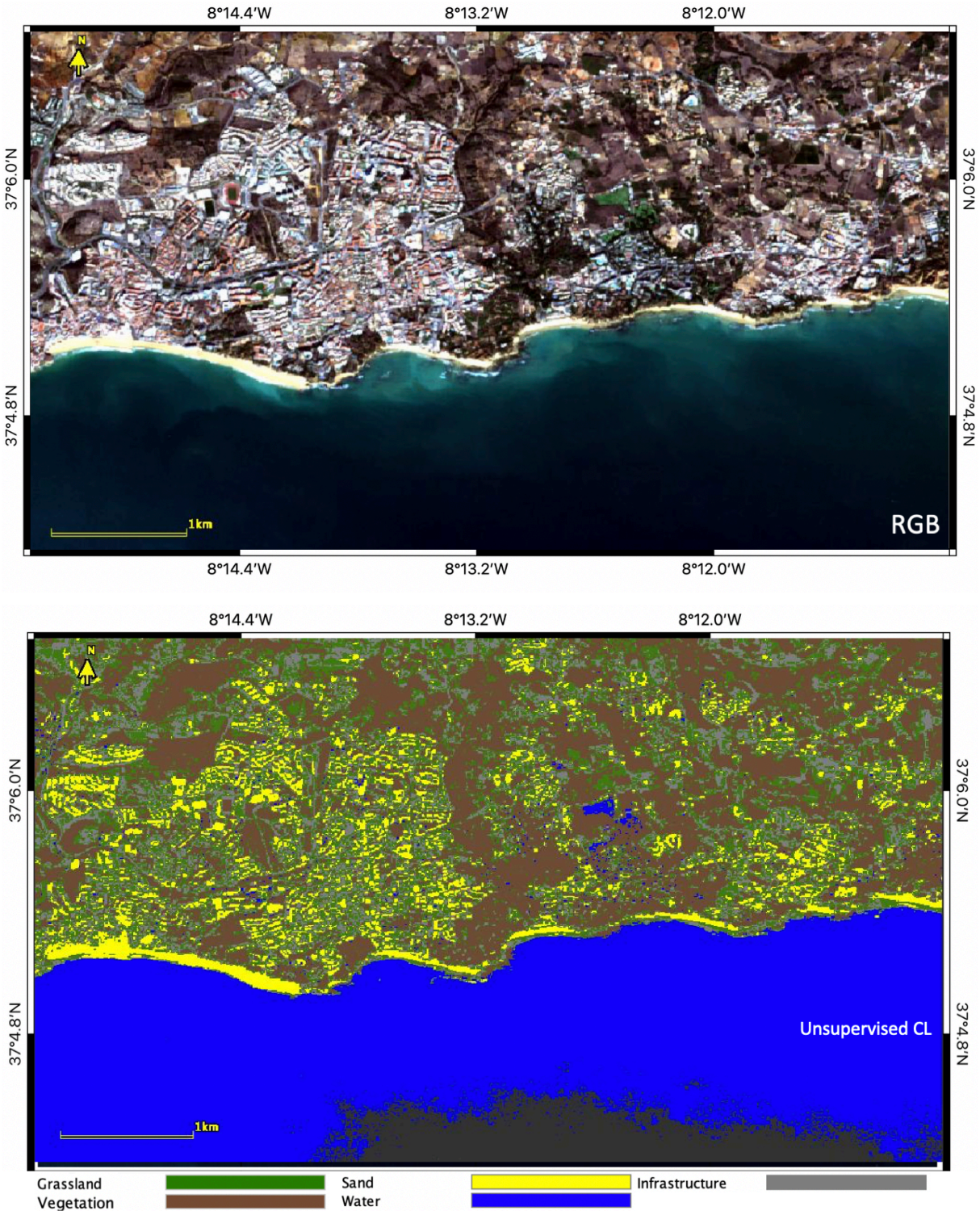

Figure 57: Subset 1 (Olhos de Água – Santa Eulália) of the resampled and reprojected RGB Sentinel-2 image from November 2019 (top). Unsupervised classification of the Sentinel-2 image from November 2019 (Subset 1) after color manipulation (bottom) (STOCK, 2020. Contains modified Copernicus Sentinel data (2019), processed by ESA).

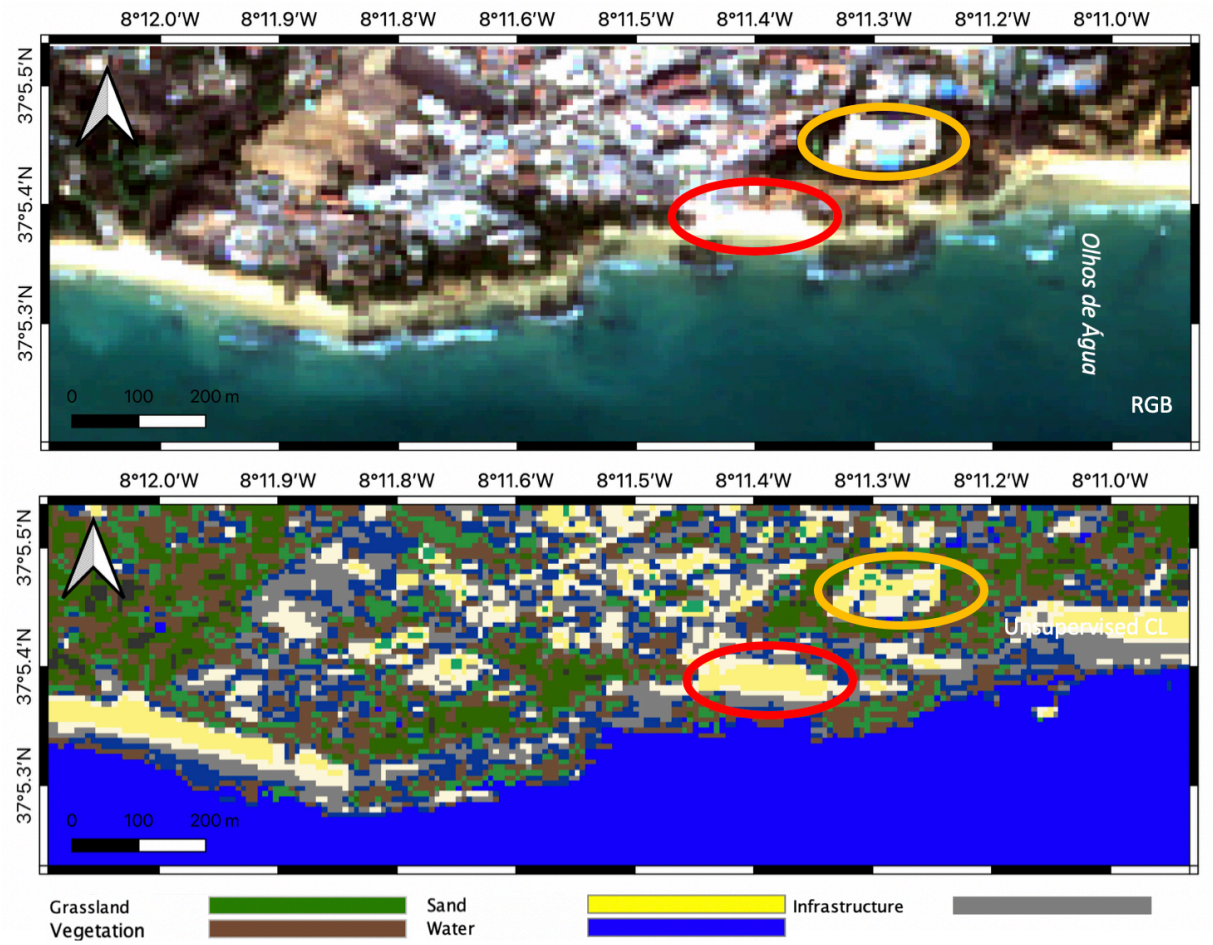

Figure 58: Resampled and reprojected RGB Sentinel-2 image from November 2019 (OA-ML) (top). Unsupervised classification of the Sentinel 2 image from November 2019 after color manipulation, showing the difficulties of classifying similar colored pixels. Red circles indicate Sand, orange circles Infrastructure (bottom) (STOCK, 2020. Contains modified Copernicus Sentinel data (2019), processed by ESA).

The same methods were applied to Sentinel-2 satellite images from August 2019 and March 2020 to examine possible seasonal differences. With the same color palette, the images from August 2019 and March 2020 show similar pattern when comparing to the results from November 2019 (Figure 59). However, on the base of visual comparison, the unsupervised classification from August and March exhibits better differentiation between Infrastructure and sand for example.

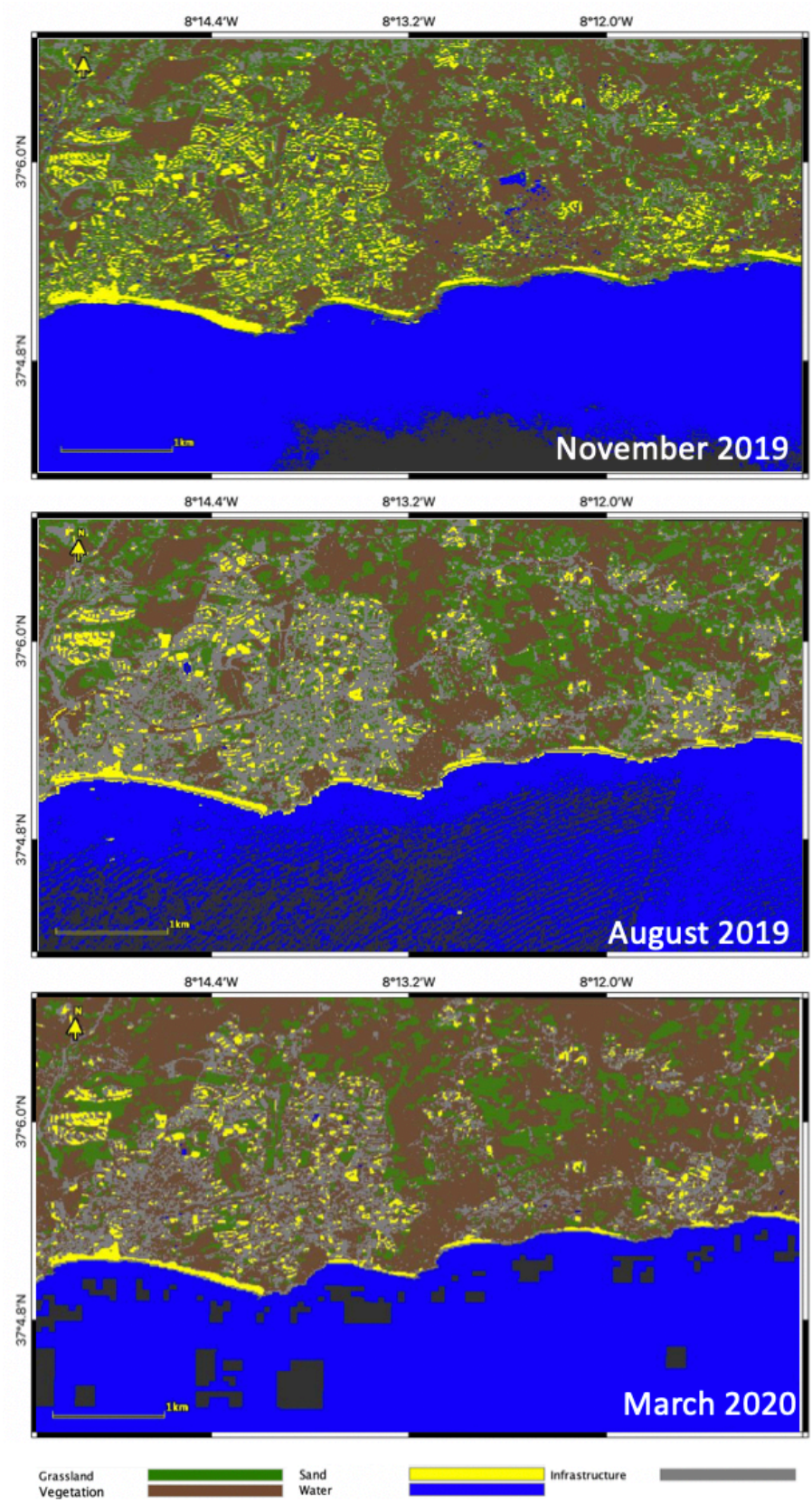

Figure 59: Unsupervised classification of Subset 1 (OA – SE) of the Sentinel-2 images from November 2019 (top), August 2019 (middle) and March 2020 (bottom), exhibiting differences in distinguishing features such as sand and infrastructure (STOCK, 2020. Contains modified Copernicus Sentinel data (2019), processed by ESA).

5.3.1.2 Sentinel-2 Supervised Classification

For the *supervised classification*, the RF and ML analysis were applied to the subsets after creating polygons as *vector container*. The classification through the chosen polygons for e.g. Subset 2 provided seven classes (see Section 6.4), *no data*, *Sand*, Dunes, *Infrastructure, Soil, Vegetation*, *Water* (Figure 60 and 61). By visual comparison, only minor differences can be detected, but without further analysis, neither of the two classification (ML, RF) can be favored.

All the images that were used and processed were exported as *kmz* files to import in *Google Earth*. With this, a comparison of surface features was possible, and the classification could be validated by overlaying the *unsupervised* and *supervised classification* (Figure 62).

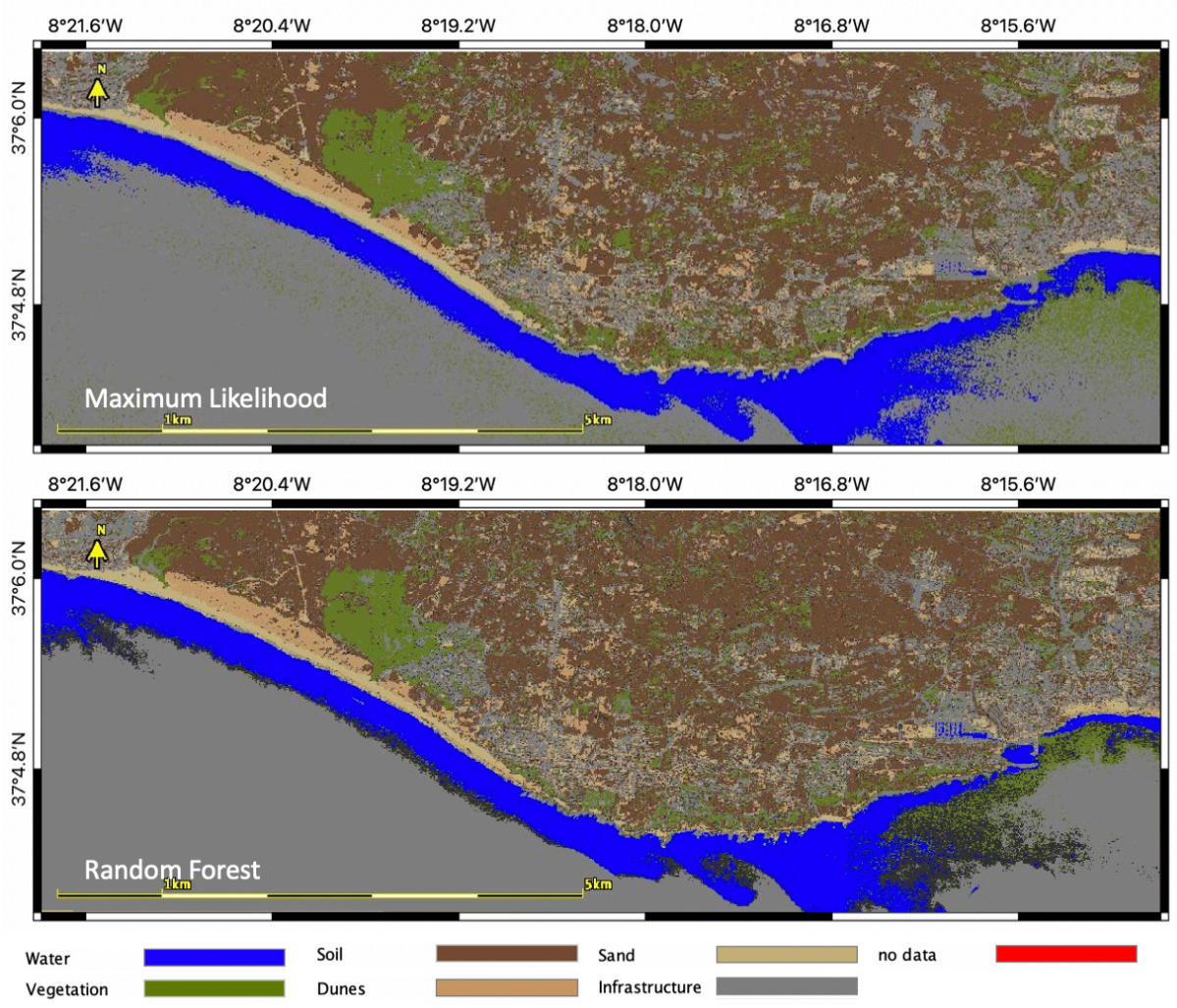

Figure 60: Comparison of Maximum Likelihood (top) and Random Forest (bottom) classification of Subset 2 (Albufeira – Armação de Pêra) of the Sentinel-2 image from November 2019 (STOCK, 2020. Contains modified Copernicus Sentinel data (2019), processed by ESA.

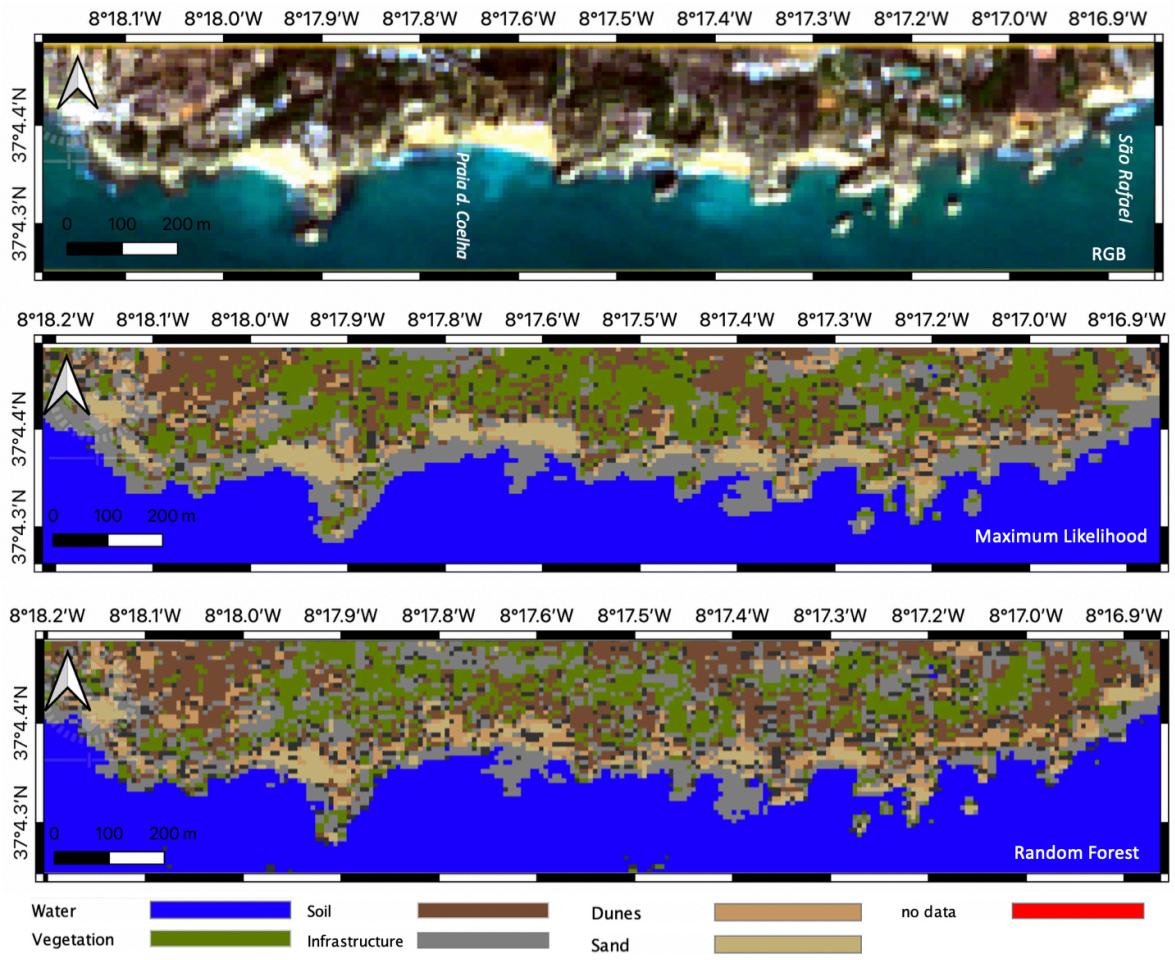

Figure 61: Zoom in into the RGB (top), Maximum Likelihood (middle) and Random Forest(bottom) classifications of the area São Rafael beach until Evaristo (Subset 2) beach from the Sentinel-2 image from November 2019, indicating a slight visual advantage of the ML classifier (STOCK, 2020. Contains modified Copernicus Sentinel data (2019), processed by ESA.

Figure 62: Zoom into the unsupervised classification of Subset 1, overlaying the Google Earth image (STOCK, 2020. Adapted from Google Earth. Contains modified Copernicus Sentinel data (2019), processed by ESA).

5.3.2 UAV image analysis

To further test the classification tool in SNAP, the same procedure as for the satellite images was applied to the captured images from the UAV during the fieldwork. The *unsupervised classification* of an UAV "top-down" image as presented in Figure 63, shows good identification of features such as vegetation, sand and sinkholes.

As this study focuses on vertical facies variation, the tool was also applied to UAV images of the cliff face. The obtained results present difficulties in proper portrayal of the horizontal layers in the cliff face due to varying lighting and reflection in the RGB image (Figure 64). Consequently, the classifier tool cannot distinguish between certain lithological different features.

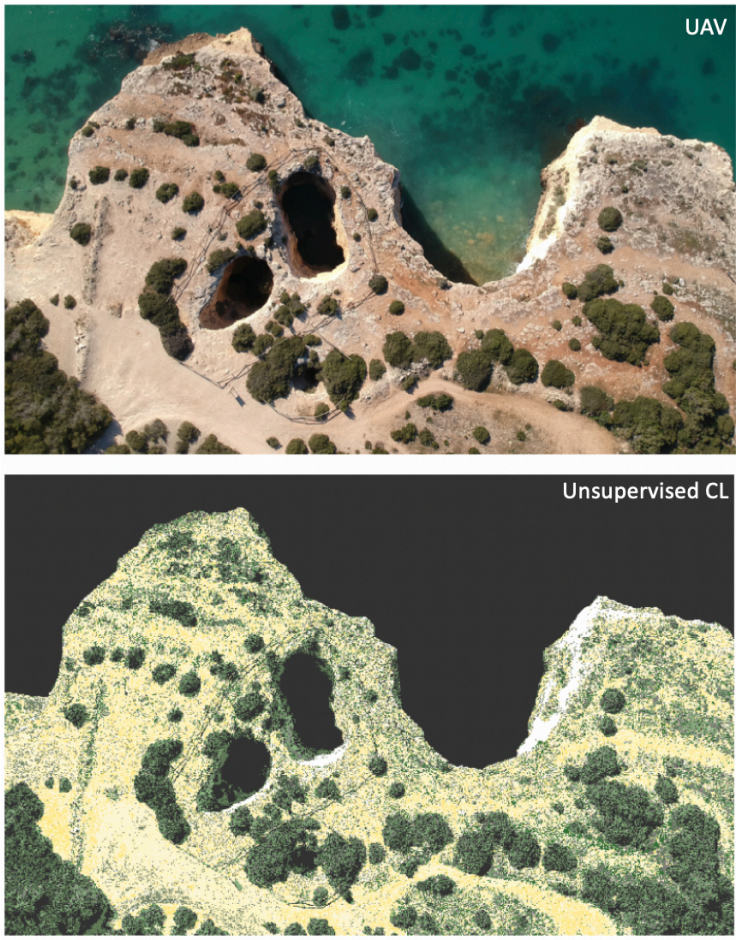

Figure 63: Unsupervised classification tool (bottom) applied to an UAV (top) image of the coast near Albandeira beach, showing distinction of different features such as vegetation, sands and sinkholes (STOCK, 2020, modified in SNAP).

Figure 64: Unsupervised classification (top) of an UAV image (bottom) of a horizontal cliff profile near Albandeira beach showing difficulties concerning accurate layer distinction (STOCK, 2020).

5.4 Photogrammetric Analysis using AgiSoft Metashape

The use of the software *AgiSoft Metashape* helped to develop orthomosaics and to explore the study area in a 3D model (Figure 65 and 66). With this, sinkholes, rockfall, sediment fans, shore platforms and marine caves could be identified more easily compared to regular, ground-level images. The created 3D model further helped to identify the overall morphology and to measure cliff heights. The height of the cliffs (topographic surface) could be identified by moving the 3D model in a profile view. As an example, Figure 65 presents the cliff profile of Sector I (A), measurements of cliff heights (B), sinkholes and shore platforms at the cliffs between *Olhos de Água* and *Maria Luisa* (C), as well as a sediment fan in a collapsed sinkhole near *Santa Eulália* beach (D).

The orthomosaic in Figure 66 shows some features in the cliffs of sector I from *Olhos de Água* to *Santa Eulália* such as sinkholes and evidence from rockfall.

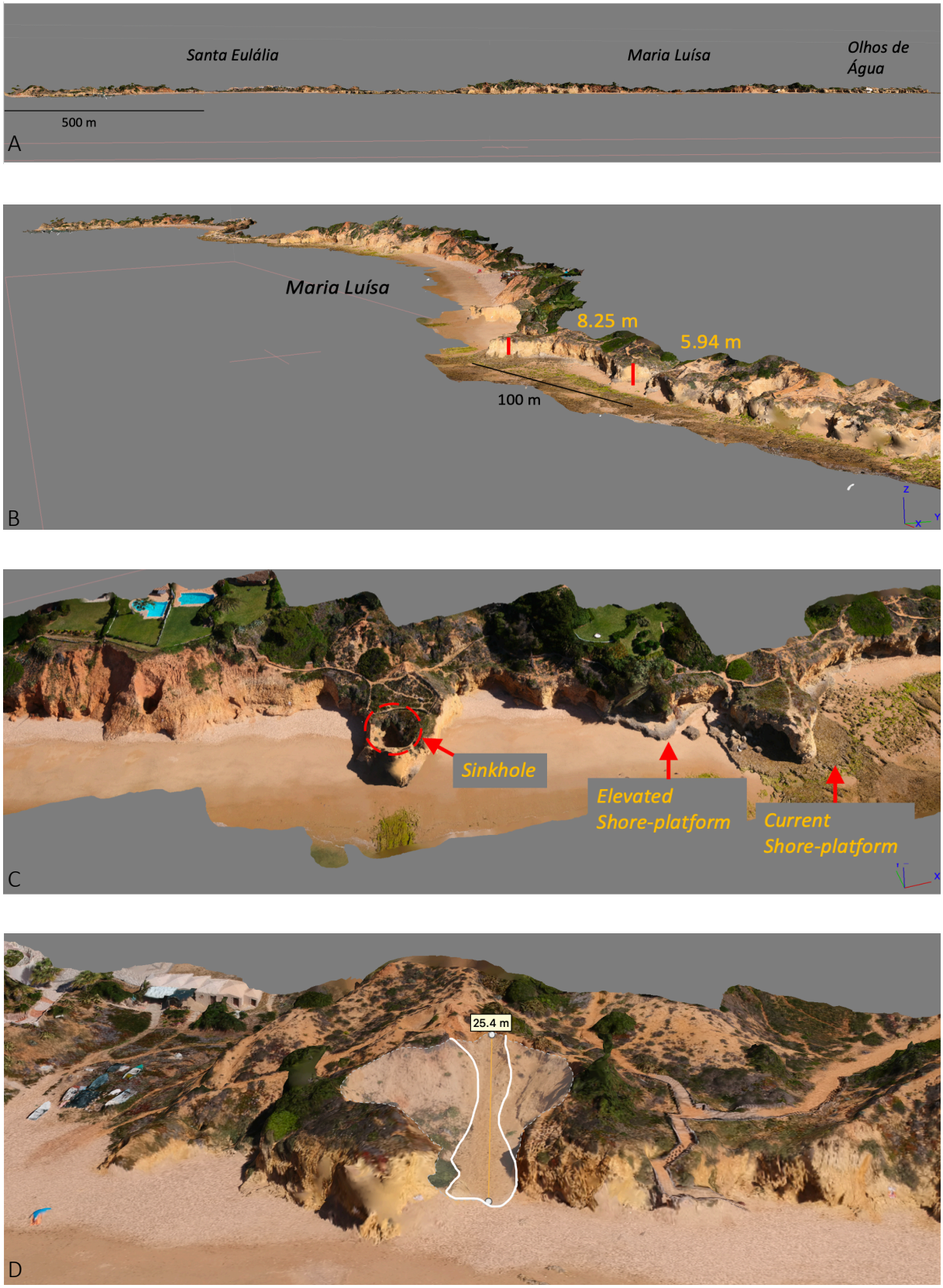

Figure 65: 3D model created in AgiSoft Metashape from UAV images, showing the cliff height between OA and SE and identifying topography (top), cliff heights (B) sinkholes and shore platforms (C) and sediment fans (D) (STOCK, 2020).

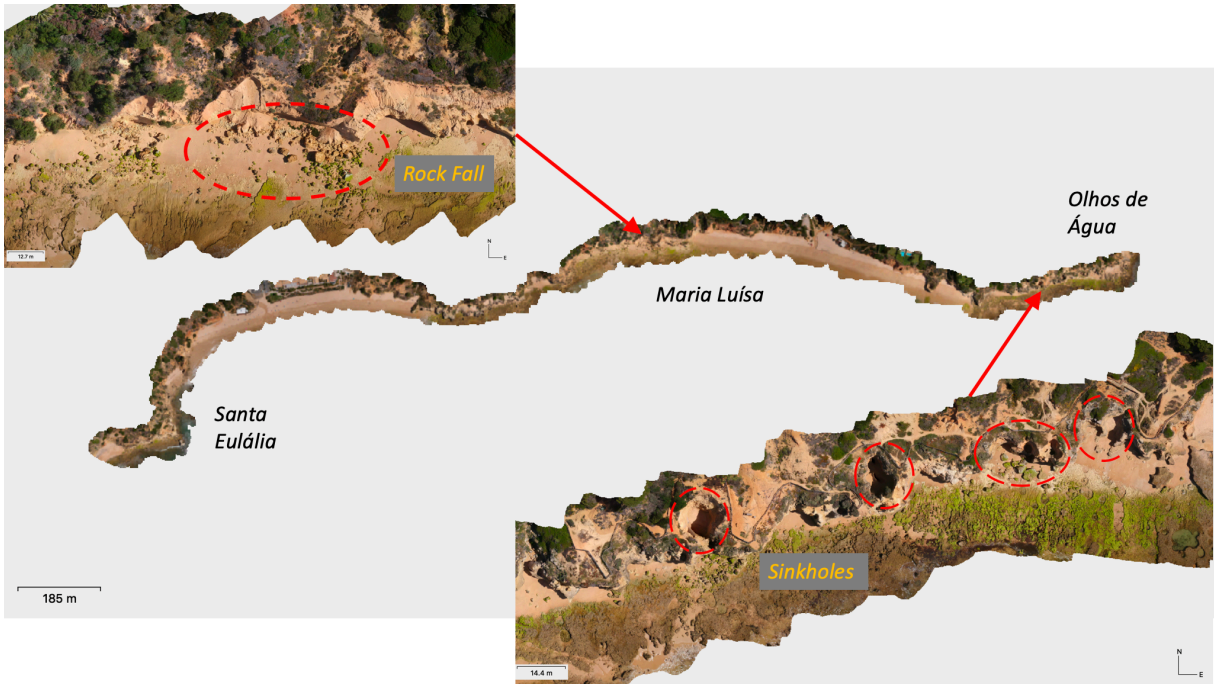

Figure 66: Orthomosaic, created in AgiSoft Metashape from UAV images, showing the part of the study area from Olhos de Água to Santa Eulália and points out to rock fall events and sinkholes (STOCK, 2020).

5.5 Parametrization and Vulnerability Evaluation

In order to perform a parametrization of the main factors that influence cliff vulnerability to erosion, the study area was divided into six subsectors according to the respective lithological properties, as it is presented in Table 6. After assigning an impact factor for every parameter, a total value as well as a weighted average concerning cliff vulnerability could be calculated for each sector (Table 7).

According to the parametrization, sector IV (Arrifes – Galé) presents the highest vulnerability with a weighted average of 3, where 4 is the highest. Followed by the sectors I, II, III and VI, which all show moderate vulnerability (weighted average 2,5; 2,4; 2,6; 2,6 respectively). The part of the study area with the lowest vulnerability is sector V (Galé – Armação de Pêra bay) with a weighted average of 1,6. However, due to the aforementioned restrictions by national security at the time of this work, information for some location and parameters are lacking, which may influence the outcome and is further discussed in Section 6.6.

With the information of the parametrization, a vulnerability map could be created, where sectors with a high vulnerability are represented by an orange rectangle (Sector IV),

moderate vulnerability is marked in yellow (Sectors I, II, III, VI) and low vulnerability is marked in green color (Sector V) (Figure 67).

Table 6: The subsections of the study area, divided according to their respective lithological properties.

Sector	Sites	Geographic Coordinates	Lithology
Sector I	Olhos de Água – Santa Eulália	37° 5'22.17" N/8°11'24.64" W – 37° 5'1.66" N/8°13'5.80" W	Detrital facies. Mainly low fossiliferous sandstones
Sector II	Santa Eulália – Albufeira	37° 5'1.66" N/8°13'5.80" W – 37° 5'9.39" N/ 8°15'4.01" W	Very fossiliferous carbonate facies at the base. Detrital facies of yellow siltstone in the upper part
Sector III	Albufeira – Arrifes	37° 5'9.39" N/ 8°15'4.01" W – 37° 4'30.09" N/8°16'41.67" W	Hard crystalline limestones from Jurassic and vertical marls from Cretaceous
Sector IV	Arrifes – Galé	37° 4'30.09" N/8°16'41.67" W – 37° 4'31.99" N/8°18'30.39" W	Biocalcarenite, fossiliferous limestone, siltstone
Sector V	Galé – Armação de Pêra	37° 4'31.99" N/8°18'30.39" W – 37° 6'6.65" N/8°22'10.05" W	Bay-beach and dunes
Sector VI	Armação de Pêra – Albandeira	37° 6'6.65" N/8°22'10.05" W – 37° 5'25.86" N/8°24'1.25" W	Detrital facies interlayered with limestone showing different amounts of fossils

Table 7: Cliff vulnerability to erosion for each parameter and sector with assigned values of 1 (low vulnerability, green), 2 (moderate vulnerability, yellow), 3 (high vulnerability, orange), 4 (very high vulnerability, red). Grey boxes indicate "no available data" (See Table 6 for the sector identification). Total vulnerability describes the sum of all parameters for each sector. Weighted average includes the sum of the used impact factor as the denominator.

Parameter	Sector I	Sector II	Sector III	Sector IV	Sector V	Sector VI	Impact Factor
Vertical Facies Variation	2,7	1	1	4	1	4	3
$CaCO_3$ %	1,7	2,7	x	x	x	1	3
Layering	2	2	3	2	x	2	2
Faults	3	4	4	4	1	3	2
Karst	3,6	1	4	4	1	4	2
Notches	3	4	1	3	1	2	2
Marine Caves	3	4	4	3	1	3	2
Exposition to waves	2,6	2	2	2,5	4	2	2
Shore platform width	1	2	1	1	4	3	1
Beach width	2,3	1	4	1	1	1	1
Total Vulnerability	24,9	23,7	24	24,5	14	19	
Weighted Average	**2,5**	**2,4**	**2,6**	**3,0**	**1,6**	**2,6**	

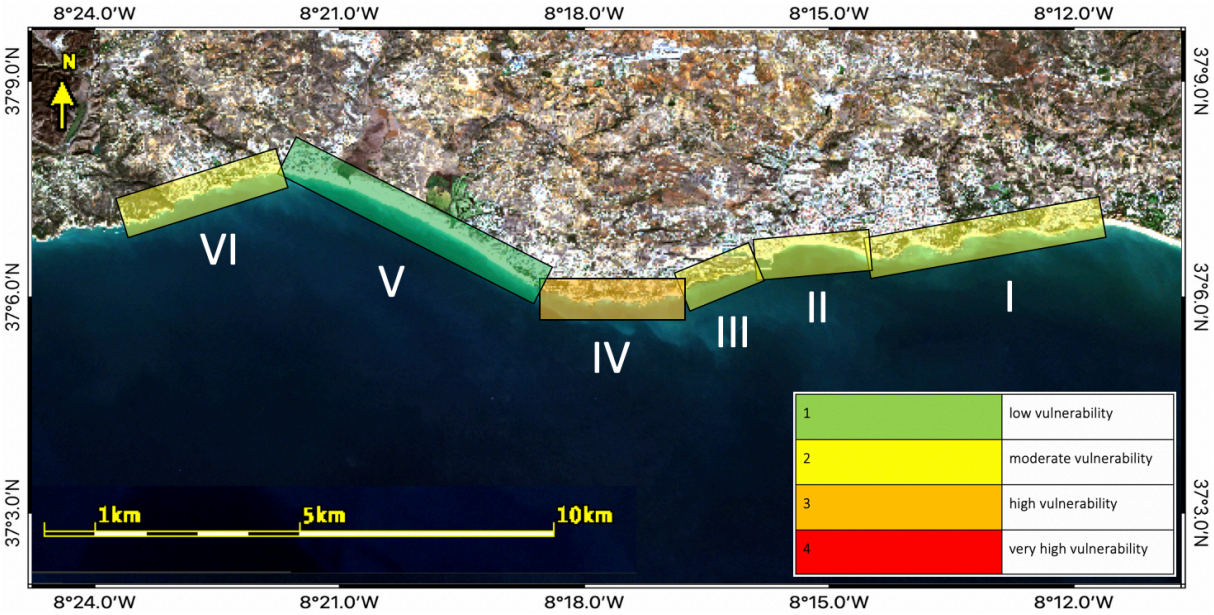

Figure 67: Sentinel-2 image of the study area with the final vulnerability classification according to the parametrization obtained from this work. Sector I, II, III and VI exhibit moderate vulnerability, sector IV high vulnerability, sector V low vulnerability (STOCK, 2020. Contains modified Copernicus Sentinel data (2019) processed by ESA).

6 DISCUSSION

In this study, various parameters that influence the state of rocky coastal cliffs have been analyzed. By reason of the high vulnerability to erosion in combination with high touristic pressure on the southern Algarve coast, research in this field and region is of utmost importance. In the following Section, the most noteworthy matters and parameters concerning the topic and methodologies of this study are discussed and compared to previous research.

6.1 Driver Mechanisms

The described processes (see Section 2.1), leading to coastline recession also apply to the southern Algarve. Here, erosion is promoted by multiple factors, while direct exposure to waves is among the strongest. Other parameters involved in the evolution of the cliffs in the study area are lithological properties, mechanical strength of the exposed cliff material, vertical facies variations and their individual thickness, geometric characteristics, number and position of siltstone layers, faults, crevices and other discontinuities, as well as intensity and distribution of karstification. This has also been investigated in multiple works (Dias and Neal, 1992; Teixeira, 2006; Marques, 2008; Bezerra et al., 2011; Moura et al., 2011a; Moura et al., 2012a; Terefenko and Terefenko, 2014), however lithological properties are widely ignored or are never a key factor.

Studies conducted by Dias and Neal (1992), Marques (1998), Nunes et al. (2009), Bezerra et al. (2011), Moura et al. (2011a), Horta et al. (2013), Proença, et al. (2011) discuss coastal retreat in the southern Algarve coast by pointing at wave energy and height and exposure to waves as the main parameters for erosional processes. According to Moura et al. (2006a), the combination of storms, wave energy, lithology and karst features are the main drivers for cliff retreat in the study area. Other authors such as Viegas et al. (2014) add that the horizontal bedding of the cliffs in the southern Algarve coast leads to abrasion and excavations at the cliff base, developing caves and ledges in highly fractured cliffs and supplementing the aforementioned susceptibilities. Moreover, Dias and Neal (1992) and Bezerra et al. (2011) indicate wave-cut and structural notches as a decreasing factor regarding cliff stability as these features promote collapse due to gravity.

Due to the lack of research in the study area that assumes lithological properties to be one of the most influencing factors concerning cliff vulnerability, the present work considers lithology a first order factor for the first time and thus, augments previous research on this topic.

6.1.1 Vertical Facies Variation

Results of the present work point to multiple different lithofacies (vertical facies variation) as a first-order factor concerning cliff instability. The presence of alternating mechanical weak and strong layers in the cliff face evocate a high sensibility towards wave impact and excavation. Owing to the faster erosion of mechanically weak facies, the more resistant layers remain and protrude at the cliff face. Particularly the number and position of the extremely weak siltstone layers, which develop structural notches, create tremendous instability and may be the reason for various cliff collapses and rock fall.

This is in accordance to previous hypothesis from Marques (2008), Bezerra et al. (2011) and Moura et al.(2011a), which suggest an increase in risk of rock fall and topples for higher cliffs with multiple vertical lithofacies. In particular Sector IV and VI exhibit highest cliffs with highest vertical facies variations, which, in combination with other parameters (Table 7), results in highest vulnerability classes. It is also suggested by the aforementioned authors, that the composition of alternating layers of fine grained calcarenites and macrofossil-rich calcarenites in the Miocene rock outcrops differ in their reaction to erosive impacts and that particularly the weak siltstone layers in various location (e.g. Albandeira) present a high risk of cliff failure.

6.1.2 $CaCO_3$ Content

The $CaCO_3$ content analysis of the samples from the cliffs in the study area exhibit correlations to rock resistance and thus, should be considered a first order factor concerning cliff vulnerability.

The results of the carbonate content analysis of this work show highest arithmetic average values for sector VI (77,9 %) and sector I (67,19 %), whereas sector II (39,68 %) reveals lowest

values (Table 5). This lateral variation results from the crossing of the current coastline of several Miocene sub environments from westerly fossiliferous and deeper, to more littoral and detrital facies in the eastern part.

Moreover, high $CaCO_3$ content values can be identified in the top lithofacies in several locations (e.g. OA-C, SE-D), which is the result of a high abundance of calcite rich fossils in these layers. Additionally, lithofacies A-A of location *Alemães*, which belongs to the LPCF, exhibits high $CaCO_3$ content (81,6 %) due to abundant fossils. Even though this cliff is affected by wave erosion in its lower part, the overlaying facies (A-B1 and A-AB2) with lower $CaCO_3$ content erode much faster (see Section 5.2, Figure 53). This has also been discovered by Teixeira (2006), where samples with high lumashell abundance presented much higher carbonate content compared to fine calcarenites, creating more resistance to chemical weathering. Research from Marques (2008) regarding geotechnical properties and rock strength, further support this assumption. Accordingly, calcarenites exhibit different values of mechanical resistance, where high macrofossils content has a compressive strength of 1 MPa to 3 MPa, whereas fine grained calcarenite only shows values of 0.5 MPa to 2 MPa. Consequently, the latter is weaker and more affected by superficial erosion. However, depending on the size of the shell particles in the substrate, porosity and thus, vulnerability to water percolation, dissolution and water hammer effect (air compression) increases with increasing shell size (Moura et al., 2012a). This is reflected in locations OA and ML for example, where, as a result of marine transgression by the end of the Miocene, large shells, sea urchins and pectinids established a heterogeneous and very porous biofacies on top of the cliffs.

Previous studies (Teixeira, 2006; Andriani and Walsh, 2007; Terefenko and Terefenko, 2014; Moura et al., 2011b) also point out the importance of carbonate cement in the rock and its impact on chemical and mechanical strength. Due to its cementing effect, calcium carbonate content correlates positively with rock strength, thus higher $CaCO_3$ content in the rock indicates higher strength and therefore higher resistance. Teixeira (2006) discovered that especially rocks that underwent secondary calcite precipitation, as the inner walls of multiple sinkholes (mainly sector I and IV of the present study), seem to incorporate very high amounts of $CaCO_3$ and are hence more resilient.

For the parametrization (Table 7) the amount of $CaCO_3$ was considered as an arithmetic average for the entire cliff. However, as layer thickness varies, weighted averages were calculated in respect to the thickness of each lithofacies (Table 5).

Concerning the cliffs at OA, regardless of the high $CaCO_3$ content of layer OA-C (93,5 %), the very low thickness compared to OA-A ($CaCO_3$ content of 41 %) and OA-B ($CaCO_3$ content of 52 %) immensely reduces its impact on the total vulnerability, resulting in a slight decrease in the weighted average of $CaCO_3$ content of the entire cliff. As for location *Alemães,* the difference of 12,6 % between arithmetic and weighted average shifts the vulnerability class of $CaCO_3$ % from "moderate" to "low". This may be caused by the amount of vertical facies (3 layers) and the respective percentage of $CaCO_3$ in each lithofacies, where the relatively thick layer A-A exhibits a high $CaCO_3$ content (81,6 %) compared to the thinner layers A-B1 and A-B2 with lower $CaCO_3$ content (4,5 % and 32,9 % respectively). When considering the entire cliff at *Alemães*, the vulnerability is low, nevertheless, the cliff shows intra-variability where layers A-B1 and A-B2 exhibit high vulnerability to erosion. *Albandeira*, having 8 vertical lithofacies of which 7 can be associated to "low vulnerability" and only one layer being "moderately vulnerable", is not affected by the layer thickness, whereas cliffs with lower vertical facies variations (e.g. *Alemães*) show stronger affection.

As for the mentioned sampling limitations (Section 4.1), only three out of the six sectors could be sampled and thus analyzed regarding $CaCO_3$ content. With data from the entire study area, the accuracy of the results may have increased, and traits could have been demonstrated more obvious. Particularly, given that this parameter is potentially a first order factor for the above exposed reasons (impact factor 3), it is likely, that with a holistic dataset, total cliff vulnerability would differ.

6.1.3 Karstification

As it can be seen in the parametrization (Table 7) four out of the six studied sectors exhibit vulnerability classes of "high" or "very high" for karst features. This indicates the strong pressure of karstification on the cliffs in the southern Algarve coast, promoting instability in multiple locations (Bezerra et al., 2011; Moura et al., 2011a). Particularly in facies of chemical weak lithologies, karst features may develop more easily, forming holes and ducts. With

increased exposure to erosional processes, these structures collapse and augment cliff retreat. Moreover, the development of sinkholes in the cliffs increase instability and present a high vulnerability, as these features are prone to collapse, which may relocate the coastline several meters. However, the reverse process also may apply, when the receding coast intercepts and destroys sinkholes and thus, contributes to the development of a highly crenulated coastline with pocket beaches and stacks. In the study area, this can be observed at the locations *Olhos de Água* (sector I) and *Coelha* (sector IV), where the coastline is characterized by collapsed sinkholes (Figure 66).

This is in accordance to multiple studies (Moura et al., 2006a; Marques, 2008; Nunes et al., 2009; Bezerra et al., 2011), which state, that the presence of karst in the southern Algarve is responsible for the exceedingly high retreat rates, mainly in the way of cliff toppling. However, this is subject to local differences regarding fault structures and synoptic conditions (Oliveira et al., 2019). As studies (Forth et al., 1999; Andriani et al., 2005; Basso et al., 2013; Zabidi et al., 2016) show, jointing and faulting is strongly correlated with sinkhole development. Thus, in a highly faulted or jointed cliff, karst features like caves and conduits may develop more easily due to the decrease in shear strength owed to the presence of susceptibilities in the rock. Moreover, dissolution processes from rain or ocean water support this process.

Most of the sinkholes in the southern Algarve coast are filled with Plio- Pleistocene sediments, others are free from sands. This may change with time, as these sediments get washed out by waves and rain and filled again by slides from the top or the back of the cliff where Plio- Pleistocene material accumulates. This exhibits the constant sediment movement, which may contribute to natural beach nourishment, and the erosive energy of the waves.

6.2 Driver Mechanisms in the Studied Sectors

The cliffs of the southern Algarve coast experience ongoing physical and chemical weathering and erosion with local differences depending on lithological properties (vertical facies variations, $CaCO_3$ content (fossil content), layering), coastline orientation, wave energy, intensity of karstification, faults, notches, caves and the presence or absence of protecting

features like shore platforms and sandy beaches (Table 7). These factors can be identified as the strongest drivers concerning vulnerability of the cliffs in the study area and are now further discusses for each studied location.

6.2.1 Sector I (Olhos de Água – Santa Eulália)

The location of *Olhos de Água* presents a more differentiated situation compared to other localities, as in addition to wave attack and weakly cemented calcarenite rocks, hydric erosion acts on the cliff and shore platforms as a result of a high abundance of brackish water, surfacing in multiple freshwater springs (Figure 19). This and other karst features like conduits and holes (Figure 16) increase the cliffs vulnerability and enhance erosional processes. The eroding state of the cliffs vary throughout this coastal stretch, which may be due to higher porosity of certain lithofacies. These promote water circulation and hence, dissolution of carbonates.

Furthermore, marine notches and caves develop in parts, where waves impact the junction of cliff and shore platform, which increases the risk of collapsing cliff units (Figures 16, 17 and 23).

The vertical facies variation with only three distinct layers is quite low, resulting in a decrease in vulnerability. The present $CaCO_3$ content in the cliff slightly decreases the overall vulnerability, as these three layers each present $CaCO_3$ content values above 40 % and an average value of 59,7 %, which is close to the lowest vulnerability class (>61).

Similar conditions are existent at *Maria Luísa* beach. However, due to a wider beach compared to *Olhos de Água*, the adjacent cliffs in the back of the beach are less affected by wave impact but not exempt. Karst exhumations in the cliff face and marine caves in the base (Figure 25 and 28) enhance erosion and create a very high vulnerability. This is further promoted by dense sinkhole occurrence and due to weakly cemented calcarenites in this location, which increases the risk of rock fall.

Furthermore, seven lithofacies in vertical succession increase cliff vulnerability due to susceptibilities and alternating grades of resistance in the contact zones. The average $CaCO_3$ content (56,9 % average) corresponds to the moderate vulnerability class and therefore,

slightly lowers the overall vulnerability. In this sector I however, the cliffs at *Maria Luísa* present the lowest amount of $CaCO_3$ content.

The quite complex geometric relationship of the five vertical lithofacies at *Santa Eulália* entails erosive contacts between the layers and karst features play a decisive role concerning driver mechanisms for erosion (Figure 33). These discontinuities provide a relatively easy way for infiltrated rain and ocean water to excavate those openings and increase cliff instability.

Concerning the low and moderate $CaCO_3$ values (average of 73 %) in the five different lithofacies, the cliffs of *Santa Eulália* have the lowest vulnerability out of the three locations in Sector I.

According to the vulnerability parametrization, Sector I presents a moderate vulnerability with a weighted average of 2,5. The most impacting factor is karstification (vulnerability value of 3,6) while the most lowering is shore platform width (vulnerability value of 1).

6.2.2 Sector II (Santa Eulália – Albufeira)

The cliffs between *Santa Eulália* and *Alemães* beach are mainly affected by marine erosion. As a result, big parts of the cliffs are carved out, creating large and deep notches and caves in the lowest part of the cliff (Figure 38). Moreover, the presence of faults and sinkholes further increases the vulnerability to erosion. The cliffs in this section are highly vulnerable and prone to rock fall and collapse as a result of a very low $CaCO_3$ content (39,68 %). In particular, the middle siltstone layer A-B1 (Figure 40), with a $CaCO_3$ content of only 4,5 % strongly reduces the stability of the cliff. The weakness of this layer can also be identified as per its position a few meters landwards compared to layer A-A (Figure 38).

The weighted average of 2,4 (moderate vulnerability) however, is the result of the protection of a very large part through a relatively long and wide beach (*Alemães* beach) as well as the low vertical facies variation (3 layers) in this sector (Figure 38).

6.2.3 Sector IV (Arrifes – Galé)

The cliffs near *Coelha*, *Castelo*, *Evaristo*, *Manuel Lourenço* and *Galé* beach are mainly suffering from rockfall and cliff collapse due to a high level of faults, karstification (sinkholes)

and plenty of marine caves at the base of the cliff (Figure 42). The presence of three almost uninterrupted siltstone layers until the cliffs of *Albandeira* beach, which developed structural notches (Figure 42), can be identified as one of the main driver mechanisms. Other features that increase the vulnerability in this location are a high abundance of sinkholes. Especially near *Castelo* beach, a high number of partially filled or collapsed sinkholes is present. Moreover, the cliffs of sector IV present a very high vertical facies variation (9), which strongly increases the vulnerability.

The cliffs in the back of the pocket beaches in this section are protected by sand to the greatest possible extend but still show signs of wave induced and sub-aerial erosion in the presence of structural notches, holes and excavations.

Protecting features in this sector are a high number of beaches and a wide shore platform.

All factors combined, this sector presents the highest vulnerability in the study area with a weighted average of 3, which corresponds to “high vulnerability”.

6.2.4 Sector VI (Armação de Pêra – Albandeira)

The relatively high cliffs westward from *Armação de Pêra* until *Albandeira* beach exhibit a very high lithofacies variation (9) (Figure 45 and 48), multiple siltstone layers, structural and marine notches (Figure 46), marine caves at the cliff base (Figure 45) and karst features (sinkholes) (Figure 10). As the siltstone layers are much softer than their surrounding lithology, wind and waves may erode this substrate relatively easy, creating structural notches which could then lead to gravitational rockfall. This may be supported by the horizontal layer structure in this location, which leads to the formation of caves and promotes cliff collapse. Additionally, large open sinkholes, which are connected to the beach or ocean, raise the vulnerability and increase the risk of cliff collapse.

Features lowering the vulnerability of the cliffs to a weighted average of 2,6, are the numerous pocket beaches (Figure 7) and a very high average amount of $CaCO_3$ (77,9 %) in the exposing cliffs.

6.3 Mass Movements

Mass movements are the result of various driver mechanisms including lithological properties, marine and structural notches, caves, discontinuities (faults, joints, cracks) and precipitation (Emery and Kuhn, 1982; Kelletat, 1989; Carter and Woodroffe, 1994; Andriani and Walsh, 2007; Bird, 2008; Sunamura, 2015).

The process of cliff collapse as a result of deep notches and rock stress release is substance of research from Marques (2008) in the southern Algarve. According to this study, the most frequent mass movements are toppling (42 %), followed by rock fall (18 %), slumps (4 %) and other processes (36 %). Research from Bezerra et al. (2011) along the coastal stretch from *Olhos de Água* to *Galé*, correlates these major mass movements to the displacement of detrital sediments from the Plio- and Pleistocene, which fossilized the present paleokarst. As the main driver mechanism, shoreline orientation, and hence, exposition to waves seems to be the most important parameter, but also lithological characteristics have high impact. Accordingly, in some sections, the authors observe direct cliff exposure to the main swell direction, and lower retreat rates compared to more sheltered locations.

When comparing the results of the present work to the study of Bezerra et al. (2011), similar results can be observed. As per Bezerra et al. (2011), highest mass movement rates could be assigned to the part from *Olhos de Água* to *Alemães* beach (Sector I and II of the present work). In this part, cliffs expose weak Miocene carbonate sandstones (average $CaCO_3$ content 56 %, see Section 5.2), but highest volumes displaced correspond to Plio- Pleistocene sediments. As previously mentioned (Section 5.1.2) and further discussed in Section 6.6, particularly the location *Maria Luísa* presents high vulnerability towards such mass fluxes.

6.4 Satellite Images Analysis

The use of the satellite data from the Sentinel-2 missions was aiming for a classification of surface features (LULC, lithology) of the cliffs in the study area and the results were expected to complement other tools used in this study to understand cliff vulnerability.

As research (Van der Meer et al., 2014; Van der Werff and Van der Meer, 2016; Zhang et al., 2017; Ge et al., 2018; Fal et al., 2019) shows, the lithological classification of images from the

Sentinel-2 mission is a powerful and useful tool and can be applied in multiple areas around the world. However, as the aforementioned studies show, for reaching best results in classifying lithological surface features, the study area should be free from vegetation and soil and expose the lithological units. This is not the case in the southern Algarve coast as it can be seen in Figure 68, which shows the NDVI (Normalized Differential Vegetation Index) of the study area from the Sentinel-2 image from November 2019. This is greatly limiting the classification of the lithological units in the present study through this tool.

Due to this, the results from the *unsupervised* and *supervised classification* tools in *SNAP* could not generate conclusions concerning lithological properties. However, the obtained classifications allow the differentiation of LULC in the study area, where vegetation, infrastructure, beaches and other categories indicating rock and soil could be identified and categorized. Moreover, by increasing the number of vector data container and training polygons, results of the *supervised classification* improved (Figure 60 and Annex C).

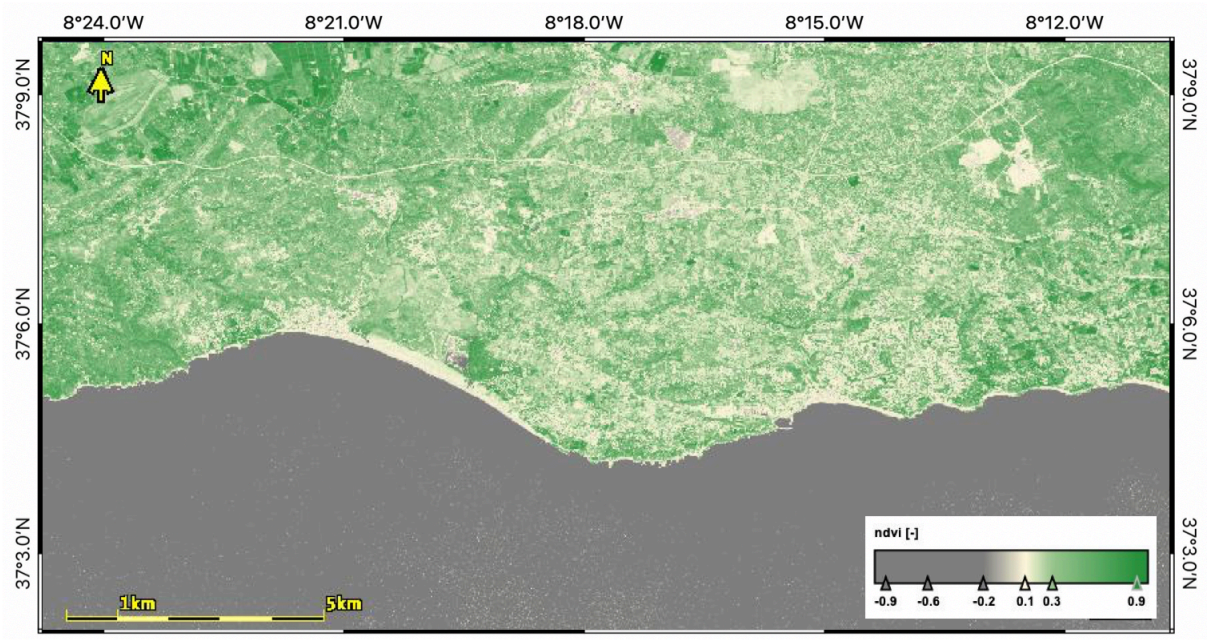

Figure 68: NDVI in the study area from November 2019, exhibiting vegetation cover (green indicating vegetation) along the coast, making a lithological classification impossible (Stock, 2020. Contains modified Copernicus Sentinel data (2019) processed by ESA).

Besides vegetation, other limitations during satellite image processing could be observed. First and foremost, the satellite images are only vertical (top-down), meaning there is no information on cliff parameters but only about cliff top features. As this study mainly focuses

on vertical changes in cliff lithofacies, the information from Satellite images, which explains general and approximate conditions of the coast, is of little use only.

Moreover, the open source satellite data used in this study does not exceed a resolution of 10 m, which would be essential for the research on cliff features and evolution. Higher resolution or other sensors, which would strongly improve the precision of the results, however, are very costly and could not be raised for this study.

The observation of karst features such as sinkholes in the satellite images was not possible due to the low resolution and hence, could not support the other used tools for this matter.

The results from open source satellite image analysis show, that for the study of lithological cliff characteristics, such as vertical facies variations, it is not an appropriate tool for the studied locations but can provide useful LULC classifications of cliff top features.

6.5 UAV image and Photogrammetric Analysis

Images from UAV were intended to complement satellite images by providing high quality images of the study area for observation and identification of certain geomorphological parameters as well as indicators for cliff retreat (e.g. rock fall).

The use of UAVs allowed to survey cliffs from different angles and positions that were not accessible by foot. This provided a wholistic observation of the cliffs and the surrounding environment. Additionally, the quantification of sinkholes and rock fall events was simplified by the use of this method. The creation of 3D models and image-mosaics of the cliffs in the study area in *AgiSoft Metashape* presented an overview of the present settings and morphological characteristics. With this, especially rockfall, marine caves and shore platform extension could be observed and quantified. Moreover, with this method, it was possible to determine even smaller sinkholes and karst features, which was crucial for the parametrization.

These advantages were also observed by Oliveira et al. (2019), who used UAV images to create orthophoto mosaics and 3D models. As for the high number and widely spread sinkholes, caves, stacks and arches, the use of remotely controlled tools such as UAVs appear to be indispensable. Additionally, the steep cliffs and surface features can often only be

reached or spotted from an aerial view, which makes the applied techniques even more useful. By using UAVs, the authors could observe and survey 6 coastal sites from the data, of which DEMs were created. With this, volume calculations were done, and risk parametrizations developed. Similar to the present work, results identify UAVs as a useful, cost efficient, accurate and sometimes necessary tool for studying coastal evolution.

Other case studies (Cruz de Oliveira et al., 2008; Redweik et al., 2008; Niethammer et al., 2012; Gilham et al., 2019; Oliveira et al., 2019; Buchanan et al., 2020) using UAV images as the preferred methodology, show similar conclusions and state, that the existence of high resolution UAV images and 3D models allows the precise identification of features and changes at coastal cliffs and helps understanding erosional processes.

6.6 Parametrization and Vulnerability evaluation

Due to the limitations and restrictions by national security at the time of this work (Covid-19), the parametrization of the studied features is lacking certain information. A particular detriment is the absence of $CaCO_3$ content values for three of the six sectors. Having all the data may have altered the outcome and should be considered when interpreting the results of this study. Additionally, as the determination and counting of features in the parametrization such as karstification, notches, and marine caves is very subjective, results may differ from other research.

Owed to the lack of information, the calculation was different for each sector, where Sector I, II and VI used ten parameters, Sector III and IV nine and Sector V only eight (Table 7). This affects the overall evaluation, but still exhibits the present vulnerability of the cliffs. As suggested by Gornitz et al. (1994) and Del Río and Gracia (2009), the weighted average presents an accurate evaluation of the importance of each parameter and thus, puts the vulnerability into perspective.

The created parametrization (Table 7) and map (Figure 67) of this study presents possible vulnerability based on the parameters lithology, karstification, faults, notches and marine caves, coastline exposition to waves, beach- and shore platform width. Previous vulnerability or hazard maps from Nunes et al. (2009) and Bezerra et al. (2011) for example, are mainly based on coastline orientation and hence, exposure to waves, morphological aspects such as

shore platforms, mechanical strength of rocks and number and type of rock falls. Lithological characteristics of the cliffs is mentioned as a possible factor, however never examined in particular. Thus, to further increase the accuracy and significance, the present study includes factors like vertical facies variation, $CaCO_3$ content, notches, karst and marine caves in the cliff.

When comparing the results of this study with those of Nunes et al. (2009) (see Section 4.3.2a), several resemblances can be observed. Both coastlines in Sector I are similar but show local differences of recession and accretion (Figure 69). A recession of multiple tens of meters can be detected in the area of *Maria Luísa*, which, in the parametrization of the present work, was also identified as an area of high vulnerability and hence, is in agreement (see Sections 5.1.2, 6.2.1, 6.3). Accretion can be observed further East of *Maria Luísa*, but may be the result of inaccurate georeferencing or drawing.

According to a separate vulnerability evaluation for each location in Sector I (*Olhos de Água, Maia Luísa, Santa Eulália*) (Table 8), *Maria Luísa* presents the highest vulnerability (weighted average 2,95), whereas *Olhos de Água* and *Santa Eulália* exhibit lower values (weighted average 2,4 and 2,15 respectively). The same relation was also determined by Nunes et al. (2009).

It is also obvious in both studies, that sector IV (*Arrifes – Galé*) presents the highest vulnerability in the studied area.

In accordance, research from Teixeira (2009) quantifies 38 mass movements of the order of 0.2 – 7 m in the years between 1995 and 2009 only at *Maria Luísa* beach, which indicates one of the highest yearly retreat rates in the area (0.13 m/year). This may be the result of the very high facies variation (7), multiple faults and notches and a south-westerly orientation in the area of *Maria Luísa* beach.

Table 8: Vulnerability classes of the locations OA, ML and SE in Sector I obtained from the parametrization (Parametrization and Vulnerability Evaluation), exhibiting ML as the most vulnerable out of the three sites.

Parameter	**OA**	**ML**	**SE**	Impact Factor
Vertical facies Variation	1	4	3	3
$CaCO_3$	1	2	1	3
Layering	2	2	2	2
Faults	4	4	1	2
Karst	4	3	4	2
Notches	3	3	3	2
Marine Caves	4	3	2	2
Platform width	1	1	1	1
Beach width	3	2	2	1
Exposition	2	4	2	2
Total Vulnerability	25	25	21	
Weighted Average	**2,4**	**2,95**	**2,15**	

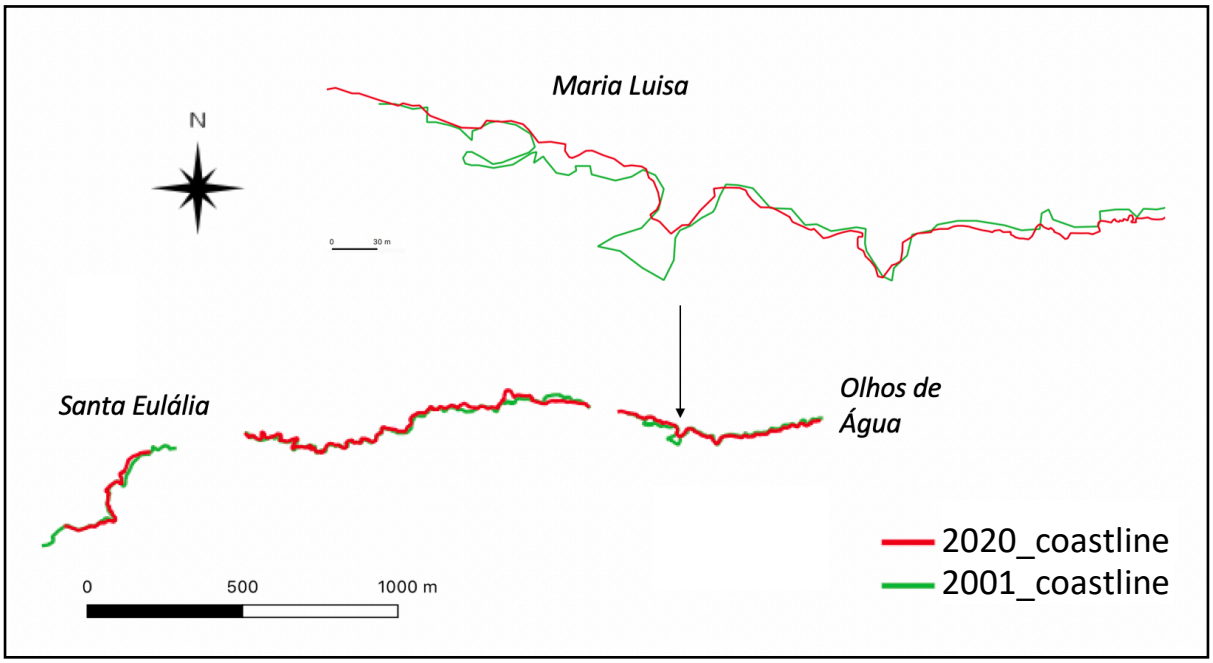

Figure 69: Comparison of coastline position from 2001 (green) with 2020 (red) using aerial and UAV images respectively (STOCK, 2020).

7 CONCLUSIONS

Coastal zones and especially rocky coasts are under constant evolution and pressures and are controlled by multiple factors. The southern Algarve region is not exempt and exhibits great vulnerability to erosional processes of physical, chemical and biological origin. The main drivers for erosion in the study area are lithological properties (vertical facies variation, $CaCO_3$ content), discontinuities in the rock (faults, joints, karst features), notches, marine caves, direct exposition to waves, narrow beaches and narrow shore platforms. During fieldwork, laboratory and computer analysis, these parameters were examined along the coastal stretch from *Olhos de Água* to *Albandeira* and a classification of cliff vulnerability was developed. The approach of this study, to include lithology, vertical facies variation and $CaCO_3$ content, and the assumption that these are first order factors concerning cliff vulnerability, developed a proportional characterization of driver mechanisms in the studied area and provides additional and more detailed analysis to previous research regarding this topic. Based on this parametrization, the study area exhibits intermediate and high vulnerability to erosion in almost all studied sectors (except *Armação de Pêra bay*), while Sector IV (*Arrifes - Galé*) was classified as most vulnerable and Sector V (*Galé - Armação de Pêra Bay*) was classified as least vulnerable. This emphasizes the pressures that the coastal cliffs of the southern Algarve region are exposed to and causes vulnerability evaluation and hazard prevention to be a crucial process. Ergo, studies like this help coastal management to understand processes on coastal cliffs and for planning towards safer tourism.

The application of multiple tools was chosen to develop LULC classifications, to identify advantages and limitations of each method and to complement one another. The main conclusions concerning the used methodology for the scope of this research are:

1. Field work is the base of all further analysis and evaluation and is therefore inevitable
2. Laboratory analysis of $CaCO_3$ content is crucial for further evaluation as it is a possible first order factor concerning cliff erosion
3. Satellite images (Sentinel-2) with a resolution of 10 m are insufficient for the study of coastal cliff features and vegetation represents a vast limitation. However, LULC classification can be done with the use of Sentinel-2 images. Satellite image analysis and vulnerability evaluation must therefore be differentiated, as LULC only provides

general information and mainly exhibits vegetated and unvegetated cliffs and beaches. Although Sentinel-2 images are free to access, it is recommended to use satellite missions with higher spatial resolution in further studies.

4. UAVs provide high quality images of coastal cliffs from multiple angles and can identify features and evidence of erosional processes (sinkholes, rockfall, sediment fans)
5. 3D modelling of UAV images supports the identification of processes and cliff features and can be used for future comparisons and accurate determinations concerning cliff evolution
6. A Parametrization and evaluation of the main driver mechanisms concerning cliff erosion provides good visualization of possible vulnerability

References

Andriani, G., & Walsh, N. (2007). Rocky coast geomorphology and erosional processes: A case study along the Murgia coastline South of Bari, Apulia - SE Italy. *Geomorphology*, *87*(3), 224–238. https://doi.org/10.1016/j.geomorph.2006.03.033

Andriani, G., Walsh, N., & Pagliarulo, R. (2005). The influence of the geological setting on the morphogenetic evolution of the Tremiti Archipelago (Apulia, Southeastern Italy). *Natural Hazards and Earth System Science*, *5*(1), 29–41. https://doi.org/10.5194/nhess-5-29-2005

Bartrum, J. (1916). High water rock platforms: a phase of shore line erosion. *Transactions and Proceedings of the New Zealand Institute*, *48*, 132–134.

Bartrum, J. (1926). "Abnormal" Shore Platforms. *The Journal of Geology*, *34*(8), 793–806.

Bartrum, J. (1938). Shore on platforms. *Journal of Gemorphology*, *13*, 266–272.

Basso, A., Bruno, E., Parise, M., & Pepe, M. (2013). Morphometric analysis of sinkholes in a karst coastal area of southern Apulia (Italy). *Environmental Earth Sciences*, *70*(6), 2545–2559. https://doi.org/10.1007/s12665-013-2297-z

Benumof, B., & Griggs, G. (1999). The Dependence of Seacliff erosion Rates on Cliff Material Properties and Physical Processes: San Diego County, California. *Shore & Beach*, *67*(4), 29–41.

Bezerra, M., Moura, D., Ferreira, Ó., & Taborda, R. (2011). Influence of Wave Action and Lithology on Sea Cliff Mass Movements in Central Algarve Coast, Portugal. *Journal of Coastal Research*, *275*, 162–171. https://doi.org/10.2112/jcoastres-d-11-00004.1

Bird, E. (2000). *Coastal Geomorphology: An Introduction*. Wiley.

Bird, E. (2008). Coastal Geomorphology: An Introduction. In *Eos, Transactions American Geophysical Union* (Vol. 82, Issue 32). https://doi.org/10.1029/01eo00219

Bird, E. (2016). *Coastal Cliffs: Morphology and Management*. https://doi.org/10.1007/978-3-319-29084-3

Bishop, M. (2013). *3.1 Remote Sensing and GIScience in Geomorphology: Introduction and Overview A2 - Shroder, John F. BT - Treatise on Geomorphology* (Vol. 3). https://doi.org/https://doi.org/10.1016/B978-0-12-374739-6.00040-3

Boye, C., & Fiadonu, E. (2020). Lithological effects on rocky coastline stability. *Heliyon*, *6*(3), e03539. https://doi.org/10.1016/j.heliyon.2020.e03539

Breiman, L. (2001). Random Forests. *Machine Learning*, *45*(1), 5–32. https://doi.org/10.1023/A:1010933404324

Buchanan, D., Naylor, L., Hurst, M., & Stephenson, W. (2020). Erosion of rocky shore platforms by block detachment from layered stratigraphy. *Earth Surface Processes and Landforms*, *45*(4), 1028–1037. https://doi.org/10.1002/esp.4797

Cachão, M., Boski, T., Moura, D., Dias, R. P., Silva, C., Santos, A., Pimentel, N., & Cabral, J. (1998). Proposta de articulação das unidades sedimentares neogénicas e quaternaries do Algarve. In *Actas V Congresso Nacional de Geologia, Comunicações do Instituto Geológico e Mineiro, Lisboa: Vol. 84/1*.

Cachão, M., & Freitas, M. (1998). Sedimentologia e interpretação paleoambiental de Areolas do Neogénico português (dados preliminaries). In *Actas V Congresso Nacional de Geologia, Comunicações do Instituto Geológico e Mineiro, Lisboa: Vol. 84/1*.

Carter, G., & Woodroffe, C. (1994). *Coastal Evolution - Late Quaternary Shoreline Morphodynamics*. The Press Syndicate of the University of Cambridge. The Pitt Building, Trumpington Street, Cambridge CB2 1RP, United Kingdom Cambridge.

Catalão, J., Catita, C., Miranda, J., & Dias, J. (2002). Photogrammetric analysis of the coastal erosion in the Algarve (Portugal) / Analyse photogrammétrique de l'érosion côtière en Algarve (Portugal). *Géomorphologie : Relief, Processus, Environnement*, *8*(2), 119–126. https://doi.org/10.3406/morfo.2002.1133

Cavacao, C. (1997). Tourismo e Demografia no Algarve. In *O Turismo em Portugal* (p. 76).

Costa, M., Silva, R., & Vitorino, J. (2001). Contribuição para o estudo do clima de agitação marítima na costa portuguesa. *2as Jornadas Portuguesas de Engenharia Costeira e Portuária.*

Cruz de Oliveira, S., Catalão, J., Ferreira, Ó., & Alveirinho Dias, J. M. (2008). Evaluation of Cliff Retreat and Beach Nourishment in Southern Portugal Using Photogrammetric Techniques. *Journal of Coastal Research*, *4*(4), 184–193. https://doi.org/10.2112/06-0781.1

Cunha, L. (2012). Geomorphology of the Central Algarve, Portugal. *Journal of Maps*.

Dana, J. (1849). *United States exploring Expedition*. Sherman, C., Philadelphia.

Dana, J. (1857). *Manual of Mineralogy*. Durrie & Peck, Philadelphia.

Davidson-Arnot, R. (2010). *Introduction to Coastal Processes and Geomorphology*. Cambridge University Press, New York.

Davidson-Arnott, R., Bauer, B., & Houser, C. (2010). Cliffed and Rocky Coasts. In *Introduction to Coastal Processes and Geomorphology* (pp. 476–516). https://doi.org/10.1017/9781108546126.014

Davis, R. A. (2013). Evolution of Coastal Landforms. In *Treatise on Geomorphology* (Vol. 10). https://doi.org/10.1016/B978-0-12-374739-6.00293-1

Davis, R., & Fitzgerald, D. (2004). Beaches and Coasts. In *Blackwell Science Ltd*. https://doi.org/10.1017/CBO9781107415324.004

Del Río, L., & Gracia, F. J. (2009). Erosion risk assessment of active coastal cliffs in temperate environments. *Geomorphology*, *112*(1–2), 82–95. https://doi.org/10.1016/j.geomorph.2009.05.009

Dias, J. (1988). Aspectos Geológicos do Litoral Algarvio. *Genovas (Lisboa)*, *10*(1), 113–128.

Dias, J. M. A., Boski, T., Rodrigues, A., & Magalhães, F. (2000). Coast line evolution in Portugal since the Last Glacial Maximum until present - A synthesis. *Marine Geology*, *170*(1–2), 177–186. https://doi.org/10.1016/S0025-3227(00)00073-6

Dias, J. M. A., & Neal, W. J. (1992). Sea Cliff Retreat in Southern Portugal. *Journal of Coastal Research*, *8*(3), 641–654.

Dias, R., & Cabral, J. (2002). Actividade neotectónica na região do Algarve, S. de Portugal.

Comunicações Do Instituto Geológico e Mineiro.

Drusch, M., Del Bello, U., Carlier, S., Colin, O., Fernandez, V., Gascon, F., Hoersch, B., Isola, C., Laberinti, P., Martimort, P., Meygret, A., Spoto, F., Sy, O., Marchese, F., & Bargellini, P. (2012). Sentinel-2: ESA's Optical High-Resolution Mission for GMES Operational Services. *Remote Sensing of Environment*, *120*, 25–36. https://doi.org/10.1016/j.rse.2011.11.026

Edwards, A. B. (1951). Wave Action in Shore Platform Formation. *Geological Magazine*, *88*(1), 41–49. https://doi.org/10.1017/S0016756800068904

Emery, K. O., & Kuhn, G. G. (1982). *Geological Society of America Bulletin Sea cliffs : Their processes , profiles , and classification*. *October 2009*, 644–654. https://doi.org/10.1130/0016-7606(1982)93<644

ESA, E. S. A. (2020a). *Copernicus Open Access Hub*. scihub.copernicus.eu/dhus/#/home. Accessed 20.01.2020

ESA, E. S. A. (2020b). *European Space Agency*. https://www.esa.int/. Accessed 20.01.2020

Estatística de Instituto National. (2019). Esttísticas do Turismo 2018. In *Journal of Chemical Information and Modeling* (Vol. 53, Issue 9). https://doi.org/10.1017/CBO9781107415324.004

Fal, S., Maanan, M., Baidder, L., & Rhinane, H. (2019). The contribution of Sentinel-2 satellite images for geological mapping in the south of Tafilalet basin (Eastern Anti-Atlas, Morocco). *International Archives of the Photogrammetry, Remote Sensing and Spatial Information Sciences - ISPRS Archives*, *42*(4/W12), 75–82. https://doi.org/10.5194/isprs-archives-XLII-4-W12-75-2019

Forst, M., Brachert, T., & Pais, J. (2000). *High-resolution correlation of coastal cliff sections in the Lagos- Portimao Formation (Lower - Middle Miocene , central Algarve , Portugal) Lagos-Portimao Formation*.

Forth, R. A., Butcher, D., & Senior, R. (1999). Hazard mapping of karst along the coast of the Algarve, Portugal. *Engineering Geology*, *52*(1–2), 67–74. https://doi.org/10.1016/S0013-7952(98)00056-8

Gabriel, S., Moura, D., Jacob, J., & Horta, J. (2013). Monitoring of waves in rocky shores: Comparison between a shore platform and the adjacent pocket beach. *Coastal Dynamics*, 1–2.

Ge, W., Cheng, Q., Jing, L., Armenakis, C., & Ding, H. (2018). Lithological discrimination using ASTER and Sentinel-2A in the Shibanjing ophiolite complex of Beishan orogenic in Inner Mongolia, China. *Advances in Space Research*, *62*(7), 1702–1716. https://doi.org/10.1016/j.asr.2018.06.036

Gilham, J., Barlow, J., & Moore, R. (2019). Detection and analysis of mass wasting events in chalk sea cliffs using UAV photogrammetry. *Engineering Geology*, *250*(January), 101–112. https://doi.org/10.1016/j.enggeo.2019.01.013

Gomez-Pujol, L., Perez-Alberti, A., Blanco-Chao, R., Costa, S., Neves, M., & Del Rio, L. (2014). The rock coast of continental Europe in the Atlantic. *Geological Society, London, Memoirs*, *40*, p77-88. https://doi.org/doi: 10.1144/M40.6

Griggs, G., & Trenhaile, A. (1994). Coastal Cliffs and Platforms. In R. Carter & C. Woodroffe

(Eds.), *Coastal Evolution - Late Quaternary Shoreline Morphodynamics* (pp. 425–450). The Press Syndicate of the University of Cambridge. The Pitt Building, Trumpington Street, Cambridge CB2 1RP, United Kingdom Cambridge.

Gupta, R. (2017). Remote sensing geology: Third edition. In *Remote Sensing Geology: Third Edition*. https://doi.org/10.1007/978-3-662-55876-8

Hayes, N., Buss, H., Moore, O., Krám, P., & Pancost, R. (2020). Controls on granitic weathering fronts in contrasting climates. *Chemical Geology*, *535*(December 2019), 119450. https://doi.org/10.1016/j.chemgeo.2019.119450

Hills, E. (1949). Shore platforms. *Geological Magazine*, *14*(3), 873–875. https://doi.org/10.1007/1-4020-3880-1_288

Horikawa, K., & Sunamura, T. (1967). A Study on Erosion of Coastal Cliffs by Using Aerial Photographs. *Coastal Engineering in Japan*, *10*(1), 67–83. https://doi.org/10.1080/05785634.1967.11924056

Horta, J., Moura, D., Gabriel, S., & Ferreira, Ó. (2013). Measurement of pocket beach morphology using geographic information technology: the MAPBeach toolbox. *Journal of Coastal Research*, *165*, 1397–1402. https://doi.org/10.2112/si65-236.1

Hulsemann, J. (1966). On The Routine Analysis of Carbonates in Unconsolidated Sediments: NOTES. *Journal of Sedimentary Petrology*, *36*(2), 622–625.

Hydrogràfico, I. (1990). *Roteiro da Costa de Portugal*. Instituto Hidrográfico.

Inman, D. L., & Nordstrom, C. E. (1971). On the Tectonic and Morphologic Classification of Coasts. *The Journal of Geology*, *79*, 21.

John, M. (1971). Properties and Classification of Rocks with Reference to Tunnelling. In *NMERE Council of Scientific & Industrial Research, Pretoria, South Africa*.

Johnsons, D. (1919). *Shore Processes and shoreline Development*. John Wiley & Sons. https://archive.org/details/shoreprocessessh01john/page/n15/mode/2up

Kaiser, A., Erhardt, A., & Eltner, A. (2018). Addressing uncertainties in interpreting soil surface changes by multitemporal high-resolution topography data across scales. *Land Degradation and Development*, *29*(8), 2264–2277. https://doi.org/10.1002/ldr.2967

Kelletat, D. (1989). Geographie der Meere und Küsten. In *Physische Geographie der Meere und Küsten*. https://doi.org/10.1007/978-3-663-12487-0_1

Komar, P. D. (1976). *Beach processes and sedimentation*. Prentice Hall, New Jersey.

Lamas, F., Irigaray, C., Oteo, C., & Chacón, J. (2005). Selection of the most appropriate method to determine the carbonate content for engineering purposes with particular regard to marls. *Engineering Geology*, *81*(1), 32–41. https://doi.org/10.1016/j.enggeo.2005.07.005

Marques, F. M. S. F. (1998). Sea cliff retreat in Portugal : overview of existing quantitative data. *Riscos Naturais*, *84*, 18–20.

Marques, F. M. S. F. (2008). Magnitude-frequency of sea cliff instabilities. *Natural Hazards and Earth System Science*, *8*(5), 1161–1171. https://doi.org/10.5194/nhess-8-1161-2008

Martins, V. N., Pires, R., & Cabral, P. (2012). Modelling of coastal vulnerability in the stretch

between the beaches of Porto de Mós and Falésia, Algarve (Portugal). *Journal of Coastal Conservation*, *16*(4), 503–510. https://doi.org/10.1007/s11852-012-0191-6

Masselink, G., & Gehrels, R. (2014). *Coastal & Global Change*. American Geophysical Union. Wiley.

Masselink, G., & Hughes, M. G. (2003). *Introduction to Coastal Processes and Geomorphology*. Arnold, London.

Miranda, P., Coelho, F., Tomé, A., Valente, M., Carvalho, A., Pires, C., Pires, H., Pires, V., & Ramalho, C. (2002). *2 20 th Century Portuguese Climate and Climate Scenarios*. *June*, 23–83.

Mottershead, D. (2013). Coastal Weathering. *Treatise on Geomorphology*, *4*, 228–244. https://doi.org/10.1016/B978-0-12-374739-6.00064-6

Moura, D., Albardeiro, L., Veiga-Pires, C., Boski, T., & Tigano, E. (2006). Morphological features and processes in the central Algarve rocky coast (South Portugal). *Geomorphology*, *81*(3–4), 345–360. https://doi.org/10.1016/j.geomorph.2006.04.014

Moura, D., Gabriel, S., Gamito, S., Santos, R., Zugasti, E., Naylor, L., Gomes, A., Tavares, A. M., & Martins, A. L. (2012). Integrated assessment of bioerosion, biocover and downwearing rates of carbonate rock shore platforms in southern Portugal. *Continental Shelf Research*, *38*, 79–88. https://doi.org/10.1016/j.csr.2012.03.003

Moura, D., Gabriel, S., & Jacob, J. (2011). Coastal morphology along the central Algarve rocky coast: Driver mechanisms. *Journal of Coastal Research*, *SPEC. ISSUE 64*, 790–794.

Moura, D., Gabriel, S., Jacob, J., Fortes, C. J. E. M., Silva, P. A., Horta, J., & Abreu, T. (2012). Erosion of rocky shores- protection promoted by sandy beaches and shore platforms. *2as Jornadas de Engenharia Hidrográfica*, *1*, 1–4.

Moura, D., Gabriel, S., Ramos-Pereira, A., Neves, M., Trindade, J., Viegas, J., Veiga-Pires, C., Ferreira, O., Matias, A., Jacob, J., Boski, T., & Santana, P. (2011). Downwearing rates on shore platforms of different calcareous lithotypes. *Marine Geology*, *286*(1–4), 112–116. https://doi.org/10.1016/j.margeo.2011.06.002

Moura, D., Veiga-Pires, C., Albardeiro, L., Boski, T., Rodrigues, A. L., & Tareco, H. (2006). Holocene sea level fluctuations and coastal evolution in the central Algarve (southern Portugal). *Marine Geology*, *237*(3–4), 127–142. https://doi.org/10.1016/j.margeo.2006.10.026

Naylor, L. A., Stephenson, W. J., & Trenhaile, A. S. (2010). Rock coast geomorphology: Recent advances and future research directions. *Geomorphology*, *114*(1–2), 3–11. https://doi.org/10.1016/j.geomorph.2009.02.004

Naylor, L., Coombes, M., & Viles, H. (2012). Reconceptualising the role of organisms in the erosion of rock coasts: A new model. *Geomorphology*, *157–158*, 17–30. https://doi.org/10.1016/j.geomorph.2011.07.015

Neumann, A. (1966). Observations on Coastal Erosion in Bermuda and Measurements of the Boring Rate of the Sponge, Cliona Lampa,. *Limnology and Oceanography*, *11*(1), 92–108. https://doi.org/10.4319/lo.1966.11.1.0092

Niculescu, S., Talab Ou Ali, H., & Billey, A. (2018). Random forest classification using Sentinel-

1 and Sentinel-2 series for vegetation monitoring in the Pays de Brest (France). *SPIE Remote Sensing*, 6. https://doi.org/10.1117/12.2325546

Niethammer, U., James, M. R., Rothmund, S., Travelletti, J., & Joswig, M. (2012). UAV-based remote sensing of the Super-Sauze landslide: Evaluation and results. *Engineering Geology*, *128*, 2–11. https://doi.org/10.1016/j.enggeo.2011.03.012

Nunes, M., Ferreira, Ó., Schaefer, M., Clifton, J., Baily, B., Moura, D., & Loureiro, C. (2009). Hazard assessment in rock cliffs at Central Algarve (Portugal): A tool for coastal management. *Ocean and Coastal Management*, *52*(10), 506–515. https://doi.org/10.1016/j.ocecoaman.2009.08.004

Oliveira, S., Moura, D., Boski, T., & Horta, J. (2019). Coastal paleokarst landforms: A morphometric approach via UAV for coastal management (Algarve, Portugal case study). *Ocean and Coastal Management*, *167*(October 2018), 245–261. https://doi.org/10.1016/j.ocecoaman.2018.10.025

Oliveira, Sónia, Moura, D., & Boski, T. (2020). The evolution of the European framework for coastal management, linked to the new environmental challenges. The Portuguese case. *Revista de Gestão Costeira Integrada*, *20*(1), 27–48. https://doi.org/10.5894/rgci-n213

Pais, J., Cunha, P., Pereira, D., Legoinha, P., Dias, R., Moura, D., Brum da Silveira, A., Kullberg, J., & Gonzalez-Delgado, J. (2012). *The Paleogene and Neogene of Western Iberia (Portugal)- A Cenozoic Record in the Europpean Atlantic Domain*. https://doi.org/10.1007/978-3-642-22401-0

Pinto, C. a, & Teixeira, S. B. (2002). Morphodynamics of the Sandy Barrier of Salgados Coastal Lagoon , Armação de Pêra Bay (Algarve – Portugal). *Litoral 2002, The Changing Coast, EUROCOAST/EUCC*, 403–409.

Pires, H. N. O., & Pessanha, L. E. V. (1997). Agitação marítima na costa portuguesa. *Instituto Nacional de Meteorologia e Geofísica (INMG)*.

Prémaillon, M., Regard, V., Dewez, T., & Auda, Y. (2018). GlobR2C2 (Global Recession Rates of Coastal Cliffs): A global relational database to investigate coastal rocky cliff erosion rate variations. *Earth Surface Dynamics*, *6*(3), 651–668. https://doi.org/10.5194/esurf-6-651-2018

Proença, B., Oliveira, F., & Sancho, F. (2011). Coastal Erosion Management in Algarve (Portugal) — A Beach Nourishment Case Study. *Journal of Coastal Research*, *61*(61), 328–334. https://doi.org/10.2112/si61-001.33

Ramos-Pereira, A., Ramos, C., & Neves, M. (2006). Dinâmica dos sistemas litorais: uma componente esquecida no ordenamento do território. O exemplo de Porto de Mós (Lagos). *Publicações Da Associação Portuguesa de Geomorfólogos*, *3*, 237–244.

Redweik, P., Marques, F., & Matildes, R. (2008). A strategy for detection and measurement of the cliff retreat in the coast of Algarve (Portugal) by photogrammetry. *EARSeL EProceedings*, *1991*(10), 92–104. http://eproceedings.org/static/vol07_2/07_2_redweik1.pdf

Richards, J. A., & Jia, X. (2006). John A. Richards · Xiuping Jia Remote Sensing Digital Image Analysis. In *Springer- Verlag*.

Roberts, H. M., & Plater, A. J. (1999). U- and Th-series disequilibria in coastal infill sediments

from Praia da Rocha (Algarve Region, Portugal): a contribution to the study of Late Quaternary weathering and erosion. *Geomorphology*, *26*, 223–228.

Romariz, C., Almeida, C., & Silva, M. O. (1979). Contributions to the geology of Algarve , Portugal. *Bol. Do Museu e Laboratório Mineralógico e Geológico Da Fac. de Ciências de Lisboa*, *16*, 253–263. http://e-geo.ineti.pt/edicoes_online/obras/costa_almeida/tp005.pdf

Singh, B., & Goel, R. K. (1999). Rock Mass Classification. A Practical Approach in Civil Engineering. In *Rock mass classification. A practical approach in civil engineering.* Elsevir Science LTD., Oxford, UK.

Stephenson, W. J., Dickson, M. E., & Trenhaile, A. S. (2013). Rock Coasts. In *Treatise on Geomorphology* (Vol. 10). Elsevier Ltd. https://doi.org/10.1016/B978-0-12-374739-6.00284-0

Stephenson, W., & Kirk, R. (2000). Development of shore platforms on Kaikoura Peninsula, South Island, New Zealand II: The role of subaerial weathering. *Geomorphology*, *32*(1–2), 43–56. https://doi.org/10.1016/S0169-555X(99)00062-8

Summerfield, M. (1991). *Global Geomorphology*. Routledge. London and New York.

Sunamura, T. (1978). Mechanisms of Shore Platform Formation on the Southeastern Coast of the Izu Peninsula, Japan. *The Journal of Geology*, *10*, 211–222.

Sunamura, T. (1992). *Geomorphology of Rocky Coasts.* Wiley, New York.

Sunamura, T. (2015). Rocky coast processes*: with special reference to the recession of soft rock cliff*. *91*(9), 481–500.

Teixeira, S. B. (2006). Slope mass movements on rocky sea-cliffs: A power-law distributed natural hazard on the Barlavento Coast, Algarve, Portugal. *Continental Shelf Research*, *26*(9), 1077–1091. https://doi.org/10.1016/j.csr.2005.12.013

Teixeira, S. B. (2009). *Geodinâmica, ocupação e risco na praia Maria Luísa (Albufeira)*.

Terefenko, P., & Terefenko, O. (2014). Determining the role of exposure, wave force, and rock chemical resistance in marine notch development. *Journal of Coastal Research*, *70*, 706–711. https://doi.org/10.2112/si70-105.1

Terrinha, P., Rocha, R., Rey, J., Cachão, M., Moura, D., Roque, C., Martins, L., Valadares, V., Cabral, J., Azevedo, M. R., Barbero, L., Clavijo, E., Dias, R. P., Gafeira, J., Matias, H., Matias, L., Madeira, J., Marques da Silva, C., Munhá, J., … Youbi, N. (2006). A bacia do Algarve: Estratigrafia, Paleografia e Tectonica. 45.

Thenkabail, P. (2015). Remotely sensed data characterization, classification, and accuracies. In *Remotely Sensed Data Characterization, Classification, and Accuracies* (Vol. 1). https://doi.org/10.1201/b19294

Toth, C., & Jóźków, G. (2016). Remote sensing platforms and sensors: A survey. *ISPRS Journal of Photogrammetry and Remote Sensing*, *115*, 22–36. https://doi.org/10.1016/j.isprsjprs.2015.10.004

Trenhaile, A. (2002). Rock coasts, with particular emphasis on shore platforms. *Geomorphology*, *48*(1–3), 7–22. https://doi.org/10.1016/S0169-555X(02)00173-3

Trenhaile, A. (2015). Coastal notches: Their morphology, formation, and function. *Earth-*

Science Reviews, *150*, 285–304. https://doi.org/10.1016/j.earscirev.2015.08.003

Trenhaile, A., & Kanyaya, J. (2007). The Role of Wave Erosion on Sloping and Horizontal Shore Platforms in Macro- and Mesotidal Environments. *Journal of Coastal Research*, *232*(2), 298–309. https://doi.org/10.2112/04-0282.1

Trenhaile, A. S. (2000). Modeling the development of wave-cut shore platforms. *Marine Geology*, *166*(1–4), 163–178. https://doi.org/10.1016/S0025-3227(00)00013-X

Van der Meer, F. D., van der Werff, H. M. A., & van Ruitenbeek, F. J. A. (2014). Potential of ESA's Sentinel-2 for geological applications. *Remote Sensing of Environment*, *148*, 124–133. https://doi.org/10.1016/j.rse.2014.03.022

Van der Werff, H., & Van der Meer, F. (2016). *Sentinel-2A MSI and Landsat 8 OLI Provide Data Continuity for Geological Remote Sensing*.

Viegas, J., Moura, D., Gabriel, S., & Pais, L. A. (2014). Influência das características geotécnicas dos maciços rochosos no recuo das arribas costeiras do algarve central. *14º Congresso Nacional de Geotecnia e 4as Jornadas Luso-Espanholas de Geotecnia*, *2004*.

Vousdoukas, M. I., Velegrakis, A. F., & Plomaritis, T. A. (2007). Beachrock occurrence, characteristics, formation mechanisms and impacts. *Earth-Science Reviews*, *85*(1–2), 23–46. https://doi.org/10.1016/j.earscirev.2007.07.002

Waltham, A. C., & Fookes, P. G. (2003). Engineering classification of karst ground conditions. *Quarterly Journal of Engineering Geology and Hydrogeology*, *36*(2), 101–118. https://doi.org/10.1144/1470-9236/2002-33

Wentworth, C. (1938). Marine bench-forming processes — water level weathering. *Journal of Gemorphology*, *1*(1), 5–32.

Wentworth, C. (1939). Wentworth, C.K., 1939. Marine bench-forming processes: II. Solution benching. *Journal of Gemorphology*, *2*(1), 3–25.

Zabidi, H., Termizi, M., Aliman, S., Ariffin, K. S., & Khalil, N. L. (2016). Geological Structure and Geomorphological Aspects in Karstified Susceptibility Mapping of Limestone Formations. *Procedia Chemistry*, *19*, 659–665. https://doi.org/10.1016/j.proche.2016.03.067

Zhang, T., Su, J., Liu, C., Chen, W., Liu, H., & Liu, G. (2017). Band selection in sentinel-2 satellite for agriculture applications. *ICAC 2017 - 2017 23rd IEEE International Conference on Automation and Computing: Addressing Global Challenges through Automation and Computing*. https://doi.org/10.23919/IConAC.2017.8081990

Annex A

ID	Layer	CaCO3	Thickness	% of cliff height / impact factor	Cliff height (m)	CaCO3 with impact factor	% / Location	CaCO3 % without impact factor	Difference (%)
1	OA-A	41,03	2,6	31,29	8,2	1283,63	60,81	62,19	1,38
2	OA-B	52,08	3,2	39,26		2044,88			
3	OA-C	93,46	2,4	29,45		2752,20			
4	ML-A	41,03	3,0	20,00	15,0	820,52	58,57	59,35	0,78
5	ML-B	52,08	1,0	6,67		347,20			
6	ML-C	93,46	2,0	13,33		1246,14			
7	ML-D	55,60	3,5	23,33		1297,23			
8	ML-F	49,33	1,5	10,00		493,34			
9	ML-G	81,04	2,0	13,33		1080,55			
10	ML-H	42,92	2,0	13,33		572,33			
11	SE-A	56,96	1,0	20,00	5,0	1139,20	79,94	80,05	0,12
12	SE-B	92,43	0,5	10,00		924,27			
14	SE-C	80,52	2,0	40,00		3220,63			
15	SE-D	90,32	1,5	30,00		2709,45			
16	A-A	81,61	7,5	150,00		12242,04	52,27	39,68	12,59
17	A-B1	4,53	4,0	80,00		362,23			
18	A-B2	32,91	1,5	30,00		987,17			
19	AL-A	89,25	0,8	5,71	14,0	510,01	75,08	76,67	1,60
20	AL-B	78,56	1,5	10,71		841,68			
21	AL-C	78,51	1,6	11,07		869,20			
22	AL-D	69,55	2,4	16,79		1167,48			
23	AL-F	87,62	1,6	11,43		1001,39			
24	AL-G	51,32	1,5	10,71		549,87			
25	AL-H	80,91	0,5	3,21		260,07			
26	AL-I	77,67	1,6	11,07		859,94			

Annex B

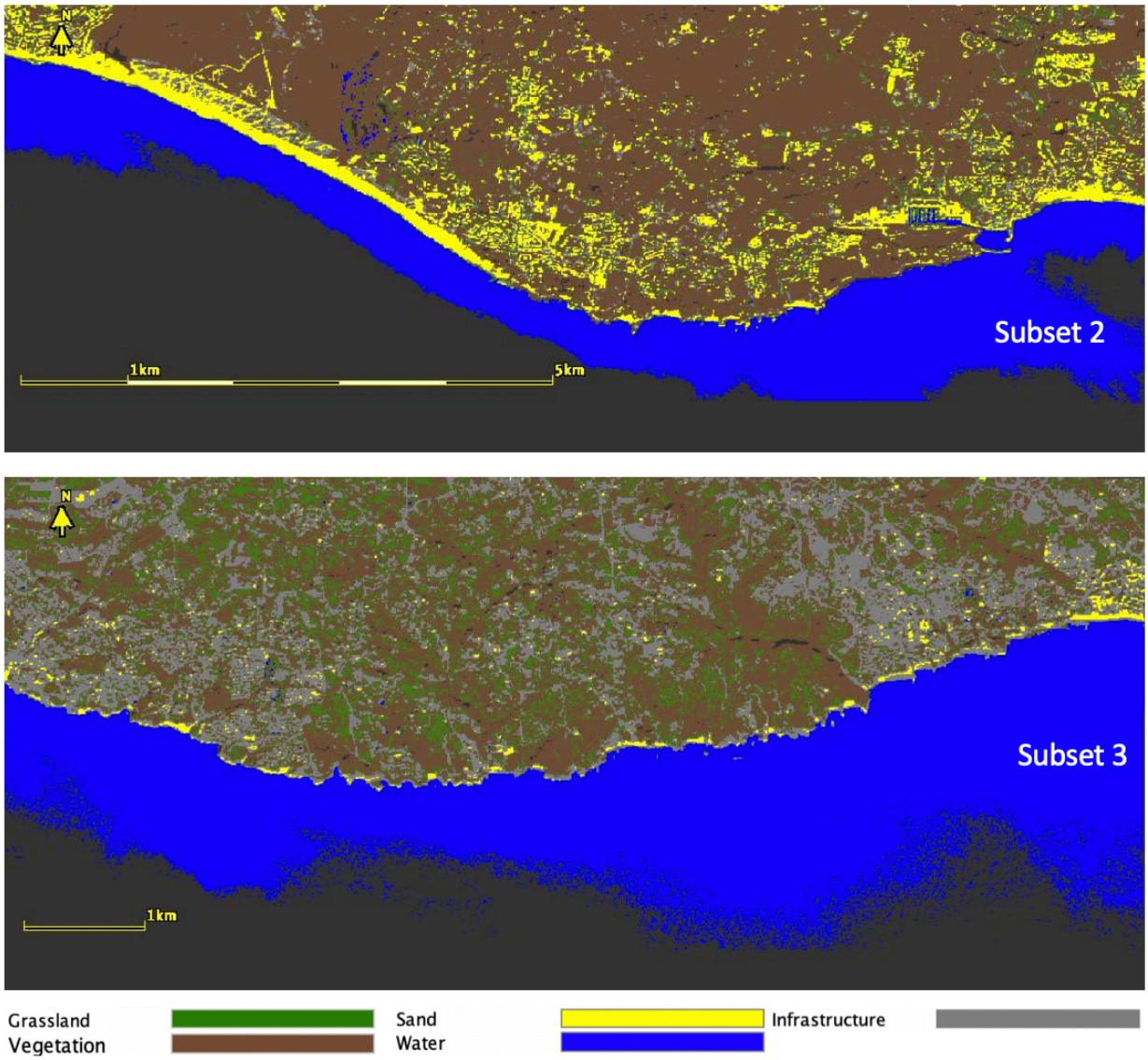

Figure 70: Sector 2 and Sector 3 of the unsupervised classification of the Sentinel-2 image from November 2019 (STOCK, 2020. Contains modified Copernicus Sentinel data (2019), processed by ESA.

Annex C

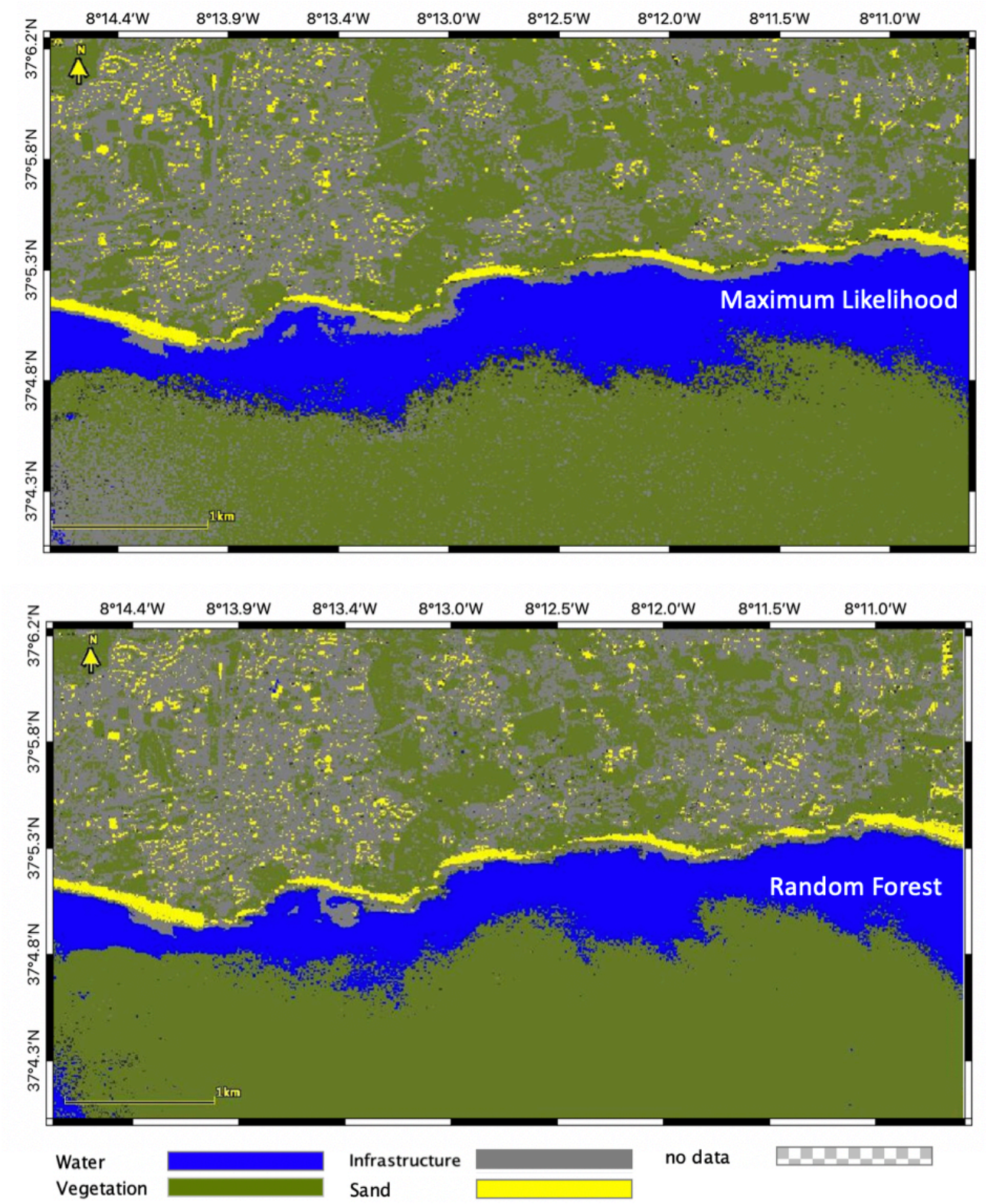

Figure 71: Result of the Maximum Likelihood (top) and Random Forest (bottom) supervised classification of Subset 1 (OA – SE) of the Sentinel-2 image from November 2019 using 5 vector data container (Stock, 2020. Contains modified Copernicus Sentinel data (2019), processed by ESA).